FAULT DETECTION AND OPTIMAL TREATMENT OF THE PERMANENT MAGNET SYNCHRONOUS MACHINE USING FIELD RECOSTRUCTION METHOD

by

AMIR KHOOBROO

Presented to the Faculty of the Graduate School of

The University of Texas at Arlington in Partial Fulfillment

of the Requirements

for the Degree of

DOCTOR OF PHILOSOPHY

THE UNIVERSITY OF TEXAS AT ARLINGTON

May 2010

ACKNOWLEDGEMENTS

I would like to take this opportunity to thank several people who have contributed to my successful completion of this dissertation. First, I would like to thank my academic supervisor Dr. Babak Fahimi for his support and guidance over the past four years. It has been an honor working with him during my PhD program and a wonderful life experience. I would also like to thank him for giving me the opportunity to present our work at various conferences and letting me be a part of various research projects which has helped both in becoming an experienced researcher and a team leader.

I would like to thank Dr. Jonathan bredow, Dr. Wei-Jen Lee, Dr. Kambiz Alavi and Dr. Frank Lewis for their agreement to be on my committee and valuable suggestions and comments.

My sincere appreciation goes to the members of the Renewable Energy and Vehicular Technology Lab at the Universty of Texas at Arlington for being supportive throughout the course of my Ph.D. work at UTA. It was my honor to be one of the members to set up and develop this lab with Dr. Fahimi and is an experience I shall always be proud of.

My gratitude goes to my family in the US and in Iran, without whose support I would have never made it this far. I am grateful to my family for the sacrifices they have made in order to provide me peace of mind, permanent support and encouragement during my long years of education.

Finally; I would like to thank my dear wife, Anahita, for giving me strength and driving force towards success over the past six years. No words can express how much I appreciate the encouragement her presence has provided. I thank her for her patience, supporting me emotionally and for being ready for my challenges. To her, I dedicate this dissertation.

May 07, 2010

ABSTRACT

FAULT DETECTION AND OPTIMAL TREATMENT OF THE PERMANENT MAGNET SYNCHRONOUS MACHINE USING FIELD RECOSTRUCTION METHOD

AMIR KHOOBROO, PhD

The University of Texas at Arlington, 2010

Supervising Professor: Babak Fahimi

Permanent magnet synchronous machines (PMSM) are used extensively in industrial applications due to their relatively high power density, high efficiency, negligible rotor losses, maintenance free operation, and ease of control. Fault tolerance has become a design criterion for adjustable speed motor drives (ASMD) which are used in high impact applications. In simple terms, a fault tolerant ASMD is expected to continue its intended function in the event of a failure compliment to its remaining components. A wide variety of the research has been done on the techniques of fault detection. Most of these researches focus solely on the fault detection and less attention is paid to treatment of the faults.

This dissertation investigates fault detection and clearance in a PMSM using the field reconstruction method. Also, the optimal excitation of the machine for optimal performance under healthy and faulty modes of operation has been investigated. Initially an accurate Finite

Element (FE) model is developed for the PMSM using the MAGNET software (©infolytica) as a reference for comparison. This model is used to analyze the electromagnetic behavior of the PMSM during normal and faulty operating conditions. As the FE analysis is time consuming, Field Reconstruction Method (FRM) is developed and implemented to minimize the computational time while maintaining an acceptable accuracy. The FRM provides a precise distribution of the magnetic field components for PMSM. A new flux estimation technique is developed to monitor magnetic flux passing through each stator tooth. Also, the flux linking each stator phase can be determined using the flux estimator.

In order to detect the faults specific signatures have been identified and detected. For the faults under study, (i.e. stator inter-turn short circuit, rotor partial demagnetization and rotor static eccentricity) there are measurable signatures in the magnetic flux that are used for detection purposes.

Finally, based on the type and location of the fault a optimal stator currents are calculated. Once a fault is detected, the faulty component would be disengaged if possible. Then, the optimal currents would be applied to the remaining stator phases to guarantee the appropriate operation of the machine. The above mentioned steps have been supported by simulation and experimental results.

TABLE OF CONTENTS

LIST OF ILLUSTRATIONS

Figure Page

LIST OF TABLES

CHAPTER 1

INTRODUCTION

In this chapter a description of the motivations, methods, and objectives of this dissertation is presented. First, the importance of PMSM in industrial applications has been discussed. Then the issues regarding the use of PMSM are explored. Later the fault tolerance concept and its implications are presented. The state-of-the-art along with their advantages and disadvantages are surveyed. This chapter is concluded by an overview of the dissertation outline and objectives.

1.1 Importance of PMSM

Permanent magnet Synchronous machines are widely used in various industrial applications due to their relatively high power density, high efficiency, negligible rotor losses, maintenance free operation, and ease of control. With rapid advancement in the area of modern power electronics, researchers have had a great deal of flexibility in implementing complex control routines. There has been significant effort to improve the control methods of the machines to enhance their efficiency and fault resilience. With nearly 65% of the electricity that is generated worldwide being consumed in electromechanical energy converters (EMEC), development of efficiency optimization for these actuators forms an integral part of any sustainable energy policy. The following items can be addressed among the various issues facing the adjustable speed electric drive systems:

- Low efficiency
- Vulnerability to various types of fault
- Lack of service during faults
- Poor energy conversion ratio (i.e. torque/amp)
- High levels of tangential and radial vibration

Over the past decades there have been numerous attempts for resolving these challenges. It is also important to note that in some cases solving a problem has resulted in counter effects on other performance indices of the EMEC. This dissertation investigates a new approach to solving these problems. It presents a design and analysis technique according to the required target specification for each system.

The PMSM has a multiphase stator whose electrical frequency is an integer multiple of the rotor speed. The difference between PMSM and conventional synchronous machine is the use of permanent magnets instead of field winding on the rotor and hence the absence of any rotor conductors as shown in figure 1.1. Permanent magnets increase the overall efficiency by eliminating the need for slip rings, need for magnetizing power and rotor copper losses. In addition, with the introduction of low cost of permanent magnets, this arrangement proves to be an efficient and affordable solution. Based on the way magnets are installed on the rotor, the PMSM can be classified into the following categories:

- Surface mount PMSM (SPMSM)
- Interior PMSM (IPMSM)

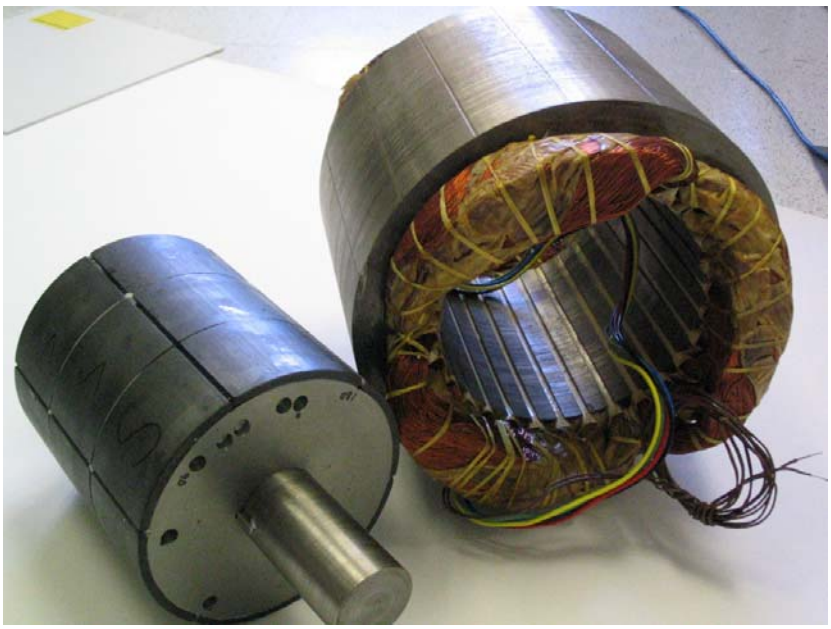

Figure 1.1: Stator and rotor laminations for 5-phase machine

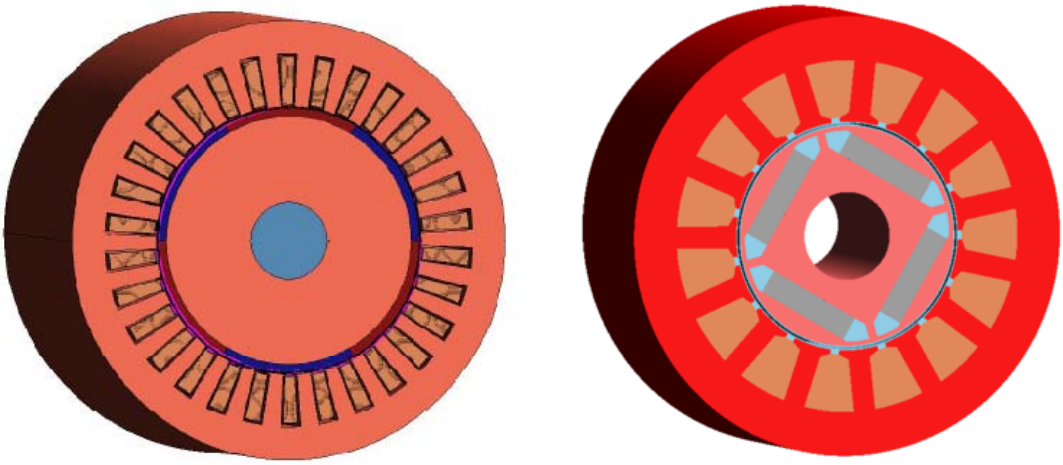

(a) (b)

Figure 1.2: The PMSM types (a) Surface Mount PMSM (b) Interior PMSM (Courtesy of infolytica)

The permanent magnets in SPMSM are mounted on the outer cylindrical surface of the rotor core. The interaction of the magnetic fields of the rotor and stator generates the torque in this machine. The interior permanent magnet synchronous machine (IPMSM) is developed by embedding the permanent magnets in the rotor structure. This leads to the magnetic saliency in the rotor, so IPMSM benefits the reaction torque as well as the reluctance torque. Figure 1.2 depicts the varoius types of the PMSM. The PMSM under study is a surface mount permanent magnet with wide magnet pole-arcs, although interior permanent magnet mounting has gained vast popularity in the recent past as well. The following subsections describe various components of the machine and provide an in-depth description of the materials chosen.

1.1.1. Rotor and Stator Laminations

The main disadvantage of the surface mount PMSM is the flow of eddy current on the surface of the rotor (the surface of the magnets are covered by a layer of metal containers to guarantee that the magnets will not fly out due to the centrifugal forces). Alloys of steel and carbon with small quantities of silicon, has higher volume resistivity, which helps to reduce eddy

current losses in the core. Silicon steels are the most popular material used to design laminations for all families of electric machines where the additional cost is justified by the increased performance. These steels are available in different grades and thicknesses.

Silicon steels are generally specified and selected on the basis of allowable core loss in watts/lb. The grades are classified in an increasing order of core loss, by numbers with a prefix 'M'; i.e. M19, M27, M36, M45 and so on, where each grade specifying a maximum core loss. Higher M numbers (and thus higher core losses) are significantly cheaper, although only a small percentage of power is saved with each step down in performance. M19 is probably the most common grade of steel used for electromechanical energy conversion devices, as it offers nearly the lowest core loss in this class of material, for a fraction of additional cost.

1.1.2. Permanent Magnet

The Permanent Magnet (PM) is a unique component in the energy conversion process. Potential energy is stored both in the magnet volume and in the external field associated with the magnet. They often operate over a dynamic cycle where energy is converted from electrical or mechanical form to field energy and then returned to the original form. A PM is characterized and compared in terms of its composition and defined unit properties obtained from the hysteresis loop of the magnet material.

The earliest manufactured magnet materials were made of hardened steel since magnets made from steel were easily magnetized. However, they had an inherent disadvantage of having very low energy and being easy to demagnetize. In recent years other magnet materials such as Aluminum Nickel and Cobalt alloys (ALNICO), Strontium Ferrite or Barium Ferrite (Ferrite), Samarium Cobalt (First generation rare earth magnet) (SmCo) and Neodymium Iron-Boron (Second generation rare earth magnet) (NdFeB) have been developed for this purpose. The frest of this section gives a brief description of the different magnet materials commonly used [1].

- Ceramic of Ferrite magnets are made of a composite of iron oxide and barium carbonate ($BaCO_3$) or strontium carbonate ($SrCO_3$). This material has been widely available since the 1950's and therefore is readily available. A commonly used type of ceramic magnet is a sintered magnet which is composed of compressed powder of alloy material being used. The magnets are hard & brittle and generally require diamond wheels to grind & shape. While these magnets are solid, their physical properties are similar to a ceramic and are therefore easily broken and chipped. Benefits of ceramic magnets include low cost, high coercive force, resistance to corrosion, and high heat tolerance. Drawbacks include low energy product (their strength), low mechanical strength, and the presence of ferrite powder on the surface of the material which tends to rub off and cause soiling.
- Alnico magnet is an alloy of aluminum (Al), nickel (Ni) and cobalt (Co) with little amounts of other elements added to enhance the properties of the magnet. These magnets have high corrosion resistance, high mechanical strength and very high working temperatures. Their drawbacks include higher cost, low coercive force, low energy product and their tendency to demagnetize due to shocks.
- Rare earth magnets are composed of alloys of Lanthanide group of elements. Neodymium (Nd) and Samarium (Sm) are two most commonly used elements for this family of magnets. The most popular varieties that are currently in use include neodymium-iron-boron ($Nd_2Fe_{14}B$, sometimes referred to as NdFeB) and samarium-cobalt ($SmCo_5$, Sm_2Co_{17}).

Samarium Cobalt (SmCo) magnets are highly resistant to oxidation, particularly resistant to temperature (upto 350° C), have higher magnetic strength than ceramic & alnico but are brittle and prone to chipping & cracking. In addition, due to the high cost of samarium, they are comparably very expensive. Neodymium-Iron-Boron (NdFeB) magnets are the most advanced and most popular permanent magnet available today. This material has properties similar to samarium-cobalt magnets, but is easily oxidized and doesn't have the same resistance to temperature. They have a strong residual field, moderate temperature stability, a

very high energy product and are more easily shaped. Although NdFeB magnets are more expensive by mass but their high flux density per unit volume (energy product) contribute to a compact design, also making it economical to most applications.

- Polymer based magnets are composed of the above-mentioned materials with various polymers to create a broad range of magnetic materials and mechanical properties. This is done mainly for enhancing material flexibility, shape complexity and direction of magnetic fields. A distinct drawback of this family of magnets is their low energy product.

- Ferrite magnets are very common for lower-performance motors. Both radial and parallel magnetizations are commonly used, depending on application. The particular choice of magnets and other design factors is important, but does not directly influence the basic principles of power converter control. The demagnetization characteristics of various magnets at normal temperature ($20℃$) is shown in figure 1.3 [2].

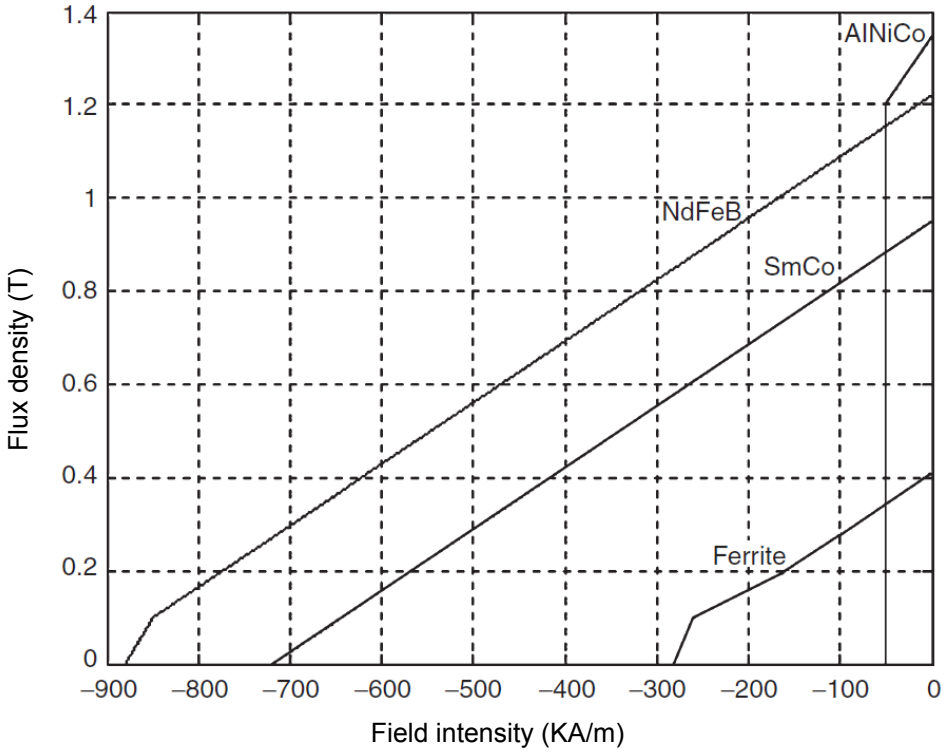

Figure 1.3: Demagnetization characteristics of various permanent magnets

According to this figure the demagnetization curve of a permanent magnet can be fully characterized by the following parameters [2]:

- Remanent Magnetism (B_r) which is where characteristic meets the B-axis.
- Coercive field intensity (H_c) which is where characteristic meets the H-axis.
- Curvature connecting these two points.

In fact, the second linear region that is close to the H-axis is considered as an unstable region. Therefore a proper operating point will be located in the first linear part, which is expressed as:

$$B = B_r + \mu_0 \mu_r H \tag{1.1}$$

Where μ_r and μ_0 stand for relative and air permeability, respectively. It must be noted that in permanent magnets μ_r is very close to 1 (relative permeability of the air). Accordingly, the energy density of a permanent magnet (assuming a linear characteristic) can be computed as:

$$E = B.H \Rightarrow E_{\max} = \frac{B_t^{\,2}}{4\mu_0 \mu_r} (KJ / m^3) \tag{1.2}$$

It must be mentioned that ferrite magnets represent a low-cost solution while offering a limited flux density. AlNiCo magnets, which are more expensive as compared to ferrite magnets, demonstrate a very high remanent magnetism. This, however, is undermined by very limited corecive field intensity. The most expensive, SmCo magnets, represent quality in every aspect including high remanent magnetism, large corecive field intensity, and a fully linear demagnetization characteristic. They also are known as highly stable in the presence of high temperature variation. Finally, the NdFeB magnets demonstrate very high energy density at room temperature. Furthermore, the cost associated with NdFeB is much less than SmCo magnets. However, corecive field intensity in NdFeB magnets is highly sensitive to temperature changes. This, in turn, results in an inadequate performance at high temperatures. In general,

the main objectives in selecting a permanent magnet for motor drive application can be summarized as [2]:

- High energy density.
- A linear demagnetization characteristic in the entire vicinity of the second quadrant (B-H plane).
- High stability with respect to temperature.
- High specific resistance to mitigate eddy currents.
- Durability against corrosion and demagnetization.
- Low cost.

Although achieving all these attributes in a single magnet is not possible, proper design can help us to optimize the performance of the drive in the context of the application. The magnetic characteristics of various magnets are summarized in table 1.1 [2].

Table 1.1 Permanent magnet characteristics

	ferrite	AlNiCo	SmCo5	NdFeB
Remanent magnetism ($B_r(T)$)	0.38 … 0.42	0.61 … 1.35	0.85 … 1.0	1.0 … 1.23
Corecive field intensity (H_c (KA/m))	390 … 280	59 … 50	1000 … 1200	1600 … 960
Max. energy density (BHmax [kJ/m3])	28 … 34	13 … 62	140 … 200	195 … 280
Temperature coefficient (KB[%/C])	–0.2 … –0.23	–0.02	–0.04 … –0.05	–0.11 … –0.13
Temperature coefficient (KH[%/C])	0.4 … 0.22	0.03 … –0.07	-0.25	–0.6 … –0.8
Reversible permeability (μrev)	1.05	<5	1.05	<1.2
Density [ρ/(kg/dm3)]	4.6 … 4.9	6.7 … 7.3	8.1 … 8.3	7.3 … 7.4
Specific electric resistance [ρCL/μΩcm]	10^{12} ... 10^{16}	40 … 70	50 … 60	140
Cost [%]	10 … 15	40 … 60	600 … 800	200 … 300

Comparing various properties of permanent magnets, the following observation can be made [2]:

- A rise in temperature will reduce the remanent magnetism in all magnet types. On a percentage basis, ferrite magnets seem to be the most sensitive magnets, while SmCo demonstrates the least sensitivity.
- Corecive field intensity portrays different behavior for various materials. While an increase in temperature results in significant decrease of corecive field in NdFeB, an opposite response is seen in ferrite magnets. Overall, SmCo offers the least sensitivity to temperature.
- SmCo is the heaviest and the most expensive alternative among all candidates. It also presents one of the lowest specific resistances, which translates to high eddy current losses.
- AlNiCo offers the highest remanent magnetism. This, however, is mainly undermined by a very limited corecive field intensity and extremely high conductivity.
- The reversible permeability in most cases is close to 1.

1.2 Fault tolerant operation of PMSM

Fault tolerance has become a design criterion for adjustable speed motor drives (ASMD) which are used in high impact applications. Fault tolerant motor drives are highly demanded in many sectors of industry including automotive, aerospace and military and domestic applications. In simple terms, a fault tolerant ASMD is expected to continue its intended function in the event of a failure compliment to its remaining components. Knowledge of magnetic field distribution in electrical machines especially the PMSM has shown to give an in-depth understanding of machine behavior in terms of force distribution and optimal excitation determination in various parts of the machine. Based on that, the availability of improved computational tools to analyze the magnetic field is of great importance. Employment of

microscopic electromechanical energy conversion scheme can be employed to give us the following benefits:

- Fault tolerant design.
- Optimal excitation for maximum energy conversion ratio (torque/Amp).
- Reduction of the torque ripple so the acoustic noise.
- Improvement in efficiency.

From an engineering point of view there is a trade off between the following goals, so depending on the application, some of these items can be of more importance in the design process. The main purpose of this project is fault tolerance design while the other factors are sought as much as possible. Fault tolerant operation of an electric drive is a prime objective in high impact applications. By manipulating the tangential and normal components of magnetic field in various parts of the machine, the flux can be observed and used to detect the fault condition. The proposed method offers new numerical techniques for analysis and design of a PMSM. These techniques are time efficient and offer an insightful version of the magnetic field in the machine. Target applications for this technique include the following areas:

- Automotive
- Domestic appliances
- Naval and Military
- Aerospace systems.

The proposed scheme would combine ideas from electromechanical energy conversion, signal reconstruction, pattern recognition, and power electronics to create novel solutions. The successful completion of this target would pave the road for development of cost effective, highly efficient, fault tolerant, and reliable electric motor drive. The most eminent attributes of this approach are:

- The magnetic filed components have been investigated in various parts of the machine.
- The fault detection scheme is based on the flux observation in the machine structure.

- The optimal excitation of the machine has been derived based on the same knowledge of the field distribution.

1.3 State-of-the-Art

The ongoing challenges in the design and control of fault tolerant electric drives have been the focus of many researches [3-8]. However improvements in these areas have been incremental. Most of the work which is done focuses on the fault tolerant design of the electrical machine [9-17]. A multi phase drive, in which each phase is regarded as a single module is the best design for this purpose. These modules should have the minimal impact on each other so that the failure in one does not affect the others. The modular approach requires:

- Minimal electrical interaction: separate single phase bridges can be used for this purpose [18].
- Minimal magnetic interaction: In case of the magnetic coupling between the phases fault current in one can induce voltages in the other which causes problems especially in the control process [19].
- Minimal thermal interaction: The stator outer surface should be cooled down properly. Also each stator slot shoul dbe used for one phase winding to separate the thermal coupling between phases.

Although effective, these techniques are not appropriate in case the design of the machine is not flexible. Principles of a fault tolerant system have been presented in [20]. For an electric drive the fault tolerance necessitates the following:

- Partitioning and redundancy
- Isolation between modules
- Fault detection and reporting
- Service continuity, Online repair

The fault tolerant design has its own disadvantages which can be caused by the unusual design or the introduction of the redundancy. Fault tolerance has been achieved in [17] by deploying a dual motor drive configuration. Same method has been used in [21, 22] to obtain fault tolerance. The disadvantage of this method is that another module of the same size and price of the main module should be used which increases the cost of the system. Also, the control strategy would be more complicated in this case. In some applications the weight and size of the electrical drive is also a restriction so the dual modular system will be inappropriate. The above mentioned methods generally deal with the fault tolerant design of the machine and increasing the redundancy of the system under operation. There are cases in which the design of the machine is not possible and due to the limitations in space and cost, deploying a secondary back up module is not feasible. In this case the system should be able to detect the fault and remove it before the remaining healthy parts are damaged. So, there should be detection schemes that constantly monitor the machine. Also, to guarantee the continous service there should be schemes to squeeze the maximum power possible out of the machine. The fault detection schemes can be classified into following:

- flux based [23, 24]
- current based [25]

In these methods the magnetic flux or the stator currents of the PMSM are monitored during operation. By performing mathematical analysis, such as FFT, Hilbert transform, etc [23, 24], specific signatures can be detected for each type of fault.

Optimal excitation of the electrical machines has been considered as a useful tool to improve the overall efficiency of the system [26]. In order to introduce the required redundancy the sizing of the semiconductors should be judiciously increased. This in turn results in more silicon and higher expense. Alternatively, the excitation of the machine can be modified in a way that yields the optimal output of interest. In this study the maximum torque per ampere is of primary interest. Therefore the target is to find the optimal stator excitation, in the event of a

fault, such that the post fault torque per ampere of the machine would be maximized. Our study uses Maxwell stress tensor method to analyze the torque behavior in normal and post fault operation. This method provides a detailed and insightful picture of the electromechanical energy conversion by providing a detailed description of the magnetic field and force distribution. Figure 1.4 summarizes the fault tolerant schemes.

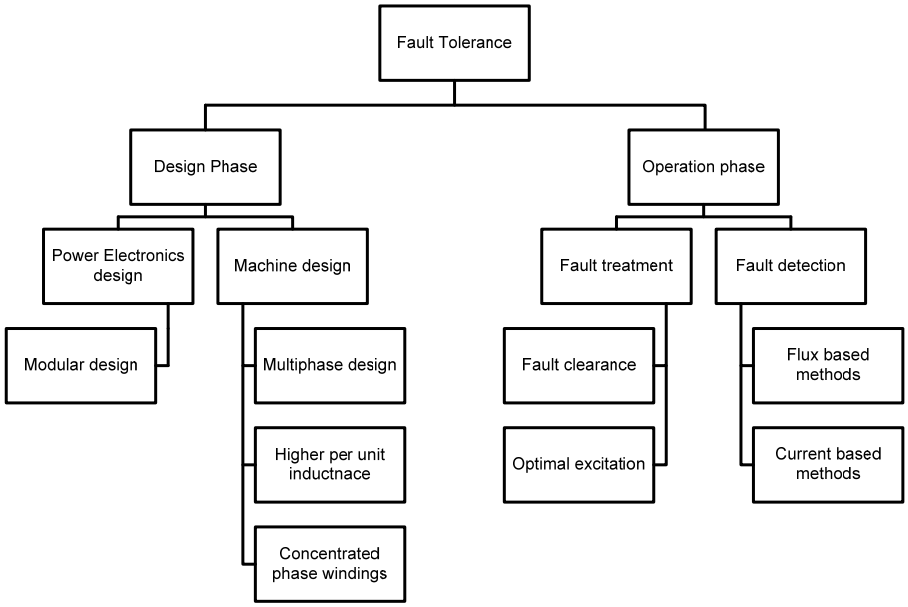

Figure 1.4: Fault tolerance summary

As mentioned before an important feature of a fault tolerant system is the ability to detect the fault and then to clear it. Flux based method, as an option for fault detection, has been used in [23, 24] to detect the inter turn short circuits inside the machine windings. In this case a set of search coils are mounted inside the machine and by monitoring the flux pattern the fault can be identified. An alternative to the search coils is to find a way to calculate flux in different parts of the machine. This will eliminate the costly and sometimes impossible burden of search coils.

Finite element Analysis has been used as a powerful tool to determine the magnetic field distribution. As the finite element procedures are tedious these methods are not applicable to all applications like real time control. Field reconstruction method is developed and

implemented to improve the process of finding magnetic field components in the electrical machines [27-30]. Field reconstruction method provides insight to microscopic electromechanical energy conversion and can be used as an alternative to FEA to analyze magnetic field distribution. Figure 1.5 illustrates some of the impacts of microscopic electromechanical energy conversion on the state of knowledge and performance.

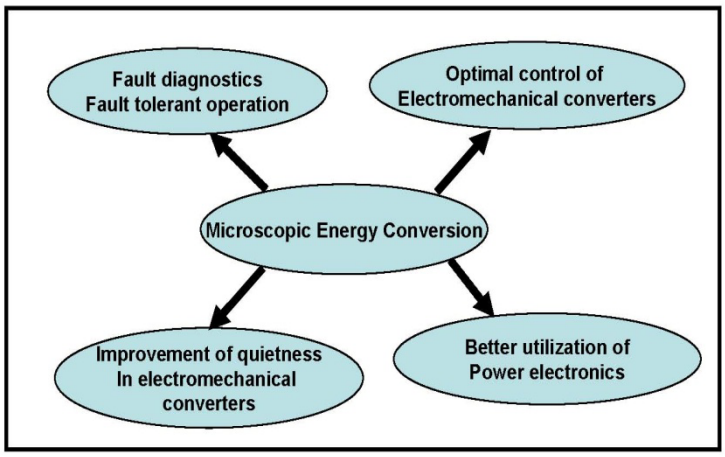

Figure 1.5: Contribution of microscopic electromechanical energy conversion to various issues in EMEC

1.4 Objectives of the Study

In this section the various tasks and objectives including the modeling of PMSM, fault detection, fault treatment and experimentation are presented.

1.4.1 Conceptualization, Design and Development of the PMSM

To validate the proposed scheme, the model of the PMSM machine should be designed using a valid model generation tool. To facilitate this process, a motor drive test bed has been designed and simulated using MAGNET software. Figure 1.5 shows the finite element model of the 5-phase, 6-pole motor that was developed and used in this research. Noteably,the size of the mesh influences the precision and computational time by a great extent.Force calculation is a post-process step, which is directly affected by field distribution calculated by

FEA. As the size of the mesh, its uniformity and aspect ratio needs to be taken into account for better accuracy the construction of the mesh has been modified as shown in Figure 1.6. Keeping the above-mentioned points in mind, a 6-pole 5-phase PMSM was modeled in 2 dimensional FEA as shown in figure 1.6a. The mesh formation in the area of interest is shown in figure 1.6b.

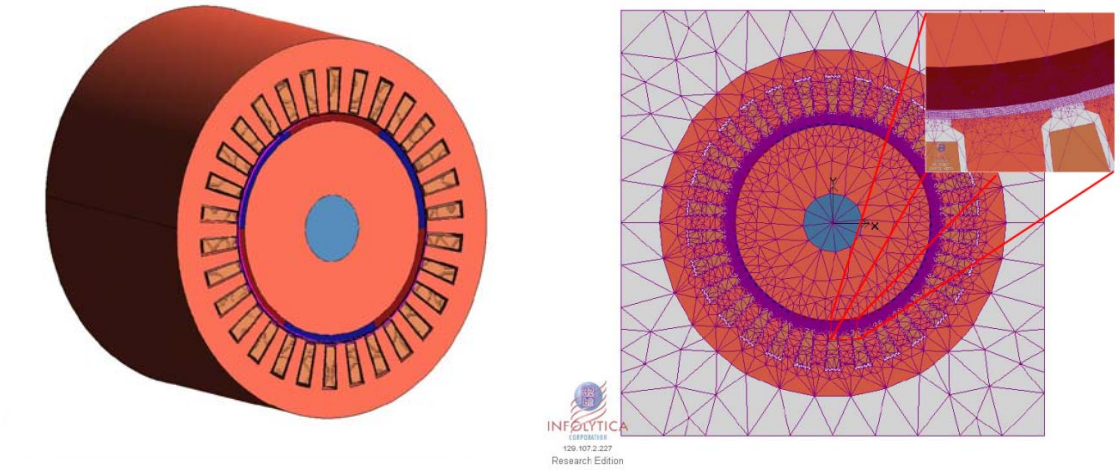

(a) (b)

Figure 1.6: The PMSM model (a) Finite element model of a surface mount 6-pole 5-phase PMSM (b) Meshing pattern in the model for enhanced accuracy

1.4.2 Development of a field reconstruction method

The field reconstruction method has been used to develop a precise magnetic model of the PMSM. The spatial distribution of the magnetic field in the airgap of an EMEC is influenced by geometry and external excitation. Access to local distribution of the magnetic field and understanding the relationship between generation of forces and geometry/excitation is of great importance. Field reconstruction method can provide accurate microscopic details of the magnetic field in a computationally efficient manner. It is much faster than the FEA methods while providing the same level of accuracy. The field reconstruction can be used to observe the magnetic flux as well as the calculation of optimal excitation in case of a fault.

1.4.3 Development of fault detection and optimization strategies

The fault tolerant system should be capable of fault detection and remediation. Also, it is desirable that the PMSM delivers maximum torque per ampere in the event of a fault. A set of look up tables can be created for each kind of fault and by monitoring the flux the type of fault can be detected. Also, based on the type of fault that happens and the place of occurrence the optimal excitation should be deployed to improve the machine performance.

1.4.4 Development of an experimental test bed

The conventional PMSM can become fault tolerant using the proposed method. For the validation of the proposed scheme, an experimental PMSM drive was designed and constructed at the Renewable Energy and Vehicular Technology Lab. This experimental system is used for validation of the flux estimation as well as the optimized fault tolerant performance using field reconstruction method. Fault detection and removal and optimization of the remaining healthy machine phase excitations are the main objectives in this experimental investigation.

1.5 Outline of the dissertation

The state-of-the-art investigation, problem identification, modeling, detection and treatment of fault tolerant PMSM are presented here. This dissertation includes 5 chapters whose outline is as follows:

Chapter 2 describes the fundamentals of the field reconstruction method. In this chapter the FRM is developed and implemented for the PMSM. To validate this model a finite element model is also created for comparison purposes. Maxwell Stress Tensor method is used to quantify electromagnetic torque in the middle of the airgap.

Chapter 3 deals with the mehtods of flux estimation in permanent magnet synchronous machines. The traditional flux estimation technique is discussed and the novel methods will be introduced in detail. These novel methods are supported by experimental and simulation results.

Chapter 4 introduces various faults under study, detection schemes and optimization strategies. The stator inter turn short circuit fault on single or multiple phases, rotor partial demagnetization and rotor eccentricity are investigated in this chapter. The experimental setup is used to support the theory and simulations.

Chapter 5 summarizes the achievements of this study and provides concluding comments on the findings.

CHAPTER 2

FIELD RECONSTRUCTION METHOD

Electromechanical energy conversion in energy conversion devices occurs in terms of magnetic fields from the media within which the electromechanical energy conversion takes place. Magnetic fields provide a controllable means within a relatively compact and highly efficient environment for energy conversion. Once the electromechanical energy converter is supplied with electric current, a magnetic field throuout the device is established. Using Maxwell stress tensor method, distribution of the radial and tangential force densities in the airgap of the machine can be expressed as:

$$f_n = \frac{1}{2\mu_0}(B_n{}^2 - B_t{}^2) \tag{2.1}$$

$$f_t = \frac{1}{\mu_0}(B_n B_t) \tag{2.2}$$

Where $f_n, f_t, B_n, B_t,$ and μ_0 denote normal and tangential component of the force density in the airgap, normal component of flux density, tangential component of flux density, and air magnetic permeability respectively. Tangential forces are partially responsible for the generation of torque on the rotor and tangential vibration of the stator frame. The tangential forces that are produced on the stator poles cause unwanted vibration in the stator frame. The resultant forces acting on the machine components can be determined by integrating the tangential and radial force densities on the surface of the desired component as follows:

$$F_t = \oint_S \vec{f}_t . ds \tag{2.3}$$

$$F_n = l \int_0^{2\pi} r f_n d\phi_s \tag{2.4}$$

Where s denotes the outer surface of a cylinder located in the airgap of the machine and $l, r, \text{and } \phi_s$ denote stack length, radius of the integrating contour, and angle component in cylindrical system of coordinates respectively.

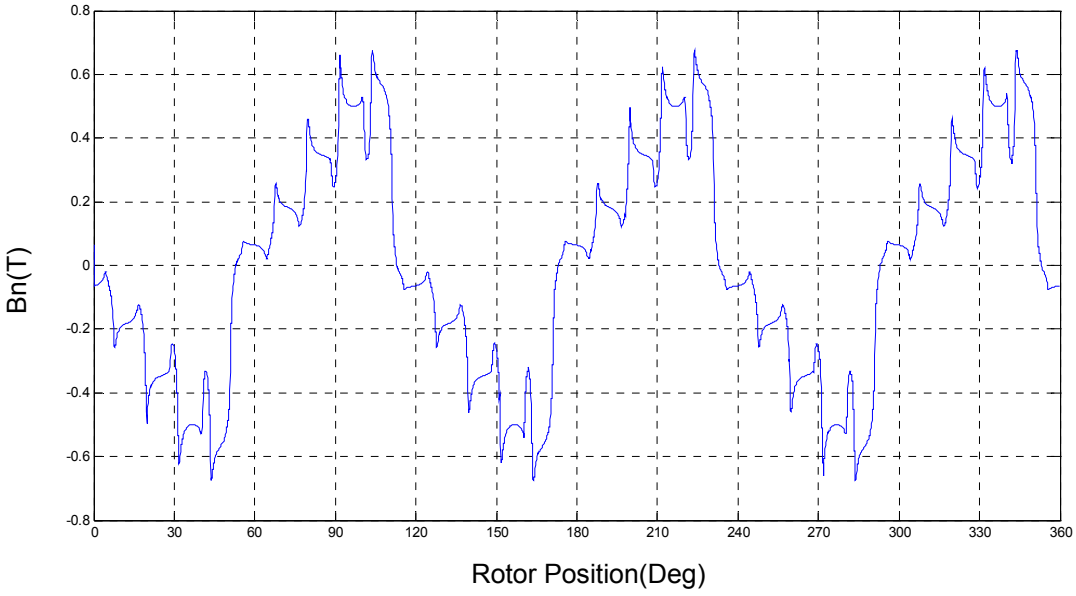

(a)

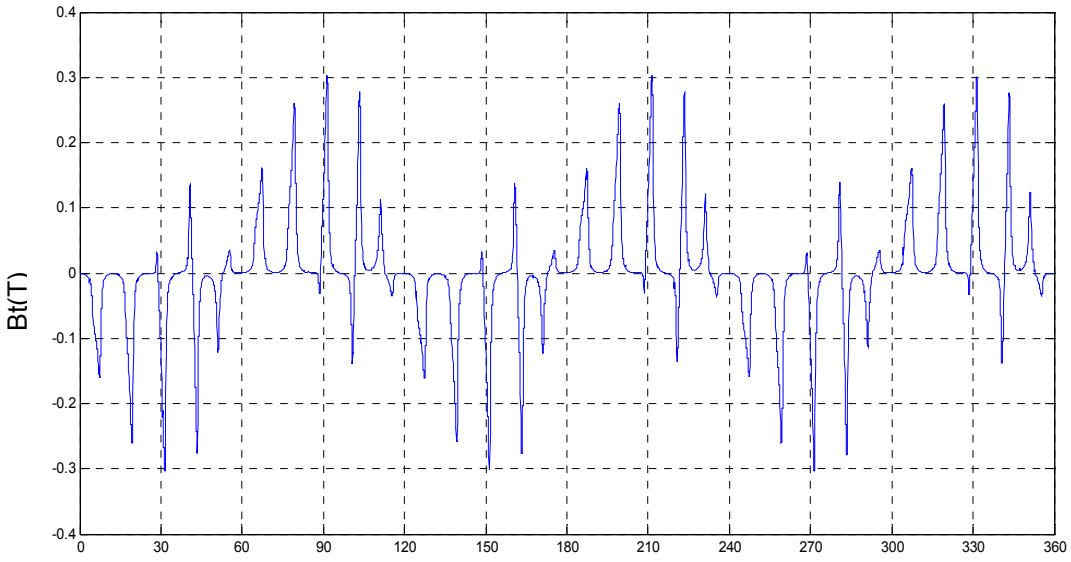

(b)

Figure 2.1: magnetic flux density in the middle of the airgap (a) Normal component (b) Tangential component

Tangential component of the force acting on the rotor is viewed as the main product of the electromechanical energy conversion process. In fact the electromagnetic torque can be expressed as:

$$T = \oint_S (\vec{r} \times \vec{f}_t).\vec{ds} \tag{2.5}$$

In (2.5), $\vec{r}$ represents a radial vector connecting the center of the rotor to an arbitrary point on the surface of integration. Figure 2.1 shows the distribution of tangential and normal components of the flux density in a PMSM. These results are obtained using a 2-dimensional transient finite element analysis (FEA).

Although FEA can be used for computation of local distribution of normal and tangential flux densities, the computational cost for iterative design procedures is very high. Moreover, lack of analytical expressions for the field components may limit one's ability to optimize the machine performance. In the next section the field reconstruction method has been introduced to address the above problems.

2.1 Development of Field Reconstruction Method

Field reconstruction method is developed to address computational time associated with FEA. This method forms the foundation for our microscopic electromechanical energy conversion technique, which is entirely based on computation and design of field components in a microscopic scale. In order to explain the idea the following assumptions are made:

- The nonlinear effects of the saturation are neglected.
- The impact of eddy currents is negligible.
- Rotor of the EMEC comprises of surface mount magnets with a uniform magnetization.
- The effect of stator end coils is neglegted.

The target EMEC for this dissertation is a 5-phase, 6-pole, surface mount, permanent magnet synchronous machine. The FEA model created for this machine is shown in figure 1.2. This FEA model is used for verification purposes. Table 2.1 depicts the characteristics of the

permanent magnet machine. Figure 2.2 shows the cross section of this machine that has been cut and rolled along the neutral axis of a pair of rotor poles.

Table 2.1 Target PMSM characteristics

Rated Power	10 hp
Number of Phases	5
Rated Speed	1800 rpm
Number of Poles	6
Number of Stator Slots	30
Stator Winding Material	Copper
Stator back iron Material	M19
Type of Permanent magnets	Surface Mount
Rotor Material	M19
Shaft Material	Cold rolled Steel
Stack length	6 in.

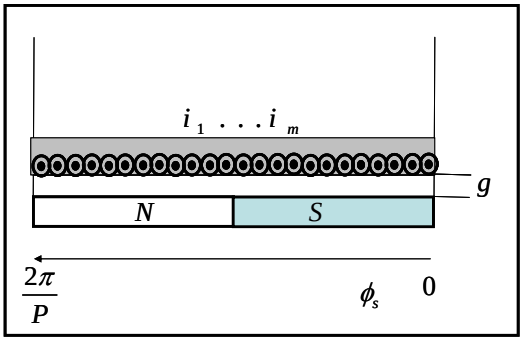

Figure 2.2: Cross section of the slot-less PM machine

In Figure 2.2, ϕ_s represents the displacement for any point on the stator and $i_1 \ldots . i_m$ represent the current in each conductor. In this configuration, the normal and tangential components of the flux density due to surface mounted permanent magnets are defined as $B_{n,pm}$ and $B_{t,pm}$ respectively. Each conductor on the stator contributes to the tangential and radial components of the flux density in the airgap. The tangential and normal components of the flux density that are contributed by a conductor (representing the k^{th} phase) located at ϕ_{sk} are given as follows:

$$B_{t,k} = B_t(i_k)h_t(\phi_s - \phi_{sk}) \qquad 0 < \phi_s < \frac{2\pi}{P}$$
$$B_{n,k} = B_n(i_k)h_n(\phi_s - \phi_{sk}) \tag{2.6}$$

Where $P, B_t, B_n, h_t, \text{and } h_n$ denote number of magnetic pole pairs, scaling function representing the dependency of the tangential and radial flux densities upon the current magnitude and impact of the geometry (for one conductor) respectively and ϕ_{sk} represents the location of the k^{th} conductor, carrying the current magnitude of i_k. Figure 2.3 illustrates the variation of the tangential and normal components of the flux density as a function of the current magnitude and displacement. It can be seen that the flux density is directly proportional to the current magnitude. Also, the flux due to the neighboring slots is a shifted version of the main component.

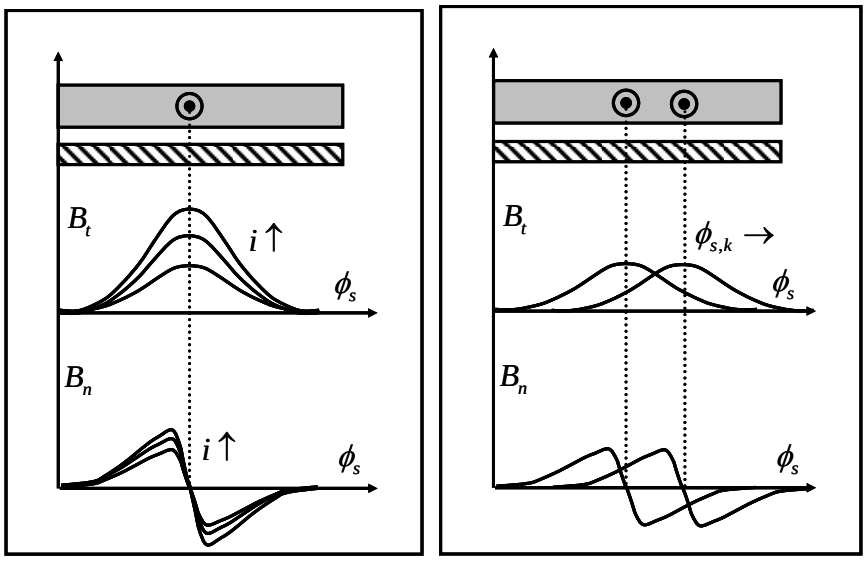

Figure 2.3: Variation of the tangential and normal components of the flux density as a function of the current magnitude and location of the conductor

Assuming superposition, the resultant tangential and normal components of the flux density in the airgap for any given rotor position can be expressed using a truncated generalized Fourier series as:

$$B_t(\phi_s, i_1, ..., i_m) = B_{t,pm} + \sum_{k=1}^{m} B_{t,k}(i_k) h_t(\phi_s - \phi_{sk})$$
$$B_n(\phi_s, i_1, ..., i_m) = B_{n,pm} + \sum_{k=1}^{m} B_{n,k}(i_k) h_n(\phi_s - \phi_{sk}) \quad (2.7)$$

The above expressions depict an elegant illustration of the separation between factors influenced by geometry (i.e. h_t, and h_n) and external excitation (i.e. $B_{t,k}$, and $B_{n,k}$). Accordingly, the tangential and normal components of the force densities can be computed as follows:

$$f_t(\phi_s, i_1, ...i_m) = \frac{1}{\mu_0}\{B_t(\phi_s, i_1, ...i_m) B_n(\phi_s, i_1, ...i_m)\}$$
$$f_n(\phi_s, i_1, ...i_m) = \frac{1}{2\mu_0}\left\{B^2{}_n(\phi_s, i_1, ...i_m) - B^2{}_t(\phi_s, i_1, ...i_m)\right\} \quad (2.8)$$

In order to calculate the resultant forces for each rotor position, one needs to integrate the force densities over the outer surface of a cylinder which is located in the middle of the airgap:

$$F_t(\theta_r) = P.L.R \int_0^{\frac{2\pi}{P}} f_t(\phi_s, i_1, ...i_m) d\phi_s \qquad 0 \le \theta_r \le \frac{2\pi}{P}$$
$$F_n(\theta_r) = P.L.R \int_0^{\frac{2\pi}{P}} f_n(\phi_s, i_1, ...i_m) d\phi_s \quad (2.9)$$

Where θ_r, L, and R represent rotor position, stack length of the machine, and radius of the integration surface respectively. In this computation a two dimensional symmetry in the geometry of the machine is assumed. As can be observed detection of the basis functions h_t, and h_n play a central role in the formulation of the field reconstruction. Under unsaturated conditions the scaling functions representing the external excitation are linear functions of the relevant currents, i.e.:

$$B_{t,k}(i_k) = B_k.i_k$$
$$B_{n,k}(i_k) = B_n.i_k \qquad (2.10)$$

Once the pattern of excitation is known and basis functions are identified, one can use (2.7) through (2.9) to identify the distribution of field/force for a given position. It must be noted that the contribution of the permanent magnets are assumed as a separate input to (2.7). Analysis of an unsaturated slot-less stator with an embedded conductor (figure 2.2) indicates that the basis functions, h_t and h_n have the following properties:

(a) Periodic with respect to ϕ_s ,

(b) h_t has an even symmetry with respect to ϕ_s ,

(c) h_n has an odd symmetry with respect to ϕ_s .

Therefore, without rotor excitation (winding or permanent magnet) the resultant tangential force will be an odd function resulting in zero average torque at every given point. However, the radial forces will exist even without any magnetic source on the rotor. One of the most important tasks of this dissertation will be to identify analytical expressions of the basis functions h_t, and h_n for the 5 phase permanent magnet synchronous machine.

Figure 2.4 shows the process of reconstruction of the flux density due to the permanent magnets and the stator phase winding currents. In this process, as the figure describes, 1A current is first applied to the conductors in a single slot of the machine. The flux density obtained due to this unit current is called the “basis function” for the given geometry. This function should be rotated by 60 degrees and superimposed to achieve the field distribution due to the current in one phase. Further, as the in the balanced 5 phase systems the consecutive phases are 72 degrees apart,this plot is rotated by 72 electrical degrees and superimposed to estimate the effective field due to current in all five phases of the machine. It must be mentioned that the flux from the permanent magnet is unchanged in magnitude. It simply rotates with rotor position.

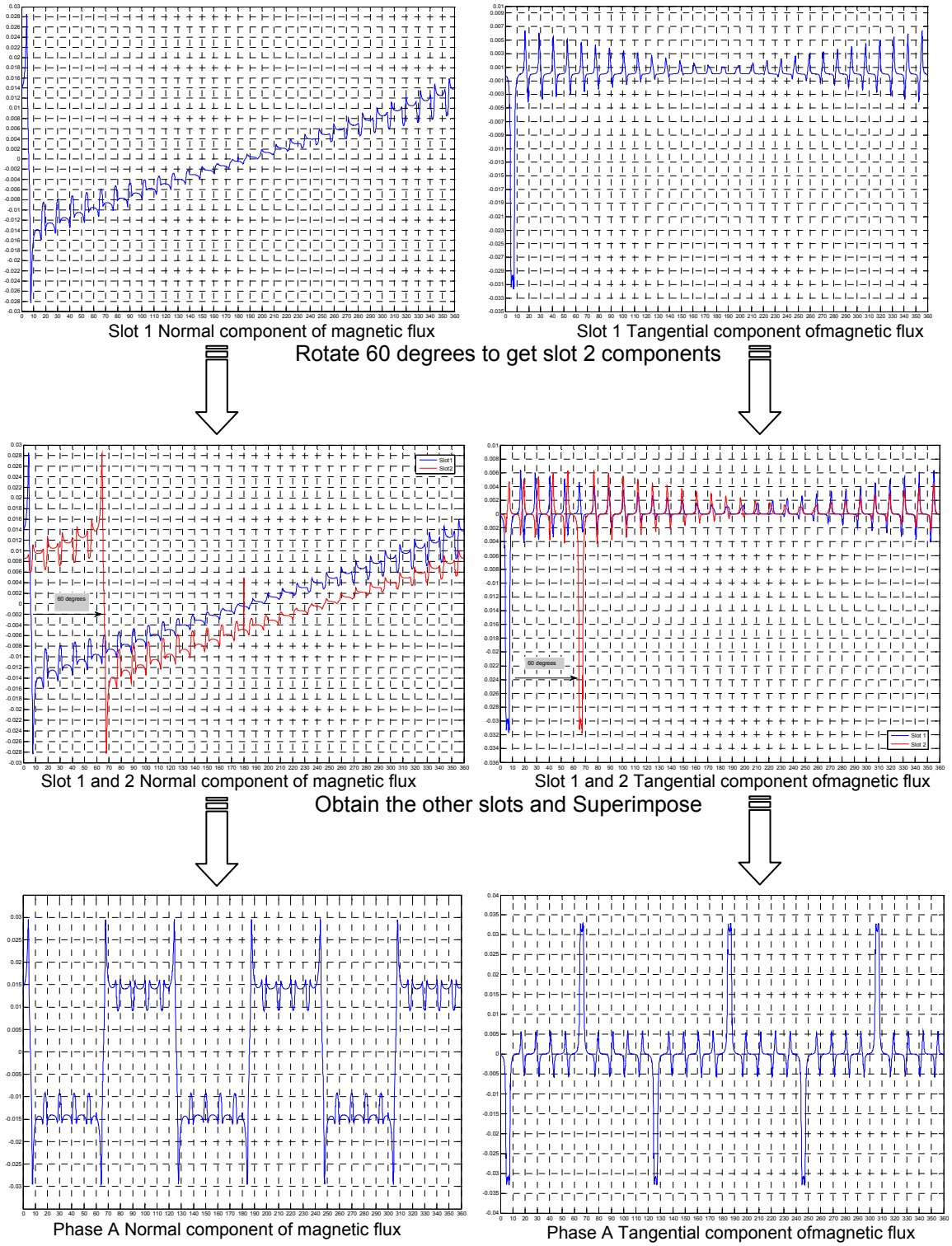

Figure 2.4: Basis functions determination for PMSM

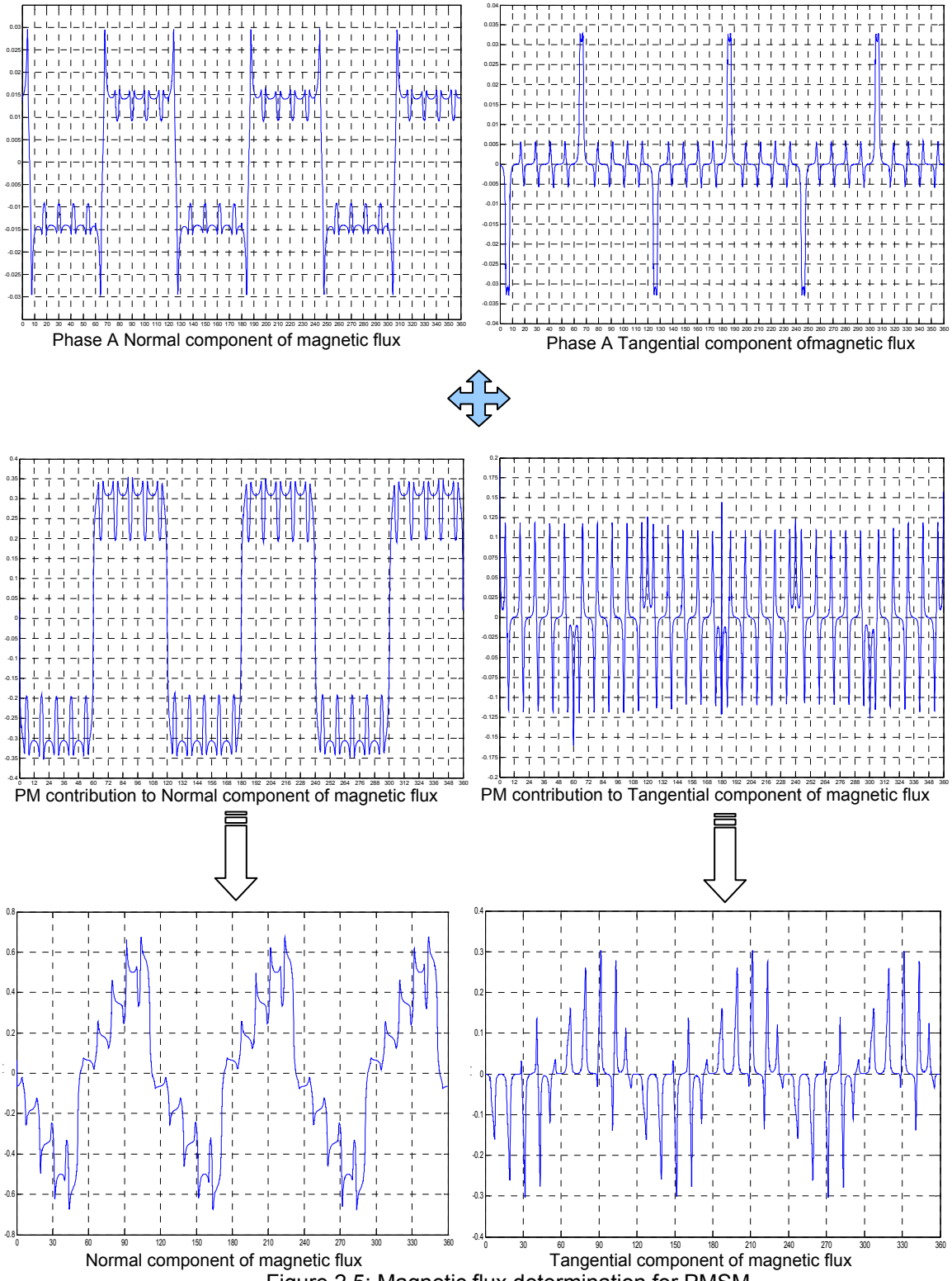

Figure 2.5: Magnetic flux determination for PMSM

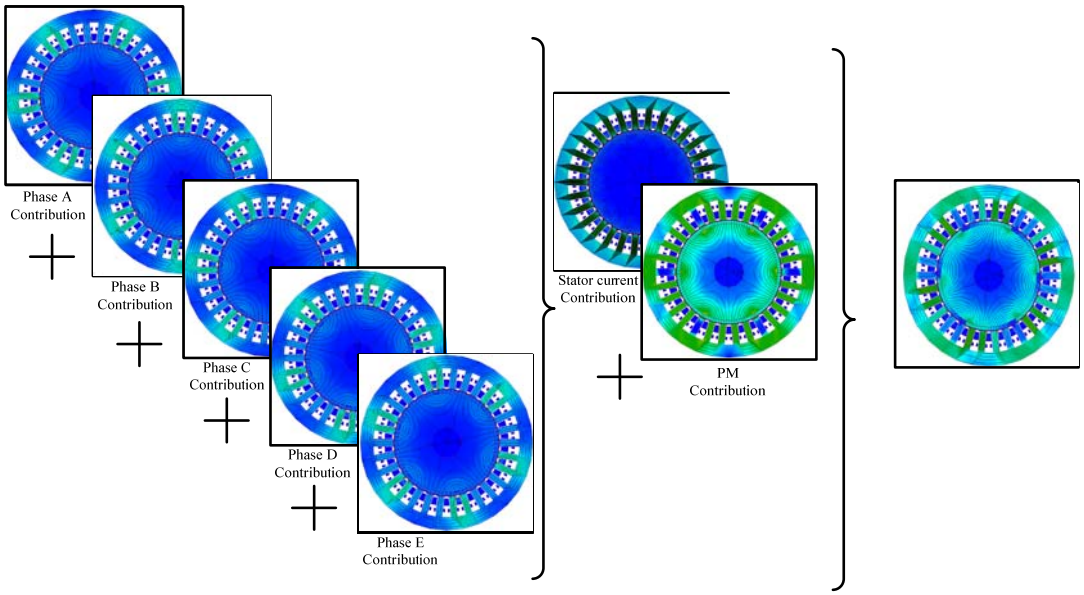

Figure 2.6: Field reconstruction method illustration.

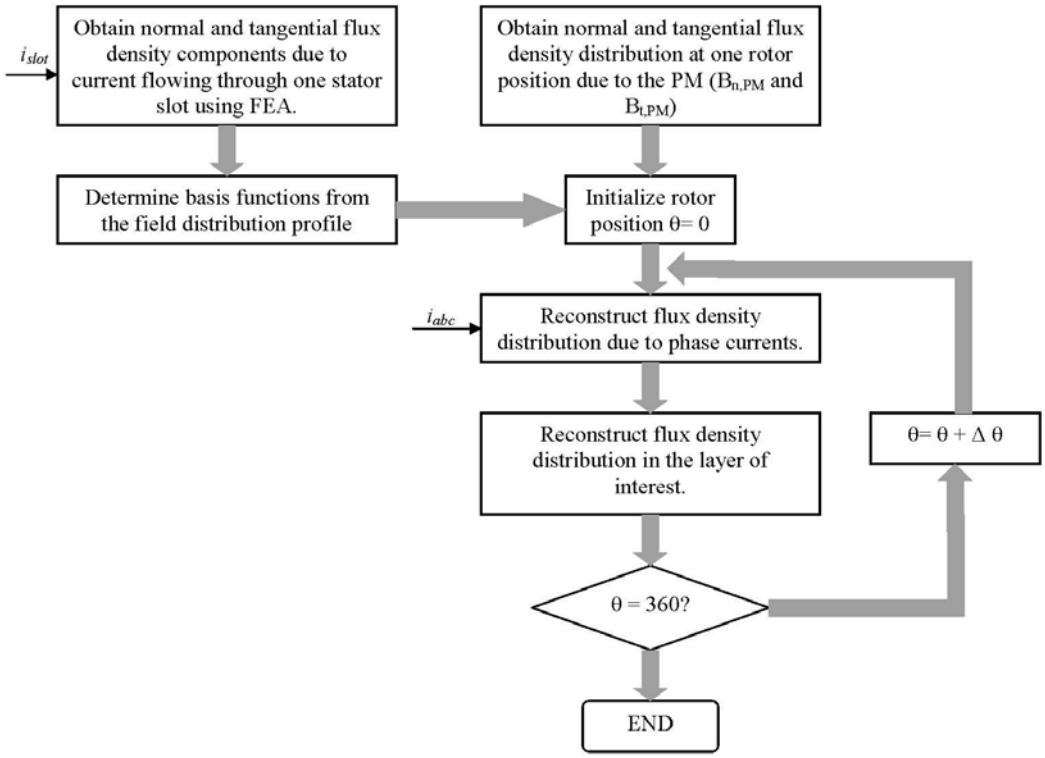

Figure 2.7: Field reconstruction method flowchart

Therefore addition of the fields due to the PM and five phase currents can be used to estimate flux distribution due to any waveform of current applied to the machine. This process is done offline and the basis functions are stored as well as the PM contribution. The basis functions calculation in this way is much faster than the case of the complete system because there is only one source of magneto-motive force (MMF) in the machine during the calculation of basis functions. This proves to be one of the major advantages of field reconstruction method. Also, this method can be applied to any type of stator current and is not just sinusoidal excitation. Figure 2.4 depicts the basis function determination for the 5 phase PM machine under study. These functions are added to the PM contribution to achive the complete system magnetic flux. The field reconstruction method is illustrated in Figures 2.5 and 2.6. According to these figure the stator phase current contribution is calculated first. Then the PM contribution is calculated and added to the stator flux to achieve the magnetic flux distribution of the complete system. The field reconstruction flowchart has been shown in Figure 2.7. In this flowchart the above modeling procedure is explained.

2.2 Voltage Driven FRM for PMSM

The field reconstruction method descibed in section 2.1 attains the distribution of the magnetic field based on the instantaneous value of the phase currents. In some applications, the permanent magnet machine is fed by a voltage source instead of the current source. In that case the field reconstruction method should be modified to account for the voltage driven applications. In order to formulize the voltage driven field reconstruction the characteristic terminal equations of the machine should be investigated.

2.2.1 Electromechanical Description

There are three basic components to be considered in order to fully describe an electromechanical device, the voltage equation, the flux linkage equation and the torque equation. The equivalent circuit of the machine, at standstill, phase winding can be modeled as

a series combination of the coil resistance and inductance of the winding. Figure 2.8 depicts this equivalent circuit.

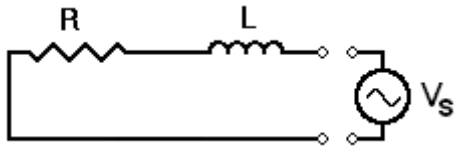

Figure 2.8: Equivalent circuit model for phase winding of the PMSM**.**

According to Faraday's law, the voltage equation of the series circuit is defined as the algebraic sum of the ohmic drop on the resistive element and the rate of change in flux linkage on the inductive component as follows:

$$v_{ks} = Ri_{ks} + \frac{d\lambda_k}{dt} \qquad k = a,b,c,d,e \tag{2.11}$$

In this equation, v_{is} and i_{is} are voltages and currents of the 5 phase stator windings respectively. *r* and λ_i are the stator winding resistance and phase flux linkages. Equation (2.11) can be rewritten and expanded as:

$$\begin{bmatrix} v_{as} \\ v_{bs} \\ v_{cs} \\ v_{ds} \\ v_{es} \end{bmatrix} = \begin{bmatrix} R_s & 0 & 0 & 0 & 0 \\ 0 & R_s & 0 & 0 & 0 \\ 0 & 0 & R_s & 0 & 0 \\ 0 & 0 & 0 & R_s & 0 \\ 0 & 0 & 0 & 0 & R_s \end{bmatrix} \begin{bmatrix} i_{as} \\ i_{bs} \\ i_{cs} \\ i_{ds} \\ i_{es} \end{bmatrix} + \begin{bmatrix} L_s & 0 & 0 & 0 & 0 \\ 0 & L_s & 0 & 0 & 0 \\ 0 & 0 & L_s & 0 & 0 \\ 0 & 0 & 0 & L_s & 0 \\ 0 & 0 & 0 & 0 & L_s \end{bmatrix} \frac{d}{dt} \begin{bmatrix} i_{as} \\ i_{bs} \\ i_{cs} \\ i_{ds} \\ i_{es} \end{bmatrix} \tag{2.12}$$

Including the effect of back motional EMF, equation 2.11 can be modified to express the equation in terms of Ohm's law as in equation 2.13:

$$V_s = Ri + L\frac{di}{dt} + E_b \tag{2.13}$$

Where V_s, *R*, *L*, λ_s and *i* denote phase voltage, winding resistance, phase inductance, flux linkage across each phase and phase current respectively. In this equation, the resistance

of the stator phase winding is a constant. This equation can be extended to represent the five phase machine used in this system as given in equation 2.14.

$$\begin{bmatrix} v_{as} \\ v_{bs} \\ v_{cs} \\ v_{ds} \\ v_{es} \end{bmatrix} = \begin{bmatrix} R_s & 0 & 0 & 0 & 0 \\ 0 & R_s & 0 & 0 & 0 \\ 0 & 0 & R_s & 0 & 0 \\ 0 & 0 & 0 & R_s & 0 \\ 0 & 0 & 0 & 0 & R_s \end{bmatrix} \begin{bmatrix} i_{as} \\ i_{bs} \\ i_{cs} \\ i_{ds} \\ i_{es} \end{bmatrix} + \begin{bmatrix} L_s & 0 & 0 & 0 & 0 \\ 0 & L_s & 0 & 0 & 0 \\ 0 & 0 & L_s & 0 & 0 \\ 0 & 0 & 0 & L_s & 0 \\ 0 & 0 & 0 & 0 & L_s \end{bmatrix} \frac{d}{dt} \begin{bmatrix} i_{as} \\ i_{bs} \\ i_{cs} \\ i_{ds} \\ i_{es} \end{bmatrix} + \begin{bmatrix} e_a \\ e_b \\ e_c \\ e_d \\ e_e \end{bmatrix} \quad (2.14)$$

Where R_s, L_s, e_i denote coil resistance, self inductance of the stator winding and induced motional back EMF in each phase respectively. Based on the notations described in equation 2.12, output mechanical torque generated (i.e. T_e) in a synchronous machine is approximated at a mechanical speed ω_m as given by equation 2.15.

$$T_e = \frac{(v_{as} i_{as} + v_{bs} i_{bs} + v_{cs} i_{cs} + v_{ds} i_{ds} + v_{es} i_{es})}{\omega_m} \quad (2.15)$$

Then, the mechanical equation governing the electromechanical system can be defined as follows:

$$T_e - T_L = J \frac{d\omega}{dt} + B\omega_m \quad (2.16)$$

Where, T_e, T_L, J, ω and B denote electrical torque (generated), mechanical load torque, moment of inertia, speed of the drive and friction respectively. Having the full description of the system, the voltage driven field reconstruction method can be implemented.

2.2.2 Formulation

Considering equation 2.11, the stator phase currents of the machine can be written as follows:

$$i_{ks} = \frac{1}{R_s}(v_{ks} - \frac{d\lambda_k}{dt}) \qquad k = a,b,c,d,e \quad (2.17)$$

For the PMSM under study the input stator phase volatges (v_{ks}) are known. Also, the stator resistances can be measured directly. Having the flux linkages for each stator phase equation 2.17 can be calculated to attain the stator phase currents. These currents can then be fed into the field reconstruction module to achieve the magnetic field distribution. The voltage equations in dq-axes coordinates for a permanent magnet machine can be written as [31]:

$$\begin{cases} v_{qs} = r_s i_{qs} + \omega\lambda_{ds} + p\lambda_{qs} \\ v_{ds} = r_s i_{ds} - \omega\lambda_{qs} + p\lambda_{ds} \\ v_{0s} = r_s i_{0s} + p\lambda_{0s} \end{cases} \tag{2.18}$$

Where r_s and ω are the coil resistance and reference frame speed, respectively. The flux linkages can be written as follows:

$$\begin{cases} \lambda_{qs} = L_{ss} i_{qs} \\ \lambda_{ds} = L_{ss} i_{ds} + \lambda_m^{'} \\ \lambda_{0s} = L_{ls} i_{0s} \end{cases} \qquad L_{ss} = L_{ls} + \frac{3}{2} L_{ms} \tag{2.19}$$

L_{ms} and L_{ls} are magnetizing and leakage inductances, respectively. Using the above equations:

$$\begin{bmatrix} \lambda_{qs}(t_{k+1}) \\ \lambda_{ds}(t_{k+1}) \end{bmatrix} = L_{ss} \begin{bmatrix} i_{qs}(t_{k+1}) \\ i_{ds}(t_{k+1}) \end{bmatrix} + \begin{bmatrix} 0 \\ \lambda_m^{'} \end{bmatrix} \tag{2.20}$$

So:

$$\begin{bmatrix} i_{qs}(t_{k+1}) \\ i_{ds}(t_{k+1}) \end{bmatrix} = \frac{1}{L_{ss}} \left(\begin{bmatrix} \lambda_{qs}(t_{k+1}) \\ \lambda_{ds}(t_{k+1}) \end{bmatrix} - \begin{bmatrix} 0 \\ \lambda_m^{'} \end{bmatrix} \right) \tag{2.21}$$

Equation 2.18 can be rewritten as:

$$\begin{cases} \dfrac{d\lambda_{qs}}{dt} = v_{qs} - r_s i_{qs} - \omega\lambda_{ds} \\ \dfrac{d\lambda_{ds}}{dt} = v_{ds} - r_s i_{ds} + \omega\lambda_{qs} \end{cases} \tag{2.22}$$

So:

$$\begin{cases} \lambda_{qs}(t_{k+1}) - \lambda_{qs}(t_k) = dt \times (v_{qs}(t_{k+1}) - r_s i_{qs}(t_{k+1}) - \omega\lambda_{ds}(t_k)) \\ \lambda_{ds}(t_{k+1}) - \lambda_{ds}(t_k) = dt \times (v_{ds}(t_{k+1}) - r_s i_{ds}(t_{k+1}) + \omega\lambda_{qs}(t_k)) \end{cases} \tag{2.23}$$

Equation 2.23 can be rewritten as:

$$\begin{cases} \lambda_{qs}(t_{k+1}) - \lambda_{qs}(t_k) = dt \times (v_{qs}(t_{k+1}) - \dfrac{r_s}{L_{ss}}\lambda_{qs}(t_{k+1}) - \omega\lambda_{ds}(t_k)) \\ \lambda_{ds}(t_{k+1}) - \lambda_{ds}(t_k) = dt \times (v_{ds}(t_{k+1}) - \dfrac{r_s}{L_{ss}}\lambda_{ds}(t_{k+1}) + \dfrac{r_s}{L_{ss}}\lambda_m^{'} + \omega\lambda_{qs}(t_k)) \end{cases} \tag{2.24}$$

So:

$$\begin{cases} \lambda_{qs}(t_{k+1})(1 + \dfrac{r_s dt}{L_{ss}}) = \lambda_{qs}(t_k) + dt \times (v_{qs}(t_{k+1}) - \omega\lambda_{ds}(t_k)) \\ \lambda_{ds}(t_{k+1})(1 + \dfrac{r_s dt}{L_{ss}}) = \lambda_{ds}(t_k) + dt \times (v_{ds}(t_{k+1}) + \dfrac{r_s}{L_{ss}}\lambda_m^{'} + \omega\lambda_{qs}(t_k)) \end{cases} \tag{2.25}$$

Finally:

$$\begin{cases} \lambda_{qs}(t_{k+1}) = \dfrac{1}{(1 + \dfrac{r_s dt}{L_{ss}})}\{\lambda_{qs}(t_k) + dt \times (v_{qs}(t_{k+1}) - \omega\lambda_{ds}(t_k))\} \\ \lambda_{ds}(t_{k+1}) = \dfrac{1}{(1 + \dfrac{r_s dt}{L_{ss}})}\{\lambda_{ds}(t_k) + dt \times (v_{ds}(t_{k+1}) + \dfrac{r_s}{L_{ss}}\lambda_m^{'} + \omega\lambda_{qs}(t_k))\} \\ \lambda_{0s}(t_{k+1}) = \lambda_{0s}(t_k) + dt \times (v_{0s}(t_{k+1}) - \dfrac{r_s}{L_{ls}}\lambda_{0s}(t_{k+1})) = \dfrac{1}{(1 + \dfrac{r_s dt}{L_{ls}})}\{\lambda_{0s}(t_k) + dt \times (v_{0s}(t_{k+1}))\} \end{cases} \tag{2.26}$$

Using equation 2.26, the flux linkages of each phase can be determined in terms of stator applied voltage. The flux linkages then will be used to derive current values using equation 2.17.

2.3 Comparison of Finite Element and Field Reconstruction

In order to validate the PMSM model the finite element analysis has been compared with the field reconstruction method in this section. This comparison includes the accuracy of the method and the time required to perform the analysis.

2.3.1 Accuracy

As stated before, field reconstruction method is developed as a replacement tool for magnetic field analysis. Finite element analysis (FEA) which is the most popular method of magnetic field analysis is chosen as a reference for comparison purposes. Figure 2.9 depicts the normal and tangential components of magnetic flux density calculated using field reconstruction method compared with those obtained using the finite element analysis. In this case the balanced sinusoidal currents have been applied to stator phase windings and motor is rotating at a constant speed. According to these figures the magnetic flux densities calculated using field reconstruction method fits properly to those of the finite element analysis. This accuracy can be even better in case the mesh used to calculate the basis functions would be of higher density. As the basis function derivation is a single magneto-static analysis, using a more dense mesh would not significantly increase the computational time necessary for field reconstruction. Having these magnetic flux densities and using Maxwell Stress Tensor (MST) method the electrical torque generated can be calculated. The torque calculated from FRM is compared wth that of the FEA as shown in Figure 2.10. The back emf of the machine measured from the experimental set up is compared to that of the field reconstruction as shown in Figure 2.11.

(a)

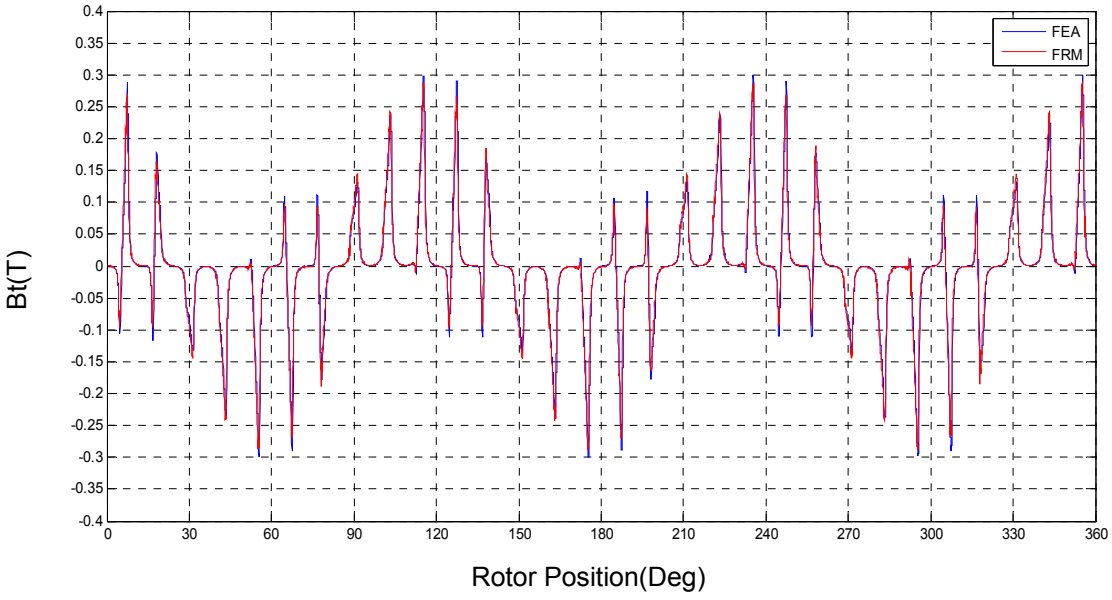

(b)

Figure 2.9: Magetic flux density, FEA vs FRM, (a) Normal component (b) tangential component.

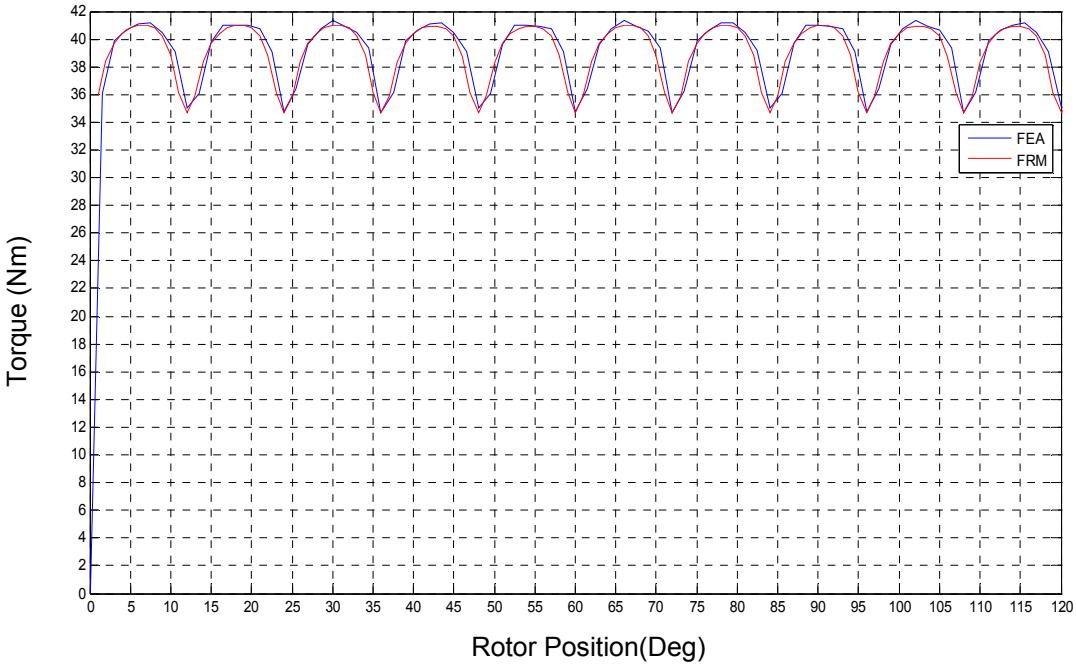

Figure 2.10: FEA and FRM torque comparison

2.3.2 Computational time

The main contribution of the field reconstruction method is the computational time which is much shorter than the conventional finite element procedures. This property makes FRM suitable for real time control applications. Besides, the shorter computational time translates into less computational costs from an economical point of view. The method has been tested on a Pentium 5, 3 GHz processor for simulation purposes. The analysis using FRM takes 30 seconds while the same analysis using FEA takes 8 hours. So, FRM provides accurate enough results while the computation time is much shorter than the FEA.

Another method ofcomputational time investigation is to implement the process on a DSP. The target device for this purpose is TMS 320F2812 dsp board. The finite element analysis can not be implemented on this DSP because of the limitations on the storage and ALU units.

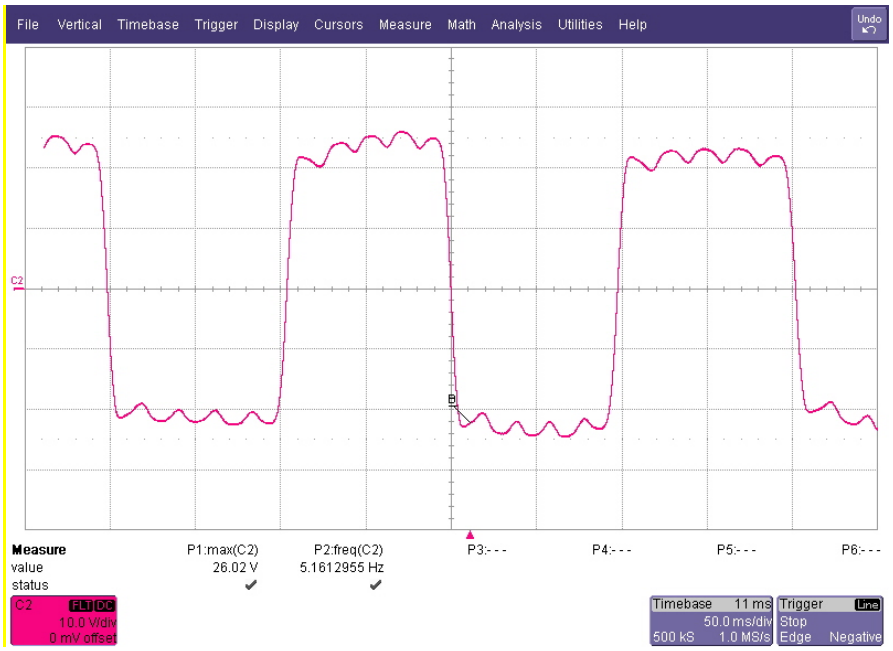

(a)

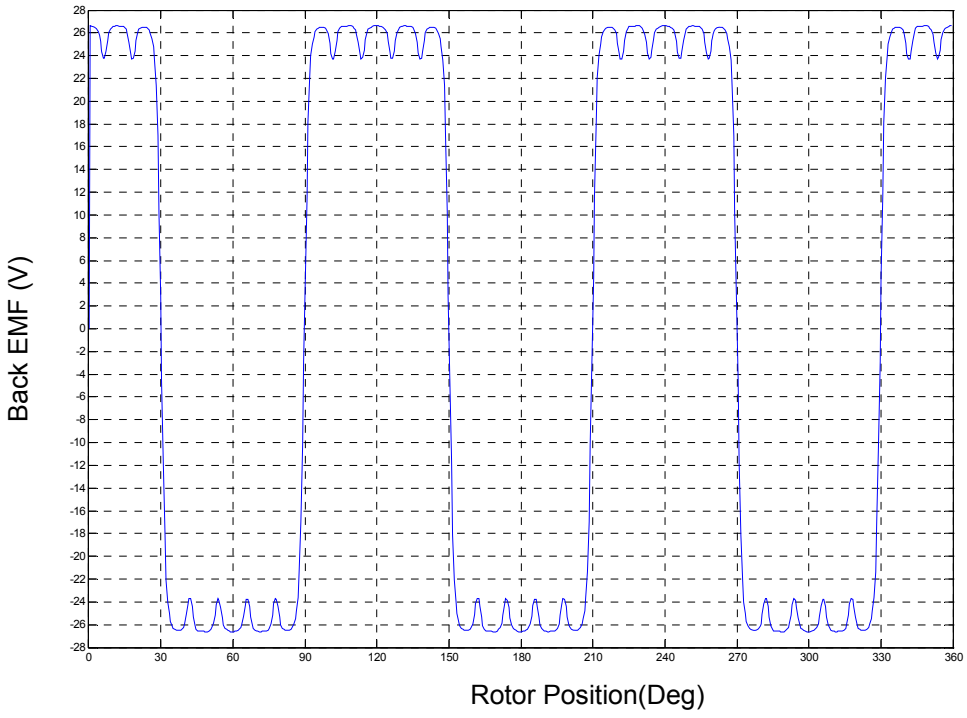

(b)

Figure 2.11: Back EMF comparison, (a) Experimental (b) field reconstruction.

In order to calculate the FRM, the following tasks should be done:

- Basis functions should be fetched from memory (10 cycles)
- Multiplication of basis functions to the current magnitude (4 cycles)
- Addition of the modulated basis functions to achieve stator contribution to magnetic flux (4 cycles)
- Addition of PM contribution to the Stator contribution to achieve complete system response(4 cycles)

As the clock frequency of this DSP is 150 MHz. each cycle takes almost 6.6 ns. It means that calculation of each time sample (which is 70 cycles) can be carried out in 462 ns. The A/D frequency for this DSP is 12 MHz so each conversion takes 83 ns. As the 5 phase currents and position should be read and converted the overall conversion time will be 498 ns. The overall calculation time is 960 ns. This short calculation time proves that FRM can be used in real time control applications where the fast response time is of great importance. The control loop implemenetd in DSP takes 3 us. So the overall time for calculation and control is almost 4 us. So, the maximum switching frequency possible is 250 MHz which is much bigger than the average switching frequency of 20 KHz.

CHAPTER 3

FLUX ESTIMATION USING FRM

Magnetic flux estimation is one of the main requirements in control of electrical machines such as direct torque control (DTC) and sensorless operation. There are also fault detection schemes that work based on the magnetic flux observation. The DTC method, for example, is used increasingly in motor control applications because of advantages such as fast dynamic response and minimal dependency on knowledge of the machine parameters. An issue in using the DTC method is obtaining an accurate estimation of the magnetic flux. Position sensorless methods are aslo being used to lower cost, reduce size, eliminate sensor cables and circuitry, and achieve better reliability.

Significant research has been reported on development of sensorless control strategies [32]–[37]. In this family of control methods, the stator flux linkage is usually calculated by integrating the voltage across the stator windings using:

$$\lambda_{si} = \int_0^t (v_{si} - r i_{si})\, dt \qquad i = A, B, C, ... \tag{3.1}$$

Where, v_{si}, r and i_{si} are stator phase voltage, stator resistance, and stator current respectively. Although straightforward, this method has its own weaknesses which include:

- Integration drifts due to offset error in current and voltage measurement.
- Errors due to variation in stator resistance as a result of temperature changes, etc.

These challenges become more severe at low speeds when the voltage drop across a stator resistor is comparable to that of the back-EMF of the machine.

A great deal of research has been done to address these issues. Chapuis and Roye proposed a constant DC offset method to eliminate the integration drift [38]. This method is

useful provided that the offset remains unchanged during the control process. Patel, et_al, presented a cascaded low pass filter (LPF) method [39] to remedy the problem. Rahman, et_al, developed low pass filtering (LPF) method for DTC in interior permanent magnet motor drives [40]. In this method, rather than a standard integrator, an LPF is used. It has been shown that in the case of a pure DC input signal, the integration method will not diverge, if the exact values of the system parameters are known [41]. Some research has been carried out to address the inevitable inaccuracies related to stator resistance. Fuzzy logic techniques have been used in [42] – [44] to tune the resistance values in DTC.

As mentioned before, besides the DTC, flux observers can be used in conjunction with specific fault detection schemes for fault tolerance motor drive and control application [45], [46]. Levi, et_al, proposed a stator resistance estimation scheme for the rotor flux-based model reference adaptive system [47].

Habetler, et_al, presented a model-based stator resistance estimation scheme for winding temperature monitoring applications [48]. The proposed method is accurate for steady state operation, while not addressing the low speed problem. All of these methods are dependant upon machine parameters such as resistance or inductance. Also, the voltage, current and speed must be monitored precisely.

A Lumped parameter method is another way to estimate the flux linkages of each stator phase. Assuming the sinusoidal distribution of the stator windings the *q*- axis and *d*-axis components of the flux linkage can be determined as follows:

$$\lambda_{ds} = L_d i_{ds} + \lambda'_{pm} \tag{3.2}$$

$$\lambda_{qs} = L_q i_{qs} \tag{3.3}$$

Where, L_d and L_q are *d* and *q* axes inductances respectively. λ'_{pm}, is the magnetic flux due to the permanent magnets. Although precise, the main drawback of this method is that the motional back-emf must be sinusoidal. In case of a small motor with low number of slots per

pole per phase, sinusoidal distribution of the windings is not achiveable. As a result lumped parameter model may not be suitable. This chapter presents a new method of magnetic flux estimation to remedy the aforementioned issues. The distribution of the magnetic field in the airgap of the machine is used to estimate flux linkages. Due to the fact that this method is independent from stator resistance value, the corresponding errors are eliminated. Furthermore, there is no integration with respect to time, which is prone to numerical drift. This eliminates the accumulation of errors at low speeds where integration would otherwise take place over a relatively longer period of time. As a result, magnetic flux can be computed accurately over the entire speed range.

3.1 Stator Tooth Flux Estimation

In this section the observations and findings which leads to the development of new flux estimation method has been discussed.

3.1.1 Method 1

The first step in each analysis is the observation of the phenomenon and its behavior in the operation range. Here, the finite element model created for the 5-phase PMSM is used to observe the behavior of the magnetic field in the machine. Figure 3.1 depicts the distribution of the magnetic field in the machine.

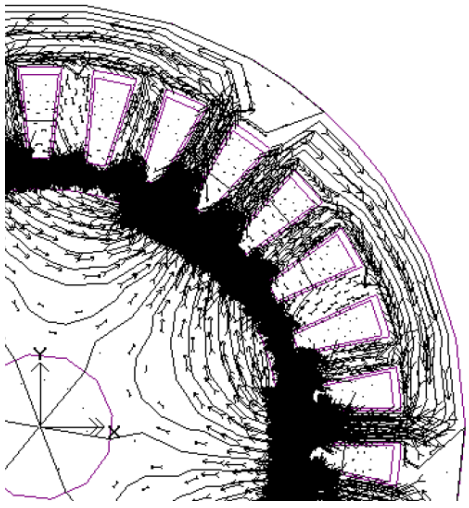

Figure 3.1: Magnetic Flux distribution in the machine

The idea is to use the normal and tangential components of the magnetic flux density attained from FRM to find the magnetic flux passing each stator tooth. According to figure 3.1 a dominant majority of the flux lines that exist in the airgap of the machine would enter the stator tooth from the top surface. So, the flux in each stator tooth can be calculated using the magnetic field components in the airgap. There would be a slight error in this calculation because of the leakage flux (i.e. some flux lines would enter the stator tooth from the tooth side surfaces instead of top surface). These flux lines are not accounted for, in the calculation and therefore result in error.

The span of magnetic field components corresponding to each stator tooth can be determined as follows:

$$S = \frac{360^{\circ}}{M} \tag{3.4}$$

Where M is the number of stator teeth. In this case, the 5-phase machine of analysis has 30 stator teeth so the magnetic components of each 12° span have been specified to one tooth. These components are to be projected on the axes passing through the middle of each stator tooth. Having partitioned the airgap, the next step is to project the magnetic field components to the axis passing through each stator tooth. Figure 3.2 illustrates the projection of the normal and tangential components to the corresponding axis.

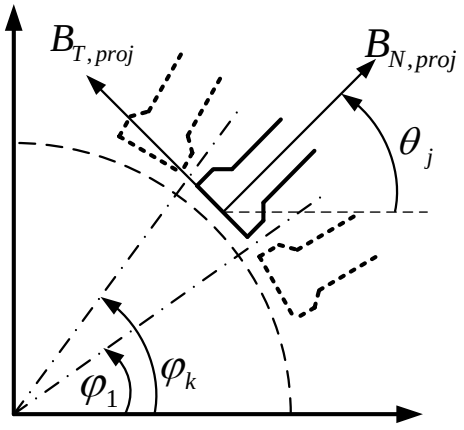

Figure 3.2: Magnetic flux component projection into stator teeth axes

Considering the relative position of each magnetic flux component to the projection axes, the flux density components can be projected on the axis using the following equation:

$$B_{proj}(j) = \sum_{i=1}^{K} \{B_{n,i} \cos(\phi_i - \theta_j) - B_{t,i} \sin(\phi_i - \theta_j)\} \tag{3.5}$$

Where ϕ and θ are the position of the field components in the airgap and the position of the projection axis in the model, respectively. The indices $i = 1...K$ and $j = 1...L$ refer to the number of field component solutions in the airgap covering one stator tooth and the respective stator teeth, respectively. Based upon normal field components, the flux in the airgap, which is almost equal to the flux in the stator tooth, can be calculated as:

$$\Phi = \iint_S \vec{B}_{proj} . d\vec{S} \tag{3.6}$$

The above integration is performed on the surface which is concentric to the rotor surface and passes through the stator teeth as shown in Figure 3.3.

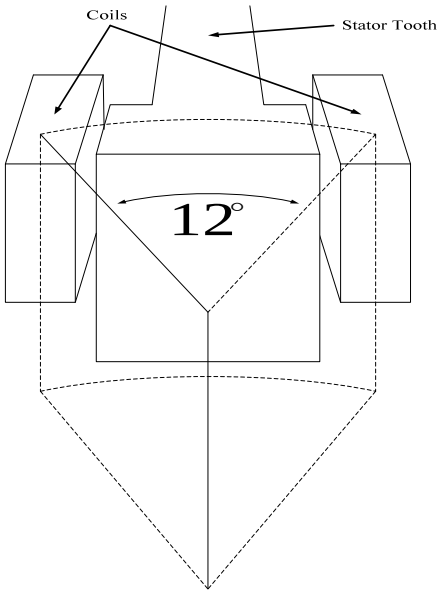

Figure 3.3: Flux Integration surface

As this method deploys field reconstruction method to obtain field components in the middle of the airgap, it generates more data than necessary for some flux targeted applications where the distribution of the magnetic field is not needed. In the next section a modified version of the current flux estimator with smaller number of computations is presented.

3.1.2 Method 2

In this section "Flux reconstruction method" is introduced which follows the same concept as of the field reconstruction. This method directly deals with the flux passing each stator tooth instead of the distribution of the magnetic flux densities in the airgap. In this method the stator tooth flux due to the PM ($\Phi_{PM,j}(\theta_r)$) for each rotor position (i.e. θ_r) is captured and stored offline while the stator windings are open circuited (PM contribution to the flux linkage). Similar to the basis function derivation in FRM, the contribution of the stator current to magnetic flux in each stator tooth would be obtained and stored offline. For this purpose 1(A) would be applied to each stator phase (one at a time) and the resulting fluxes will be stored ($\Phi_{A,j}, \Phi_{B,j}, \Phi_{C,j}, \Phi_{d,j}, \Phi_{e,j}$). Having the contribution of the permanent magnet and stator currents, the magnetic flux in each stator tooth can be determined as follows:

$$\Phi_j(\theta_r) = \Phi_{PM,j}(\theta_r) + i_A(\theta_r).\Phi_{A,j} + i_B(\theta_r).\Phi_{B,j} + i_C(\theta_r).\Phi_{C,j} + i_d(\theta_r).\Phi_{d,j} + i_e(\theta_r).\Phi_{e,j} \quad (3.7)$$

Where, *j* is the stator tooth index. i_A ,i_B ,i_c , i_d and i_e are stator winding phase currents. Using equation 3.7 the distribution of the flux in the machine can be achieved. This data can be used to calculate the flux linking each of the stator phases.

3.2 Stator Phase Flux Estimation

The magnetic flux for each magnetic pole can be calculated and multiplied by the number of pole pairs in order to calculate the stator phase flux linkage. Figure 3.4 depicts the flux corresponding to the first pole which passes through the A1-A2 frame (linking A1-A2). A1

and A2 are the wires of first and second slot of the phase “A” winding (there are 6 slots per each phase).

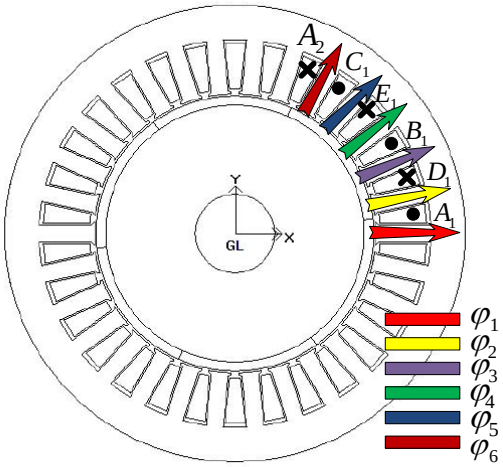

Figure 3.4: Flux assignment to stator teeth

Based on the flux assigment of figure 3.4 and considering the flux distribution shown in figure 3.1, the flux linkage of this winding is as follows:

$$\lambda_{A1-A2} = N(\Phi_2 + \Phi_3 + \Phi_4 + \Phi_5 + \Phi_6) \tag{3.8}$$

Where, N denotes the number of conductors in each slot. Phase A flux linkage then can be determined as follows:

$$\lambda_A = 3N(\Phi_2 + \Phi_3 + \Phi_4 + \Phi_5 + \Phi_6) \tag{3.9}$$

In genral, once all stator tooth fluxes are known one can compute the flux linking each phase. In order to accomplish this task one needs to know the number of magnetic poles (i.e. 2P). Following equations denote the flux linking five phases of stator (Similar derivation can be used for machines with higher number of phases).

$$\lambda_A = P\sum_{j=1}^{q} N_j \Phi_j(\theta_r) \tag{3.10}$$

$$\lambda_B = P\sum_{j=q+1}^{2q} N_j \Phi_j(\theta_r) \tag{3.11}$$

$$\lambda_C = P \sum_{j=2q+1}^{3q} N_j \Phi_j(\theta_r) \tag{3.12}$$

$$\lambda_D = P \sum_{j=3q+1}^{4q} N_j \Phi_j(\theta_r) \tag{3.13}$$

$$\lambda_E = P \sum_{j=4q+1}^{5q} N_j \Phi_j(\theta_r) \tag{3.14}$$

In which q and N_j represent the number of staor slots forming one full pole pitch and the numer of conductors inside the j-th stator slot respectively. In case of the 5-phase machine, the order of the phases is A, D, B, E and C as shown in Figure 3.4. The flux estimation scheme has been illustrated in Figure 3.5.

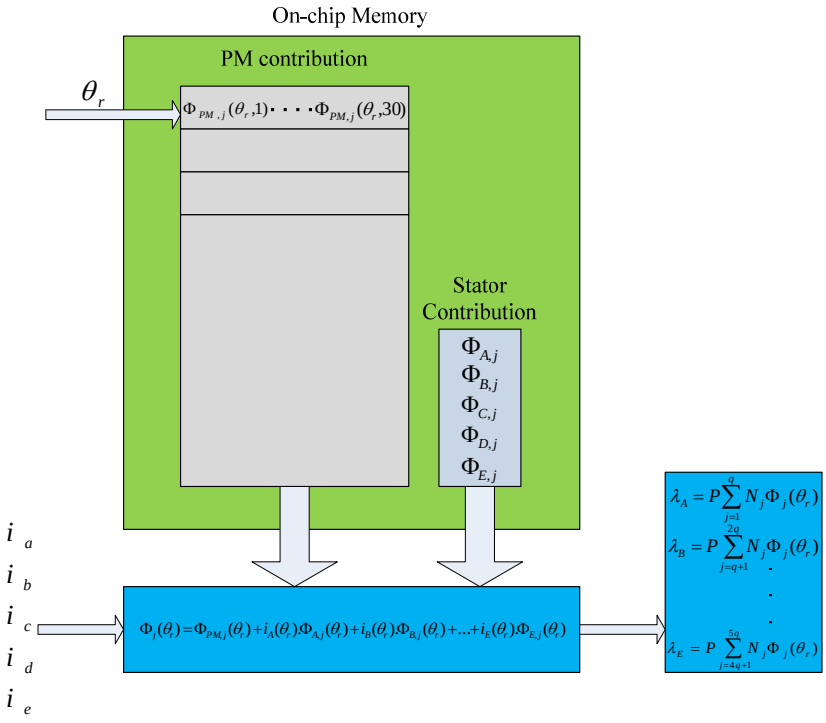

Figure 3.5: Flux estimation schematic

According to Figure 3.5 for each instant of time, the microcontroller should fetch one number from memory. Also, 32 multiplication and 31 additions are necessary to calculate the

flux linkage of each stator phase. For the typical CPU each operation would be carried out in 4 machine cycles. So in this case 252 machine cycles are required to fetch the data from memory, fetch the instruction, execute (add or multiply) and store the 5 phase flux values. Considering 150MIPS processing speed of TMS320F2812 along with the state-of-art compilers the time required to implement this calculation is roughly $6-10$ us.This example clearly shows that the proposed flux estimation technique is useful for other demanding real time applications such as position sensorless operation.

3.3 Comparison of Finite Element and Field Reconstruction

The flux estimation schemes presented in section 3.2 has been verified using the finite element model of PMSM. Figure 3.6 depicts the flux passing 5 arbitrary teeth of the PMSM stator. The blue curves are those of the field reconstruction method while the red ones are the finite element analysis results.

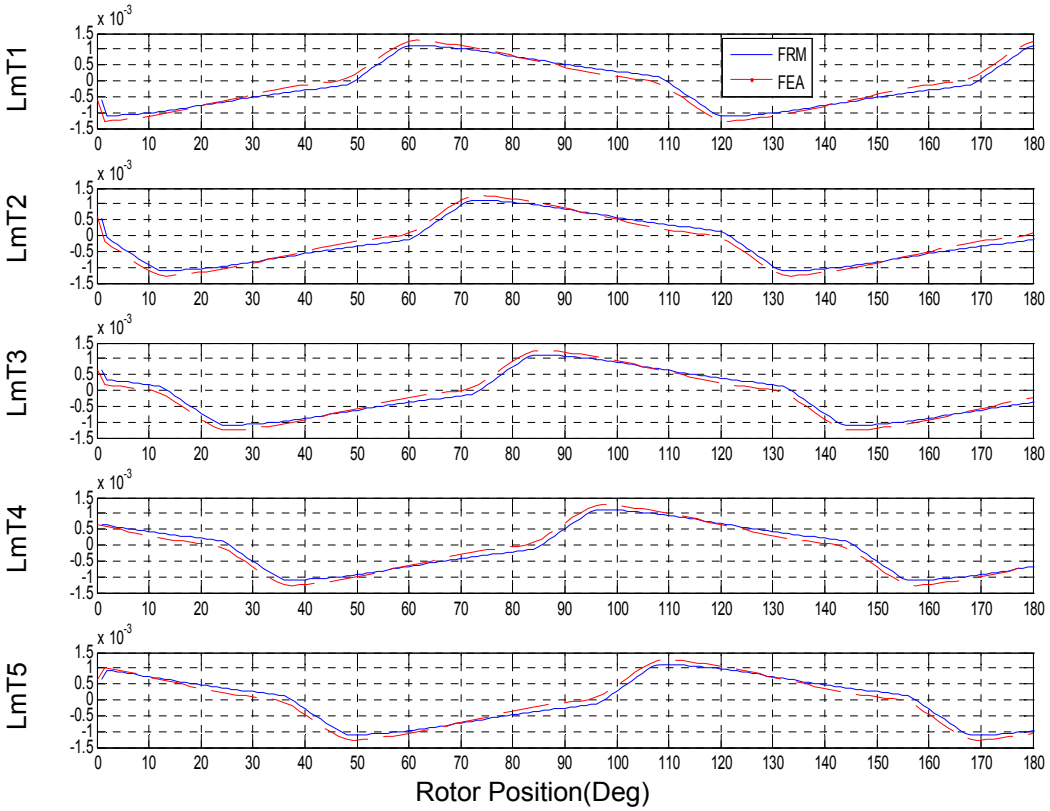

Figure 3.6: Comparison of stator teeth flux obtained from FEA and FRM

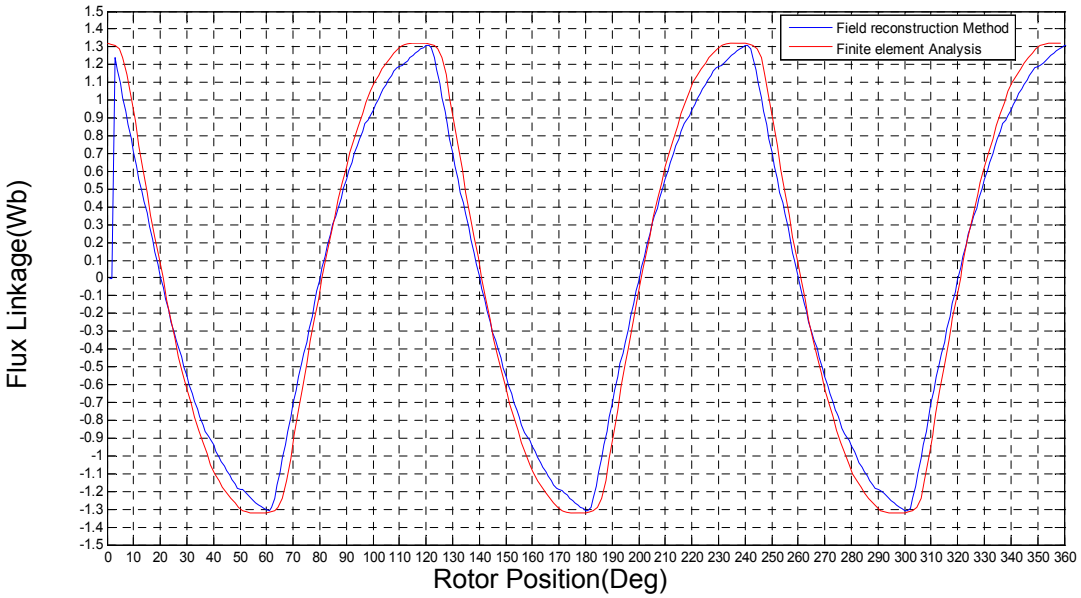

Figure 3.7: Comparison of Phase A flux linkage obtained from FEA and FRM

It can be seen that the flux estimation scheme has acceptable accuracy while as mentioned its computational time is much shorter than the FEA. Figure 3.7 illustrates the flux linkage of the machine derived using the flux passing each stator tooth. The blue curve is the flux linkage obtained using field reconstruction method while the red one is that of the finite element analysis. It should be noted that the waveform derived using each of the described methods are very close. The only difference is the computational time that is much shorter in the proposed technique where flux reconstruction method is deployed. In order to verify the proposed method, an experimental setup has been developed. The method has been tested on a 3 phase and 5 phase permanent magnet synchronous machines. It is shown in chapter 2 that the permanent magnet synchronous machine can be modeled as follows:

$$v_{ks} = Ri_{ks} + \frac{d\lambda_k}{dt} \qquad k = a,b,c,d,e \tag{3.15}$$

Where, v_{ks}, i_{ks}, λ_{ks} and R are stator terminal voltage, current, flux linkage and resistance, respectively. Equation (3.15) can be rewritten in discrete time domain as follows:

$$(v_{ks}[n] - ri_{ks}[n]) \times \Delta t = \lambda_{ks}[n] - \lambda_{ks}[n-1] \qquad k = a, b, c, .d, e \tag{3.16}$$

The voltage applied to stator windings can be determined knowing the flux linkage and the phase current. To verify the flux estimation method the voltage of the stator windings would be monitored and compared to those of the FRM method. This method has been examined for stator open circuit condition. Assuming that the stator windings are open-circuited, the open circuit voltage of stator phases can be determined as follows:

$$(v_{ks}[n]) \times \Delta t = \lambda_{ks}[n] - \lambda_{ks}[n-1] \qquad k = a, b, c, .d, e \tag{3.17}$$

The estimated flux linkages of stator 5 phases have been used to calculate the open circuit voltages of the machine while rotating at 100 rpms. Figure 3.8 depicts the back EMF of the PMSM obtained using FRM compared with those of finite element analysis and experimental setup. It must be mentioned that, the flux linkage obtained from FRM has been differentiated to attain back EMF. This differentiation induces some error in the calculated back EMF compared to that of FEA. The flux linkages of the stator phase "A" have been compared in Figure 3.9.

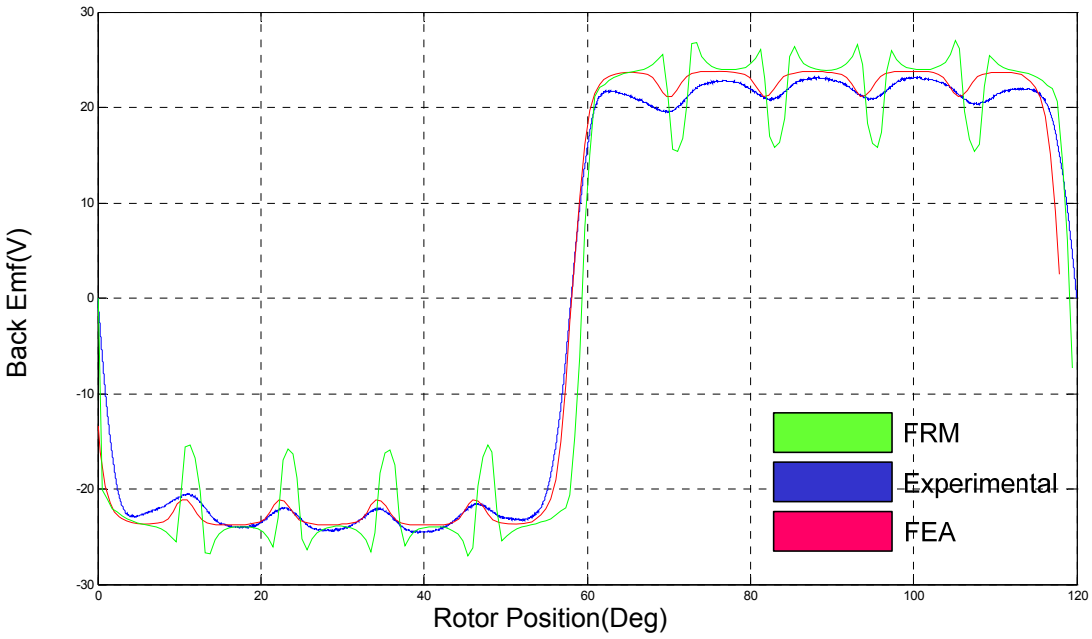

Figure 3.8: Comparison of Phase A back EMF obtained from FEA, FRM and experimental setup at 100 RPM

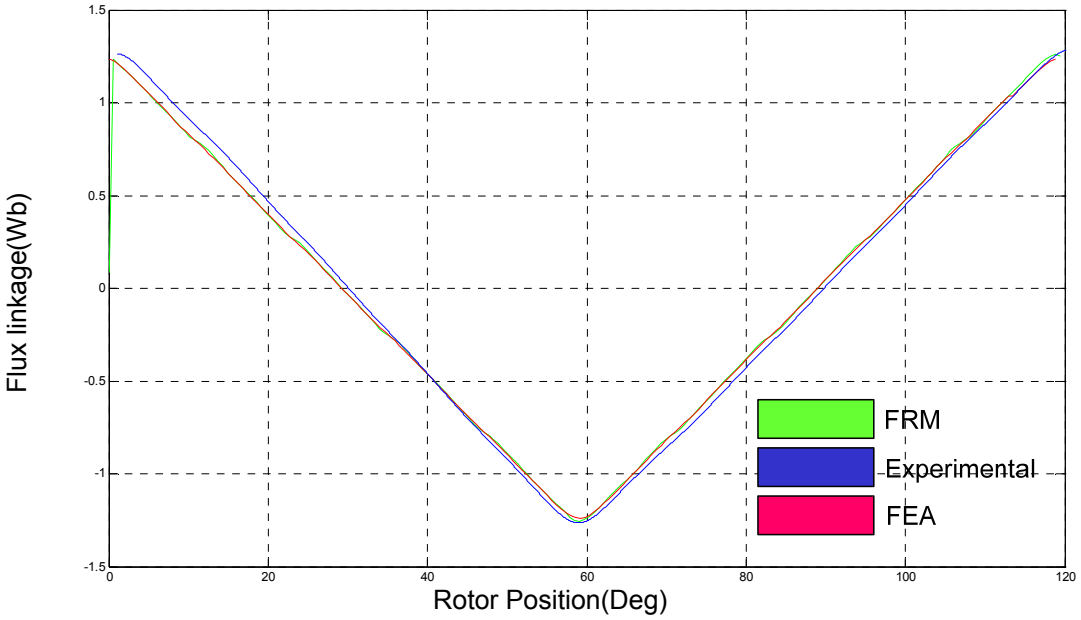

Figure 3.9: Comparison of Phase "A: flux linkage obtained from FEA, FRM and experimental setup at 100 RPM

To obtain the actual flux linkage, the measured terminal volateg is integrated. The comparison of the results validates the accuracy of the flux linkage values calculated using the flux estimator. The flux estimator is also tested on the 3 phase setup at REVT. The experimental setup is shown in Figure 3.10. Equations 3.15 – 3.17 can be rewritten for 3-phase PMSM as follows:

$$v_{ks} = Ri_{ks} + \frac{d\lambda_k}{dt} \qquad k = a,b,c \tag{3.18}$$

$$(v_{ks}[n] - ri_{ks}[n]) \times \Delta t = \lambda_{ks}[n] - \lambda_{ks}[n-1] \qquad k = a,b,c \tag{3.19}$$

$$(v_{ks}[n]) \times \Delta t = \lambda_{ks}[n] - \lambda_{ks}[n-1] \qquad k = a,b,c \tag{3.20}$$

The estimated flux linkages of stator 3 phases have been used to calculate the open circuit voltages of the machine while rotating at 1000 rpm. Figures 3.11 and 3.12 depict the back EMF of the PMSM obtained using FRM and experimental setup respectively. The back

EMF waveforms from FEA, FRM and experimental setup are compared in Figure 3.13. It must be mentioned that, the flux linkage obtained from FRM has been differentiated to attain back EMF. This differentiation induces some error in the calculated back EMF compared to that of FEA. The flux linkages of the stator phase “A” have been compared in Figure 3.14. To obtain the actual flux linkage, the measured terminal volateg is integrated. The comparison of the results validates the accuracy of the flux linkage values calculated using the flux estimator.

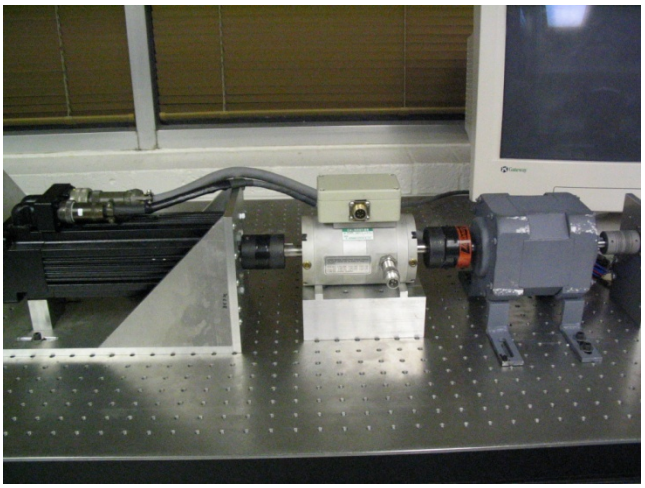

Figure 3.10: 3-phase experimental setup developed for method verification

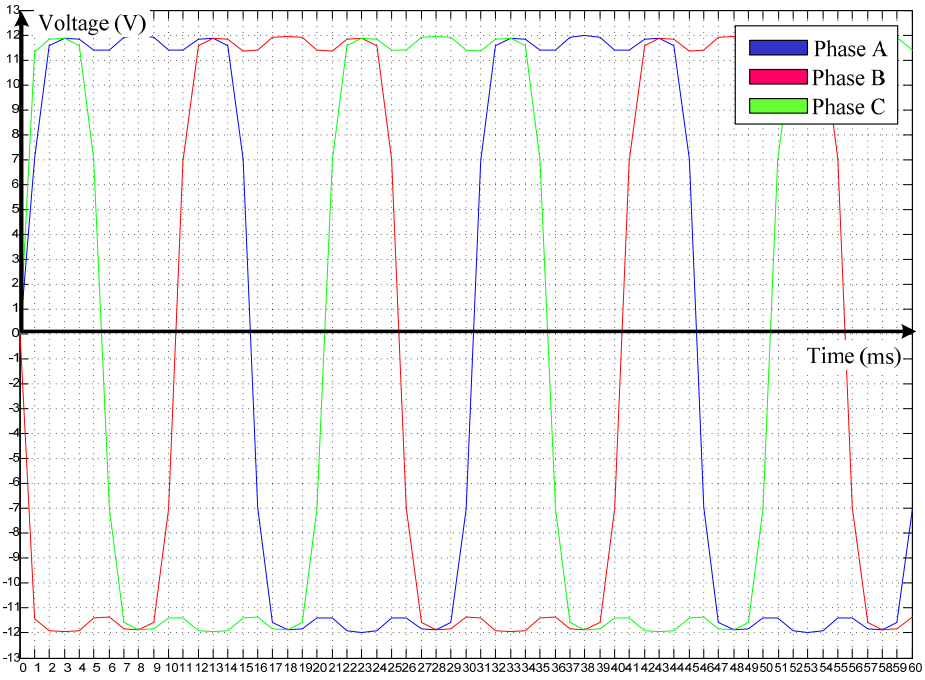

Figure 3.11: 3-phase PMSM back EMF at 1000 RPMs using FEA

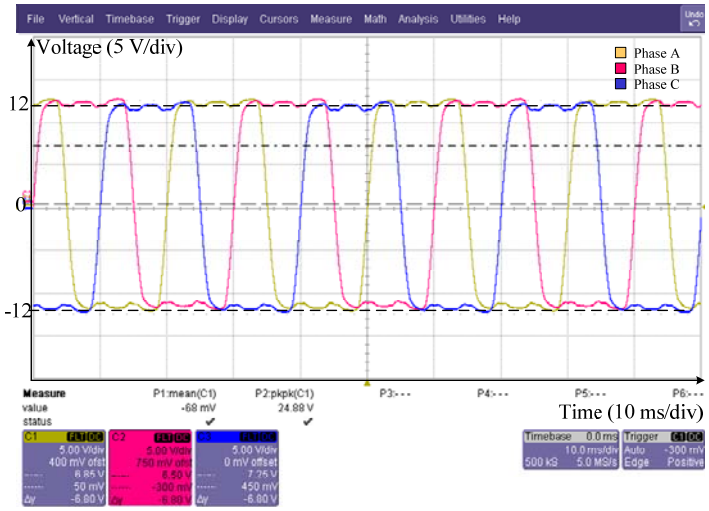

Figure 3.12: 3-phase PMSM back EMF at 1000 RPMs using experimental setup

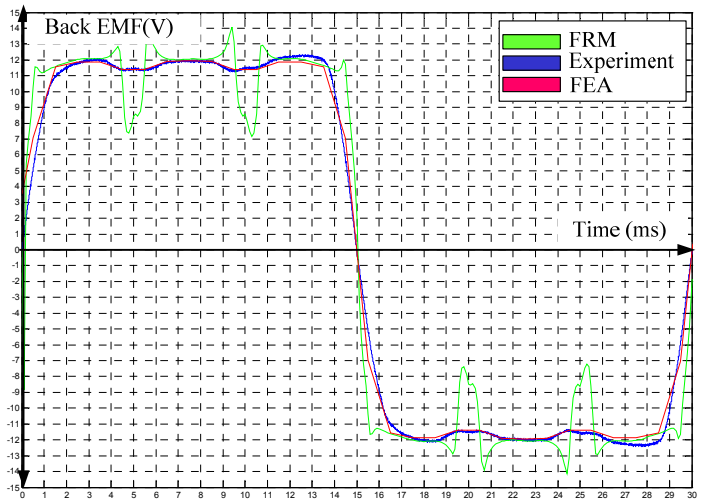

Figure 3.13: Comparison of back EMF at 1000 RPMs

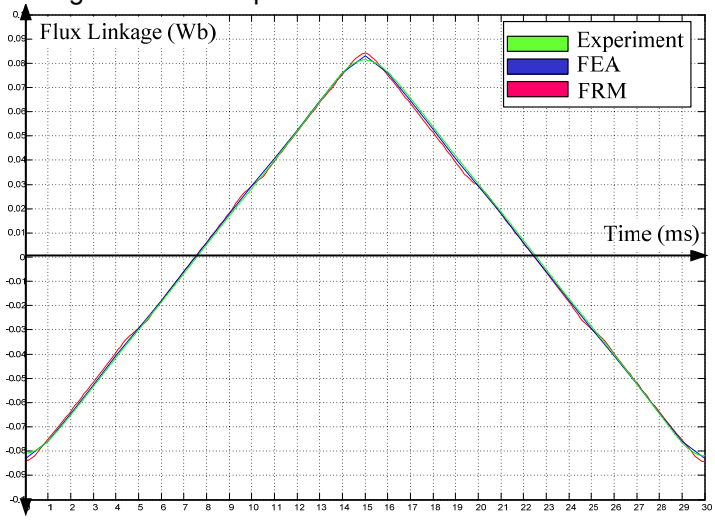

Figure 3.14: Comparison of flux linkages at 1000 RPMs

In the second case, the resistive load of 4 ohms has been connected to stator phases and the PMSM has been rotated by a prime mover at 500 rpm (Generation Mode). In this case the voltage induced in stator phases due to magnet rotation would appear across the stator resistance and the resistive load. As a result the phase voltage equation can be written as:

$$(r + r_s)i_{si}[n] \times \Delta t = \lambda_{si}[n] - \lambda_{si}[n-1] \quad i = a, b, c \tag{3.21}$$

The measured stator resistance is 0.8 ohms. The current of stator phase "A" and the voltage across the resistive load obtained from the experimental setup, is shown in Figure 3.15.

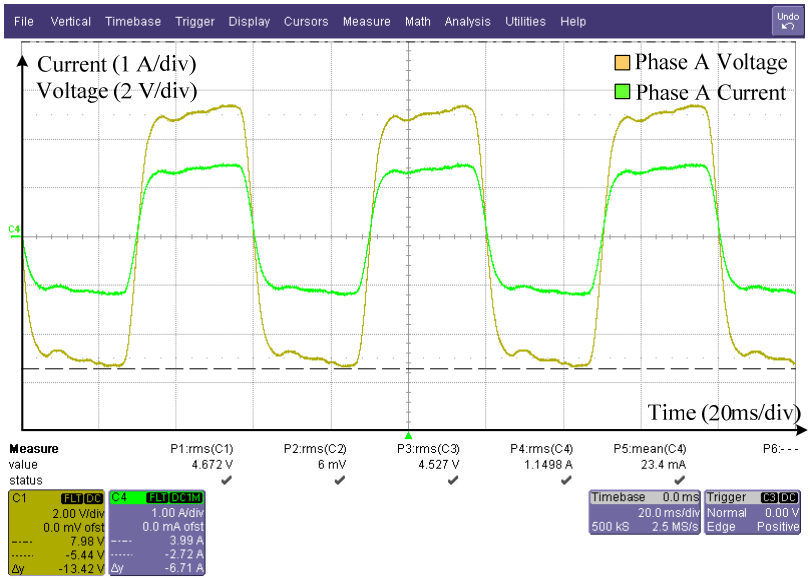

Figure 3.15: PMSM actual stator current and voltage at 500 RPMs

By applying the measured current, obtained from experiments, to the FRM, the voltage across the load, which is also the voltage at PMSM stator terminals, can be calculated using 3.21. Then, this calculated voltage can be compared to that of the experimental setup. The 3-phase experimental voltages are shown in Figure 3.16. Using the experimentally recorded currents, the flux linkage of each phase has been calculated by the FRM. The voltage across the resistors is added to the voltage drop across the stator resistor to calculate the back EMF. The calculated back EMF is compared to those of the FEA and FRM (as shown in Fig. 3.17). In order to achieve the actual flux linkage equation 3.18 is rewritten as:

$$\lambda_{ks} = \int (v_{ks} + r i_{ks})\, dt \quad i = a, b, c \tag{3.22}$$

The flux linkage of phase “A” obtained from FRM is compared to those of FEA and experimental in Figure 3.17. It should be mentioned that equation 3.22 has been used here only to compare the results. The flux observer can calculate the back EMF accurately, except for the notches which represent stator slots. This error can be alleviated by using more accurate basis functions in FRM code. Also, indirect comparison using differentiation may induce some error in the measured quantities.

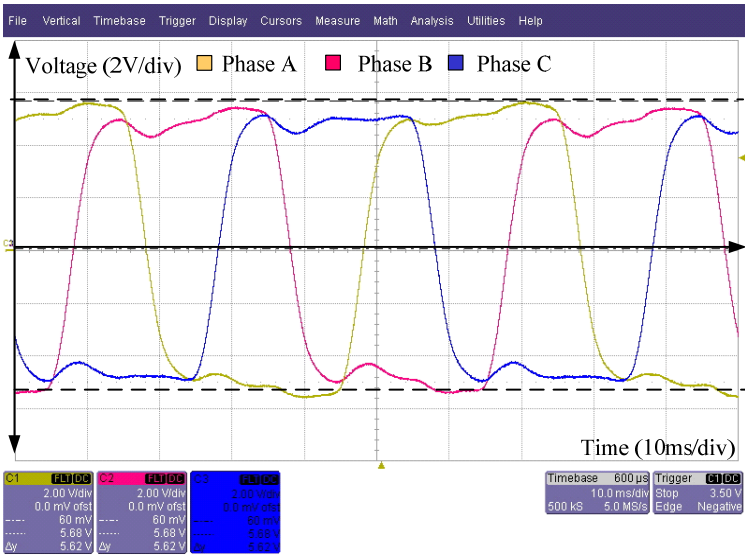

Figure 3.16: PMSM stator terminal voltages (Generation Mode)

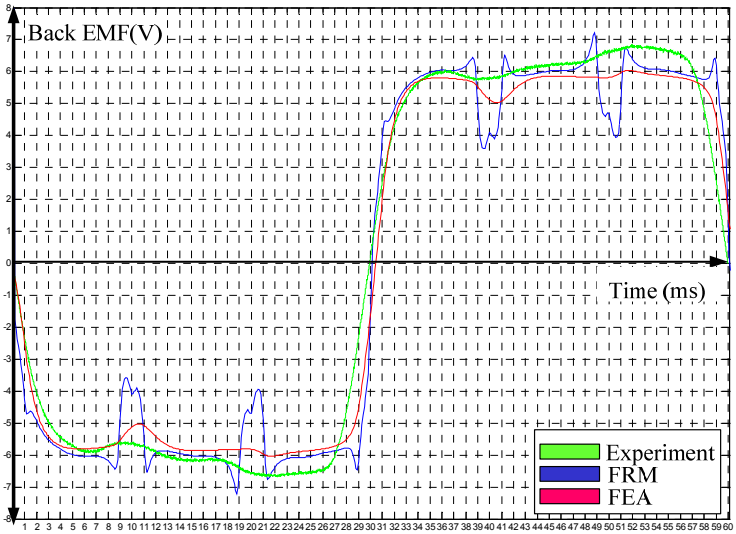

Figure 3.17: Comparison of back EMF at 500 RPMs (Generation Mode)

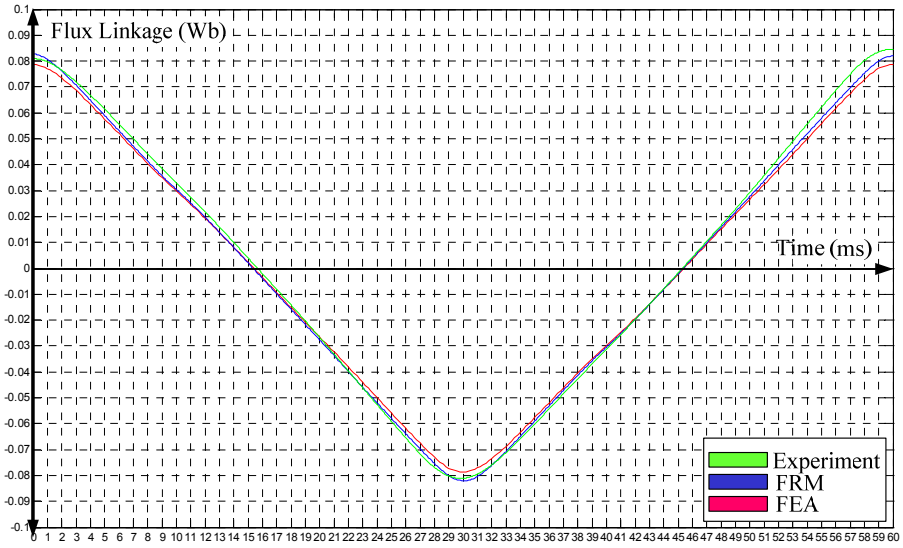

Figure 3.18: Comparison of flux linkages at 500 RPMs (Generation Mode)

In order to be able to compare the fluxes directly, search coils should be installed inside the machine. The same analysis can be done by comparing FRM results with those of the experimental setup. The flux linkage values match appropriately for FRM, FEA and experimental setup.

3.4 Resolution and Error Analysis

The typical results of flux estimation are shown in figures 3.6 and 3.7. The main question that arises is that whether the accuracy of these methods can be improved. It should be mentioned that the error associated with this method mainly is a result of following factors:

- Numerical errors
- Low resolution data tables
- Low quality mesh

The numerical errors are associated with all types of calculations and there are ways of improving the precision. As explained previously, in order to perform the field reconstruction or flux reconstruction methods first the basis functions should be obtained and stored. In order to obtain this basis functions, a finite element model is developed and the basis functions are

derived. If high resolution mesh is deployed in this process, the resulting basis function will be more accurate. However, a denser mesh means a longer simulation time which is not always desirable. Another factor that affects the accuracy is the number of points being stored in the data tables of basis functions. This resolution can vary between a few samples per degree to a sample per multiple degrees. Therefore, by increasing the mesh density the accuracy of basis functions is guaranteed while having high resolution in basis functions improves the estimation accuracy. The accuracy of the current measurements using current sensors is another factor that affects the quality of the basis functions.

CHAPTER 4

FAULT TOLERANT OPERATION IN PMSM

The present chapter introduces various types of faults that can occur in an adjustable speed PMSM drive, their methods of detection, clearance and treatment.

4.1 Classification of Faults in PMSM

Generally, the most frequently occuring faults in the permanent magnet motor drive can be classified into the following categories:

- Faults related to electrical structure
- Faults related to mechanical structure

As mentioned before a multi phase drive, in which each phase is regarded as a single module is the best design for fault tolerant purposes (increasing redundancy). These modules should have the minimal impact on each other so that the failure in one does not affect the others. The modular approach requires:

- Separate single phase bridges (Minimal electrical interaction).
- In case of the magnetic coupling between the phases, fault current in one can induce voltages in the remaining phases, which in turn causes problems especially in the control process (Minimal magnetic interaction).
- The stator outer surface should be cooled down properly (Minimal thermal interaction).

To achieve the above mentioned goals the PMSM should be excited using separate full bridges per each phase. In this case if any of the stator phases or their corresponding power electronics experience a fault it can be disengaged from the healthy components. Based on this arrangement the faults possible on the power electronics components and electrical machine phases can be illustrated as shown in Figure 4.1.

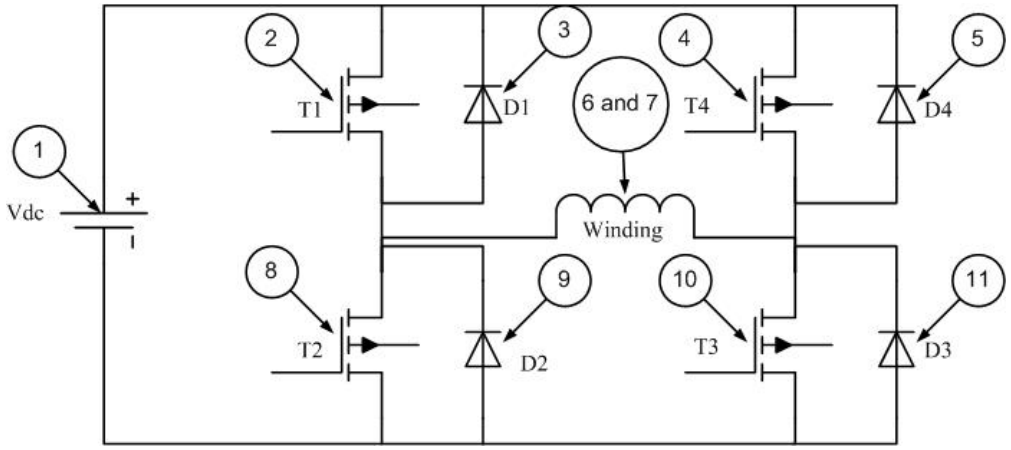

Figure 4.1: Full bridge converter for one phase of PMSM

According to figure 4.1 the faults can be classified into the following:

- Short and open circuit faults on the DC link (1)
- Short and open circuit faults on switches (2, 4, 8, 10)
- Short and open circuit faults on the diodes (3, 5, 9, 11)
- Open circuit fault on the machine phase winding (6)
- Partial and complete short circuit faults on the machine phase sinding (7)

Besides these faults, there are a set of faults that can happen on the sensors measuring current, voltage and position. These types of fault will undermine the control accuracy and functionality. The second set of faults that can happen in an EMEC are from a magnetic or mechnical nature. Among these faults, partial demagnetization of the rotor magnets and static rotor shaft eccentricity has been considered here.

4.1.1 Open-circuit faults

The open circuit faults can either happen on the power electronics components or on the machine stator windings. In case an open circuit happens in one or more of the phases. Consequently, the current flowing into that phase will be zero. The open circuit faults will harm performane of the machine in terms of magnetic field generation and distribution which results

in the loss of synchronism and torque. In this dissertation various types of the open circuits in stator windings have been considered. The modeling of the machine would not be any different from that of the healthy machine. In case an open circuit happens, the current corresponding to that phase will zero in the field reconstruction model. Based on that the magnetic field distribution and hence the flux linking each of the phases can be monitored for fault detection purposes.

4.1.2 Rotor partial demagnetization

In case of a PMSM motor drive, besides the regular monitoring of the current and voltage levels, maximum operating temperature is also limited due to the thermal limitations of the permanent magnets and stator windings. This thermal limit can be exceeded due to poor ventilation (excessive heat) or excessive currents (extreme magnetic field) caused by short circuits. These would change the magnetic properties of the permanent magnets resulting in potential demagnetization. This demagnetization will affect the performance of the machine by a great extent. The demagnetization of the magnets can be classified into the following:

- Thermal shock [49]
- Mechanical shock [49]
- Magnetic shock [50]

The permanent magnet can maintain its properties as long as its temperature is within the safe range. In the case of some faults such as short circuit, or overheating due to poor cooling, the temperature of the PM machine increases and can result in partial demagnetization.

In this case a degradation of the coercive force of the permanent magnet can occur. As discussed in [50], variation of temperature can degrade the performance of permanent magnets. Also, mechanical shock can partially or totally damage the permanent magnets. Magnet degradation, especially for Nd-Fe-B permanent magnets, can occur in case of inclined field which normally leads to a phase displacement between the magnetization direction of the

magnet and the applied field during machine operation. In this study a partial demagnetization of two magnets has been investigated as shown in Figure 4.2. The demagnetized volume of the magnet is assumed to be almost 30%.

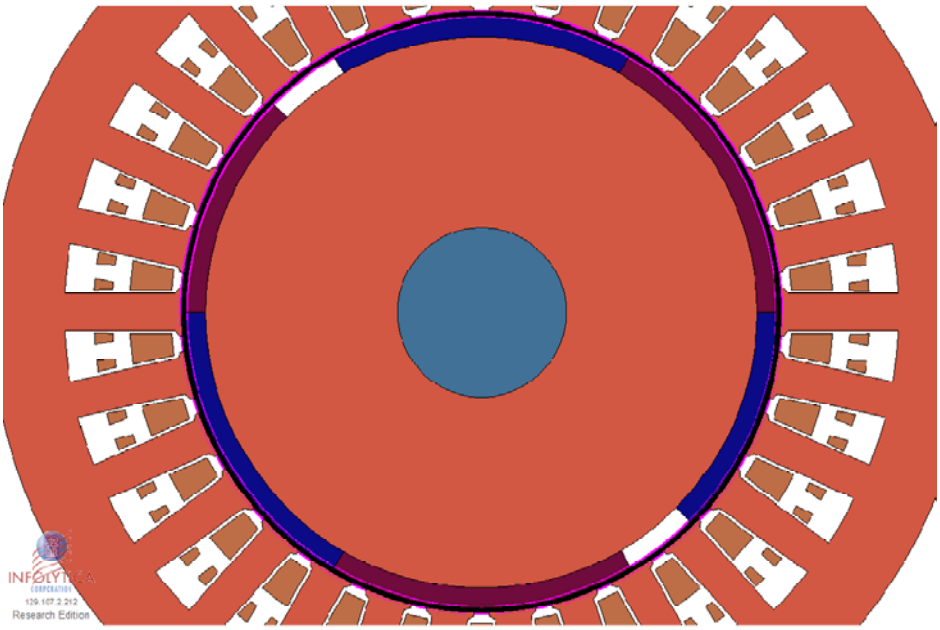

Figure 4.2: Demagnetized area of the PMSM rotor

The demagnetization of the magnets has attracted considerable attention because demagnetization of the magnets in high power ratings is one of the main issues. There is a wide variety of the research on the topic [51] – [53]. In these papers the harmonic content of the stator current is used to detect the demagnetization fault. However, this method is not able to distinguish between the harmoics due to demagnetization and the ones due to eccentricity.

4.1.3 Rotor eccentricity

The eccentricity of the rotor is one of the major faults in electrical machines due to the faulty bearings, unbalanced mass and shaft bending. This eccentricity can be in horizontal, vertical or both directions. The rotor eccentricity is equal to introducing unequal airgap between

the stator and the rotor that causes an asymmetric distribution of the magnetic field in the airgap. The eccentricity of the rotor can be classified into the following categories:

- Static eccentricity
- Dynamic eccentricity

In case of a static eccentricity, the position of minimal radial airgap length is constant during the rotation of the rotor meaning that the rotor is shifted towards one side but it does not move during rotation. In the case of static eccentricity, the amplitude of the forces exerting on the stator teeth would alter and result in unbalanced radial forces. This can cause magnetic and dynamic issues resulting in vibrations, noises and torque pulsations. There are various methods of eccentricity fault detection, such as current spectrum analysis [54].

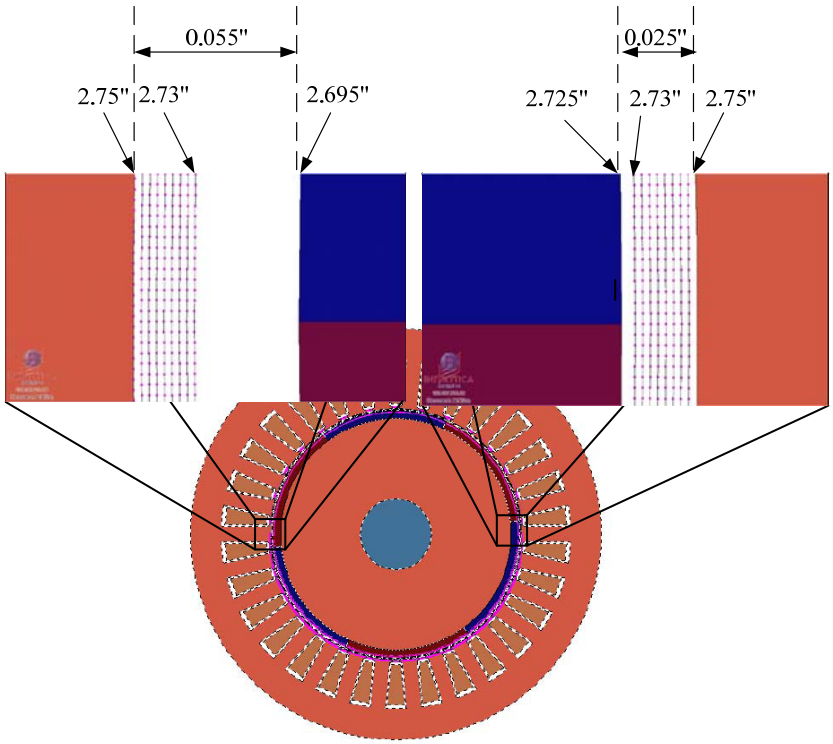

Figure 4.3: Eccentric 5-phase PMSM

In case of a dynamic ecentricity, the center of the shaft is eccentric and the airgap changes dynamically during rotation. In this dissertation, it is assumed that the rotor has 40%

static eccentricity in horizontal direction as shown in Figure 4.3. It means that the center of the shaft is replaced by 40% of the airgap length in horizontal direction.

4.2 FRM modeling of the Faulty machine

As described in the previous chapters a finite element model should be developed to analyze the behavior of the machine under healthy and faulty operations. It has been shown that to develop a comprehensive model for the PMSM, the basis functions and PM contribution to the magnetic field components should be measured and stored. The process of obtaining the basis functions and PM contribution has been described in section 2.1.

In case of a fault in the PMSM, the arrangement of the machine components would be lost or at least altered compared with the healthy case. So, the basis functions and/or PM contribution should be modified and replaced by the ones that include the fault impact. For example, in case of the rotor permanent magnet partial demagnetization, the PM contribution to the magnetic field is altered because of the change in the magnetic properties of the PMs on the rotor.

4.2.1 FRM modeling of partial demagetization

In this study, the demagnetized volume of the magnet is assumed to be almost 15%. To achieve the radial and tangential components of the magnetic field, the FR model should be modified to comply with the changes made, to account for the demagnetized volume of the permanent magnets. In case of demagnetization the PM contribution to the magnetic field is different from that of the healthy machine, so the magnetic field distribution due to the magnets should be captured and used instead of the healthy PM contribution.

Figure 4.4 illustrates the PM contribution to the magnetic field for healthy case and partially demagnetized cases. In case of demagnetization, the corresponding data would be used instead of the healthy case data.

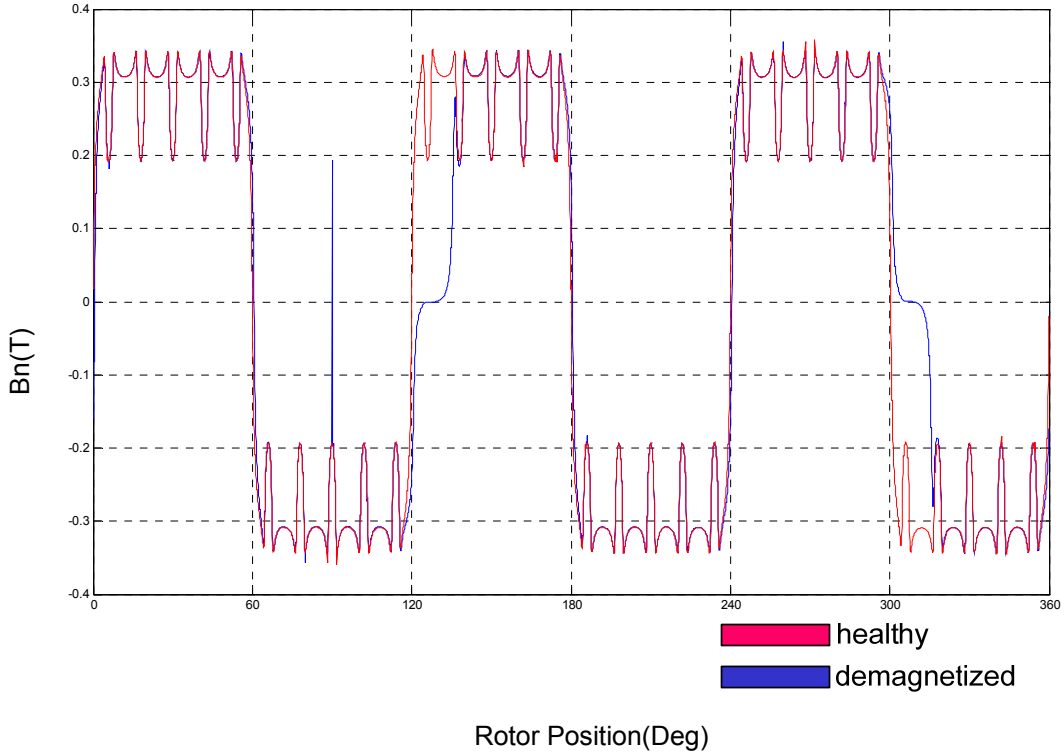

(a)

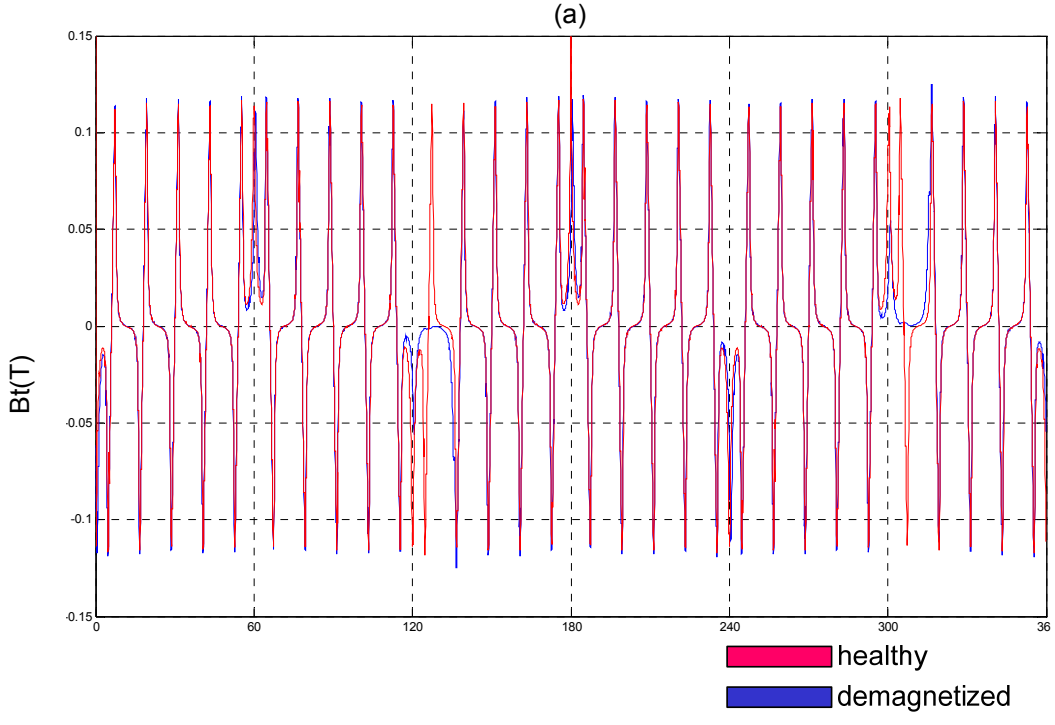

(b)

Figure 4.4: Demagnetization: PM contribution. (a) Normal (b) Tangential

4.2.2 FRM modeling of rotor eccentricity

In case of an eccentric rotor as the relative position of permanent magnets are altered compared with the normal case their contribution to magnetic field is different from that of the healthy machine. In this case the FRM model should be modified to account for the new magnet arrangement. Also, in case of an eccentric rotor as the stator windings are sitting around a non uniform airgap the basis functions which are the contribution of the stator phase currents to the magnetic field would be different. So, the basis functions and PM contribution should be modified to comply with the new condition. In order to capture the new basis function the finite element model created using MAGNET software is modified to include 40% eccentricity as shown in figure 4.3. Then, a current of 1(A) is applied to the each of the five stator phases, one at a time, to capture the magnetic field distribution and hence the modified basis functions.

Figure 4.5 depicts the PM contribution to normal and tangential components of the magnetic field in case of a healthy machine compared with that of an eccentric rotor. It is clear that in case of an eccentric rotor the PM contribution would be different because the rotor is shifted towards one end and the airgap is not uniform. Hence, it should be used instead of the healthy machine model.

Figure 4.6 depicts the stator phase "A" basis functions. In this case a current of 1(A) is applied to phase "A" slots. The basis functions which are the normal and tangential components of the magnetic field in the airgap are captured. The basis functions of phases B, C, D and E are the same but 72° shifted. These new basis functions should substitute the healthy case ones. Using the modified model the radial and tangential magnetic field components can be determined.

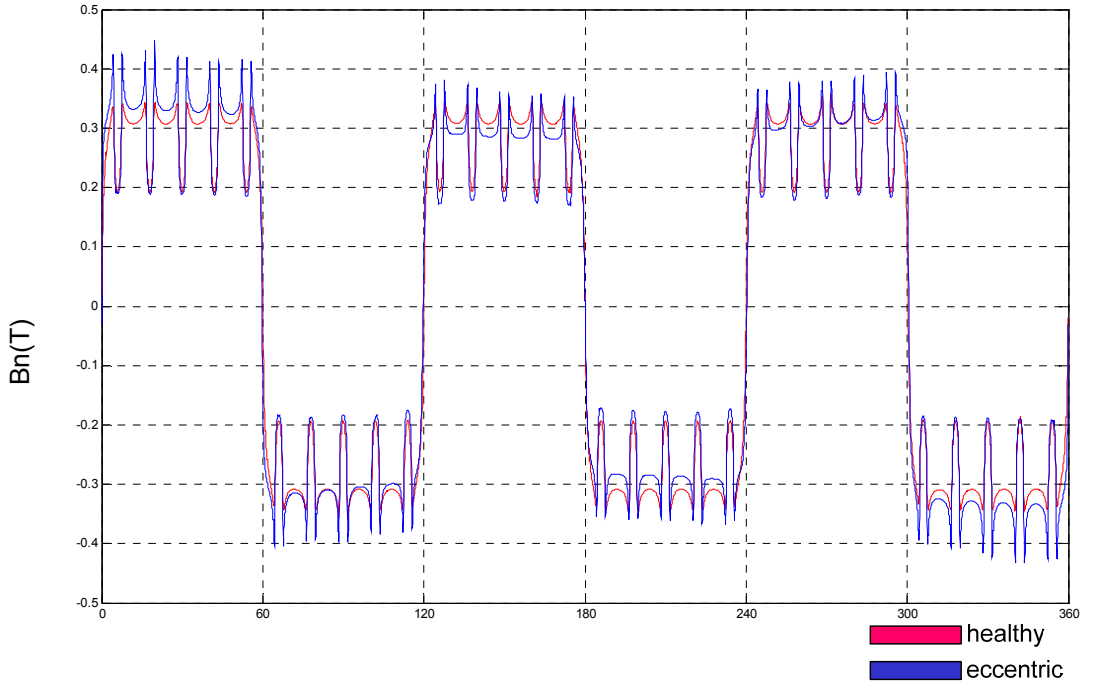

(a)

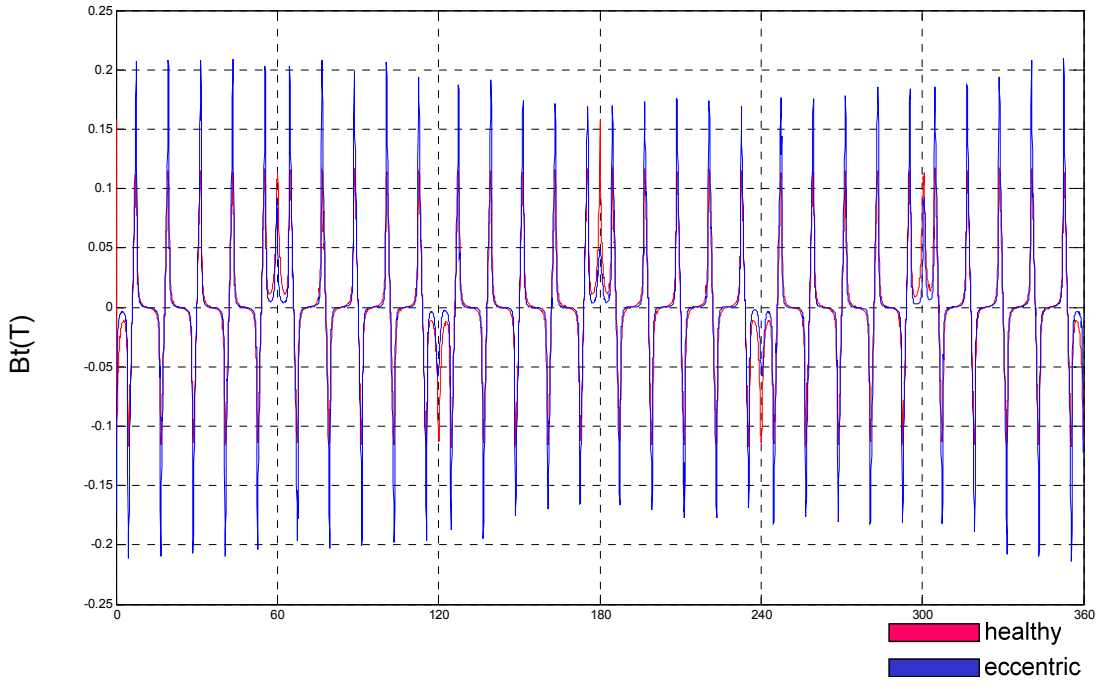

(b)

Figure 4.5: Rotor Eccentricity: PM contribution. (a) Normal (b) Tangential

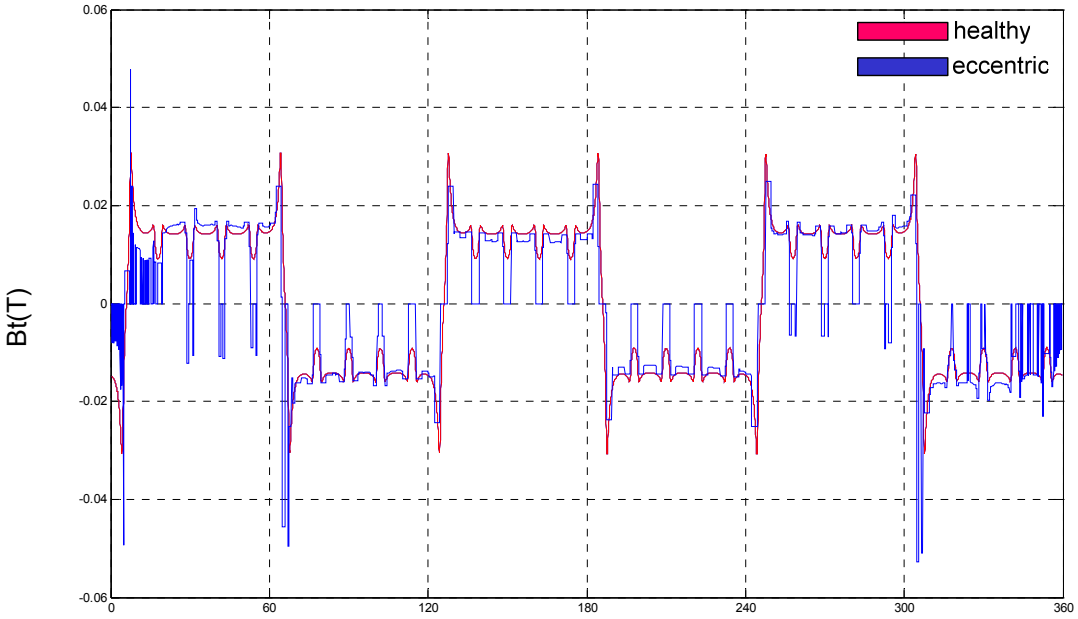

(a)

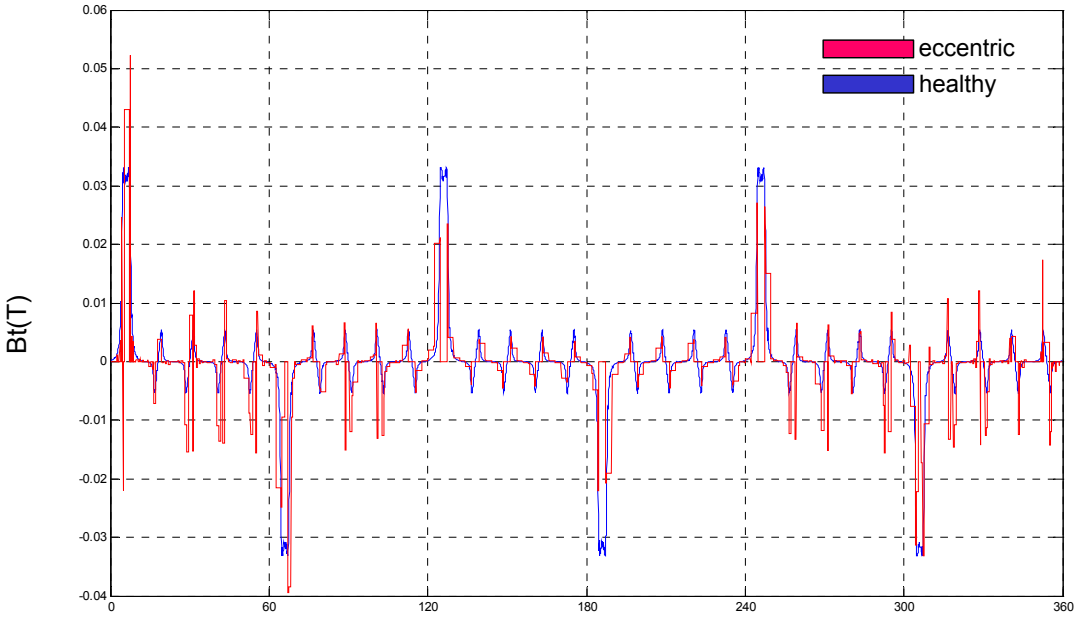

(b)

Figure 4.6: Rotor Eccentricity: Phase “A” basis function. (a) Normal (b) Tangential

4.3 Fault detection Using FRM

In this dissertation a combination of the flux based and current based techniques has been considered to detect the fault. This technique includes the injection of the measured currents into the field reconstruction module and detrmination of the flux linkages due to that current and then comparison of the resulting fluxes with those of the healthy machine. In case of not matching flux linkages, the flux linkage can be investigated to determine the type of the fault. The fault detection scheme has been depicted in figure 4.7. The detection signatures for each type of fault and the treatment to obtain maximum average torque have been presented in the following sections.

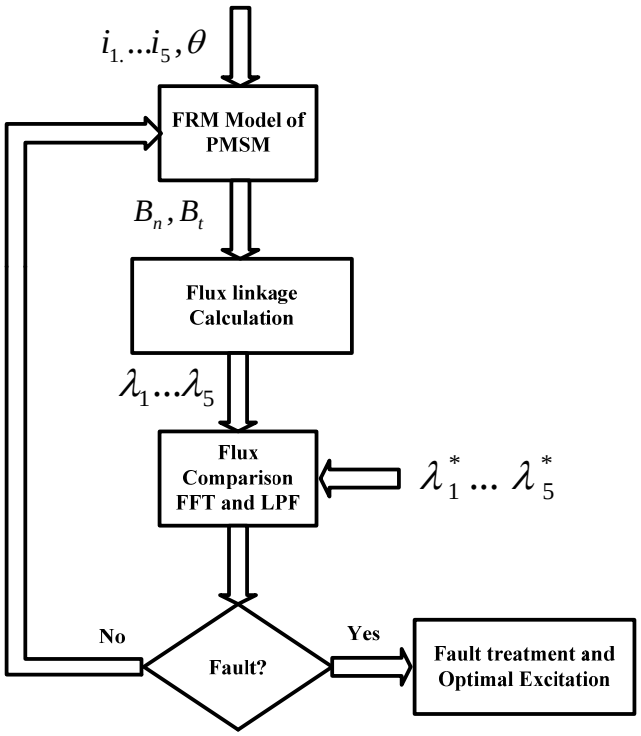

Figure 4.7: Fault detection flowchart

4.3.1 Open-circuit fault detection

The electrical power is supplied to the machine through the stator phases. Loss of any of phases would result in lower input power to the motor and hence the output torque would be

lower than expected. This lower output will endanger the machine operation. So, the fault should be detected immediately and remedial actions should be carried out. The open-circuit fault is not a catastrophic fault as compared to the short circuit faults which should be cleared immediately, but the stator excitation should be modified to compensate for the lack of energy if possible. In order to detect the faults in the stator phases the applied current is fed into the FRM unit. As mentioned before the normal and tangential components of the magnetic field can be calculated using the FRM. Then these field components would be used to calculate the flux in each of the stator teeth. The calculated fluxes would be compared to the expected values.

Based on the number of lost phases and their location different scenarios can be considered. In this dissertation, loss of 1, 2 and 3 phases has been investigated. Figure 4.8 depicts the arrangement of the phase windings in the machine for a single phase open circuit fault on phase “A”.

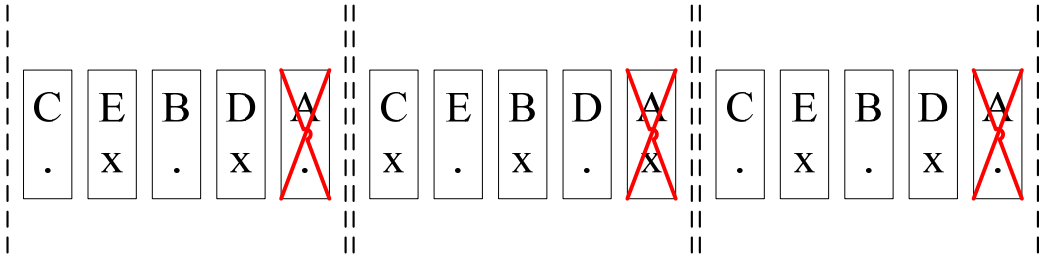

Figure 4.8: Phase “A” open-circuit Fault

In order to detect the fault the sum of the 5 phase flux linkages has been considered as the fault signature. This sum should be equal to zero in case of a balanced system with sinusoidally magnetized permanent magnets. The machine under study contains radially magnetized magnets so the sum of phase flux linkages is not equal to zero, but in case a fault happens this sum is different from the healthy case. The fault signature in case of the healthy operation and phase “A” open circuit fault has been shown in figure 4.9. This study shows that in case of single phase open circuit fault on any stator phase the difference between the healthy case and faulty case signature would be a sinusoidal whose amplitude and phase shift is

different depending on the place of fault. Table 4.1 summarizes the fault detection signatures in case of a single phase open circuit fault.

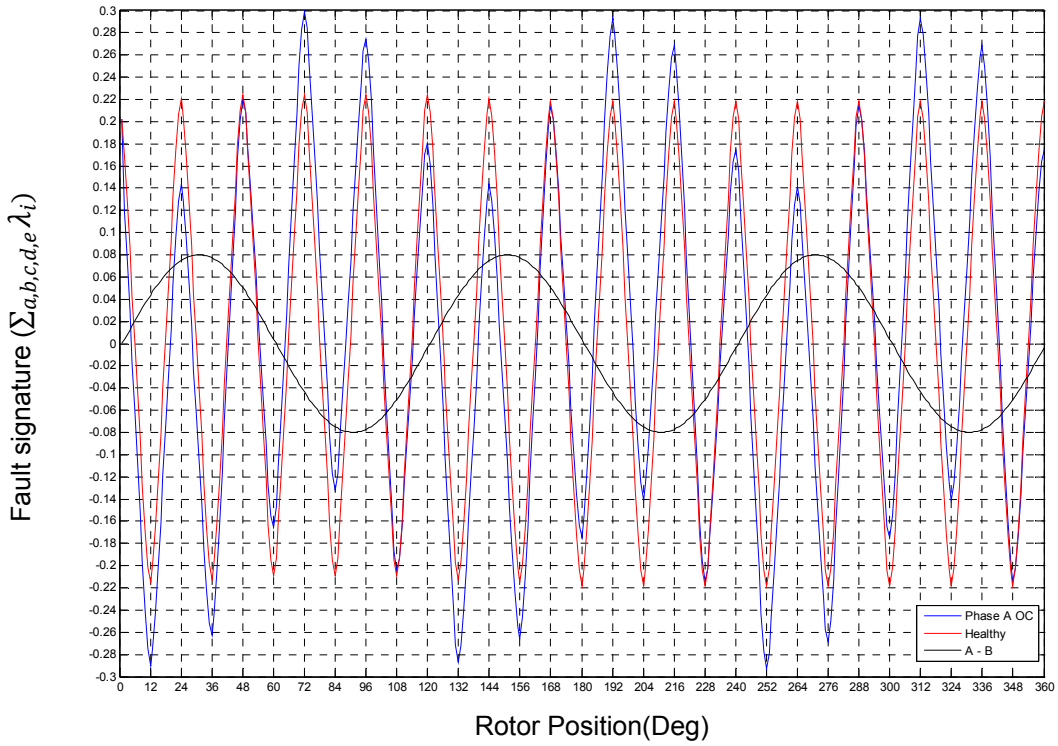

Figure 4.9: Phase "A" open-circuit Fault signature

Table 4.1 Single phase Open circuit signature

Faulty phase	Signature ($\sum_{i=a,b,c,d,e}^{healthy} \lambda_i - \sum_{i=a,b,c,d,e}^{faulty} \lambda_i$)
A	$K_1 \sin(\varphi)$
B	$K_1 \sin(\varphi - 72)$
C	$K_1 \sin(\varphi - 144)$
D	$K_1 \sin(\varphi + 144)$
E	$K_1 \sin(\varphi + 72)$

The same method can be used to detect double and even triples open circuit faults in the machine. In case of the double and triple open phases besides the number of open phases and their location there is another factor that affects the fault signature and the postfault

treatment scheme. It is important whether adjacent or nonadjacent phases are missing. Figure 4.10 depicts the case of an adjacent open circuit fault on phases “A” and “C”.

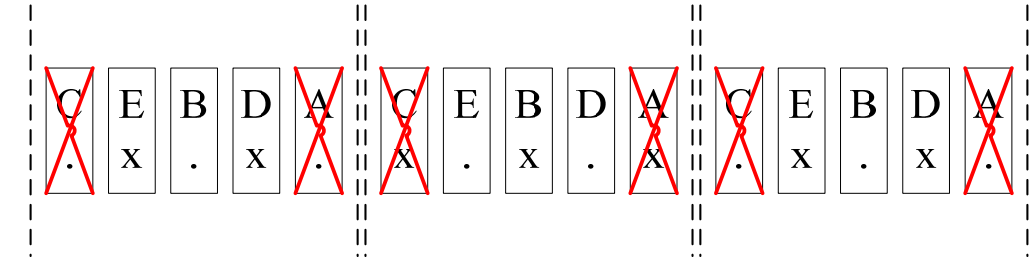

(a)

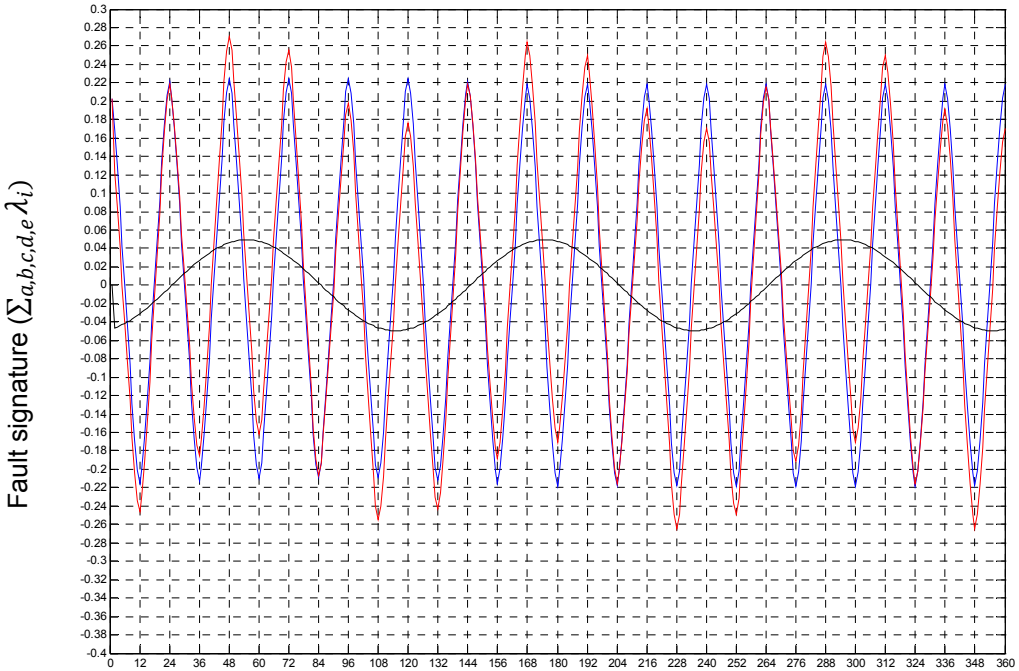

(b)

Figure 4.10: Adjacent double open circuit (a) Winding arrangement, (b) Fault signature.

In case of a non-adjacent double open circuit the signature will be different from that of the adjacent case. Figure 4.11 depicts the winding arrangement and fault signature for this case. In this figure, the sum of the flux linkages for healthy and faulty cases has been presented with blue and red curves, respetively. Table 4.2 summarizes the fault detection signatures in case of an adjacent or non-adjacent double phase open circuit fault. According to the table, the

double open circuit faults can be determined uniquely for each case using the signature. Comparing this table with that of the single phase case it can be seen that the single and double phase open circuits can be uniquely determined using the specified signature.

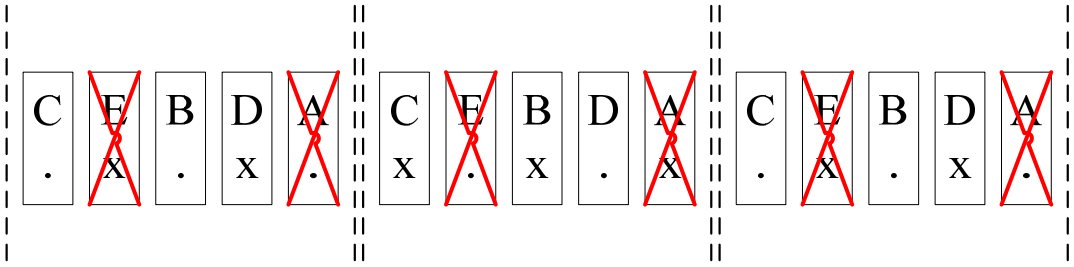

(a)

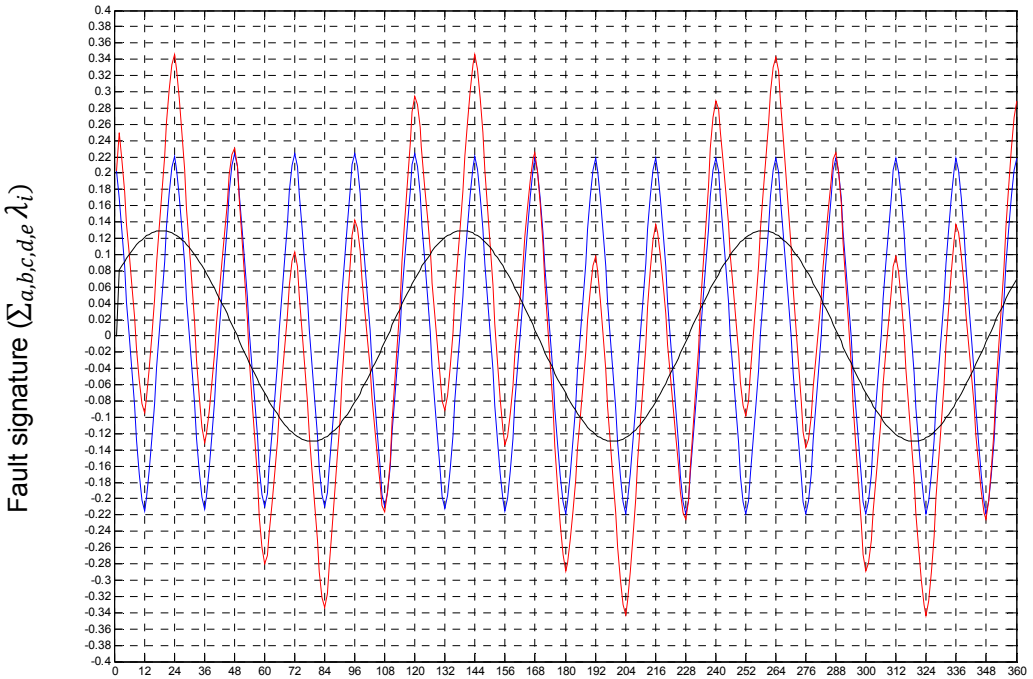

(b)

Figure 4.11: Non-Adjacent double open circuit (a) Winding arrangement, (b) Fault signature.

Triple phase open circuits can also happen on adjacent and non adjacent phases as shown in figures 4.12 and 4.13. A triple open-circuit fault on phases “A”, “B” and “C” is considered as a non-adjacent and a triple open-circuit fault on phases “A”, “B” and “D” is considered as an adjacent fault as illustrated in figure 4.12. The corresponding fault signatures

for each of these cases have been shown in figure 4.13. Again by analyzing these figures the signature to detect each fault can be determined as summarized in table 4.3.

Table 4.2 Double phase Open-circuit signature

Faulty Phase		Signature ($\sum_{i=a,b,c,d,e}^{healthy}\lambda_i - \sum_{i=a,b,c,d,e}^{faulty}\lambda_i$)
Adjacent phases	AD	$K_2 \sin(\varphi + 72)$
	AC	$K_2 \sin(\varphi - 72)$
	BD	$K_2 \sin(\varphi + 144)$
	BE	$K_2 \sin(\varphi)$
	CE	$K_2 \sin(\varphi - 144)$
Non Adjacent phases	AB	$K_3 \sin(\varphi - 36)$
	AE	$K_3 \sin(\varphi + 36)$
	BC	$K_3 \sin(\varphi - 108)$
	CD	$K_3 \sin(\varphi - 180)$
	DE	$K_3 \sin(\varphi + 108)$

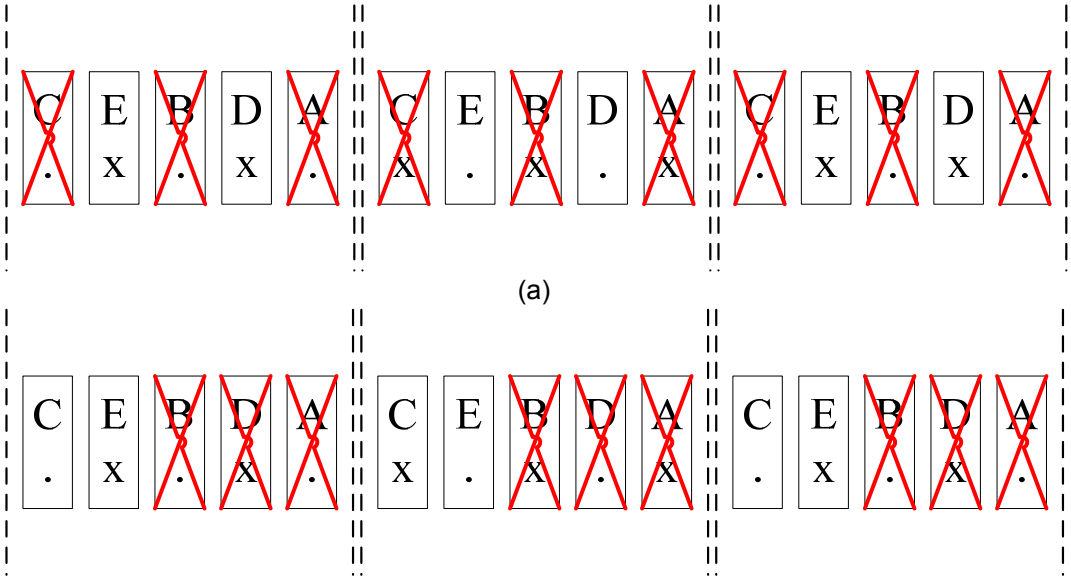

Figure 4.12: Triple phase open-circuit wire arrangement (a) Non-adjacent, (b) Adjacent.

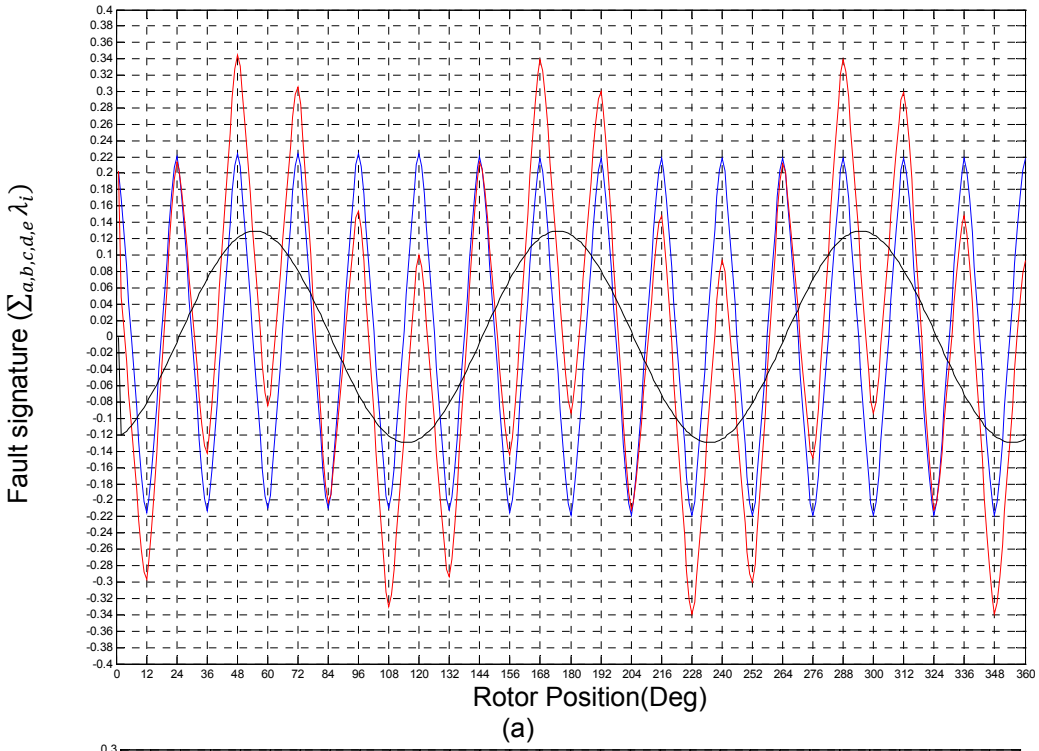

(a)

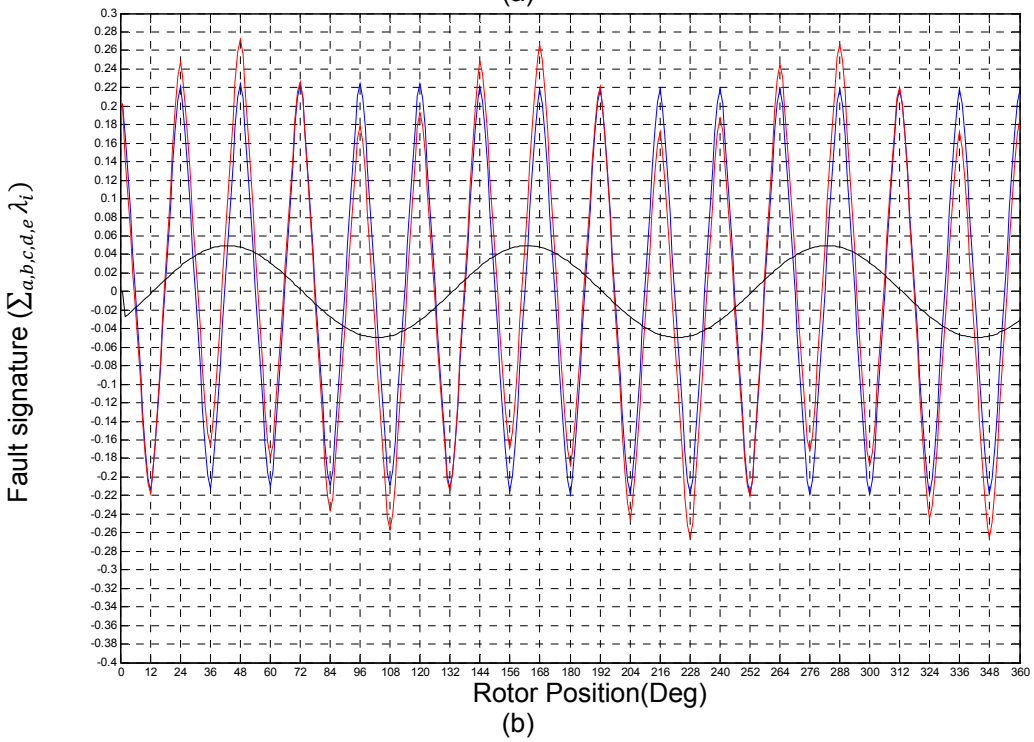

(b)

Figure 4.13: Triple phase open circuit fault (a) Non-adjacent, (b) Adjacent.

Table 4.3 Triple phase Open-circuit signature

Faulty phase		Signature ($\sum_{i=a,b,c,d,e}^{healthy}\lambda_i - \sum_{i=a,b,c,d,e}^{faulty}\lambda_i$)
Adjacent phases	ABD	$K_2 \sin(\varphi - 36)$
	ACE	$K_2 \sin(\varphi + 36)$
	BDE	$K_2 \sin(\varphi + 108)$
	BCE	$K_2 \sin(\varphi - 108)$
	ADC	$K_2 \sin(\varphi - 180)$
Non Adjacent phases	ABC	$K_3 \sin(\varphi - 72)$
	ABE	$K_3 \sin(\varphi)$
	BCD	$K_3 \sin(\varphi - 144)$
	CDE	$K_3 \sin(\varphi + 144)$
	ADE	$K_3 \sin(\varphi + 72)$

In all cases, the flux linkages of the stator phases will be calculated using the FRM. Then the signature will be calculated and compared with each of the table presented here. Based on the matching case the type and place of the fault can be determined.

4.3.2 Partial demagnetization detection

As stated before, in case of a PMSM motor drive, besides the regular monitoring of the current and voltage levels, maximum operating temperature should also be monitored due to the thermal limitations of the permanent magnets and stator windings. This thermal limit can be exceeded due to poor ventilation (excessive heat) or excessive currents (extreme magnetic field) caused by short circuits. These would change the magnetic properties of the permanent magnetc resulting in partial demagnetization. This demagnetization would affect the performance of the machine by a great extent. Increased torque ripple and accoustic noise and decreased average torque are among the problems associated with this fault. The permanent magnet can maintain its properties as long as its temperature is within the safe range. So, the demagnetization of the rotor should be avoided at the first hand and detected and cleared as soon as possible at the second handin case it had happened.

The most important task in fault detection is to find unique signatures that can be detected in case of the fault occurrence. For this purpose, generally the quantities such as current, voltage, etc are monitored. In case of a healthy machine, while the phase voltages are balanced the sum the voltages and therefore the flux linkages would be zero. Reconsidering equation 3.7:

$$\Phi_j(\theta_r) = \Phi_{PM,j}(\theta_r) + i_A(\theta_r).\Phi_{A,j} + i_B(\theta_r).\Phi_{B,j} + i_C(\theta_r).\Phi_{C,j} + i_d(\theta_r).\Phi_{d,j} + i_e(\theta_r).\Phi_{e,j} \quad (4.1)$$

In this equation the flux in one stator tooth has been related to the permanent magnet flux and stator current fluxes, one can rewrite this equation as:

$$\Phi_j(\theta_e) = \Phi_{PM,j}(\theta_e) + \sum_{j=1}^{5} i_j(\theta_e - j\frac{2\pi}{5}).\Phi_j(\phi_S - j\frac{2\pi}{5}) \quad (4.2)$$

In case the PMSM operates under normal condition, it can be proven that :

$$\left.\begin{array}{l} \int_0^{2\pi} \Phi_{PM,j}(\theta_e)d\theta_e = 0 \\ \int_0^{2\pi} i_A(\theta_e)d\theta_e = 0 \end{array}\right\} \Rightarrow \int_0^{2\pi} \Phi_j(\theta_e)d\theta_e = 0 \quad (4.3)$$

Given this assumption then demagnetization will result in:

$$\int_0^{2\pi} \Phi_{PM,j}(\theta_e)d\theta_e \neq 0 \quad (4.4)$$

Similar to what we did for open circuit faults, $S = \sum_{i=a,b,c,d,e} \lambda_i$ has been monitored to detect the fault. As shown in equations 4.3 and 4.4, in case of a healthy machine this sum would be zero while in case of a demagnetized rotor it will no longer be zero. Table 4.4 depicts possible demagnetization faults in the PMSM under study. The frequncy spectrum of the fault signature *S* for single magnet and double pair magnet demagnetization are shown in figures 4.14 and 4.15. The same analysis has been performed on the other possible cases of demagnetization. It

is shown that in case of the rotor magnet demagnetization a set of frequencies would be present in the FFT spectrum of *S* as summarized in Table 4.4.

Table 4.4: Demagnetization scenarios

Fault Scenario	Place	Frequencies to detect
Single magnet demagnetization	N2	$f_1 = 4.89$ $f_2 = 9.78$ $f_3 = 14.67$ $f_4 = 19.56$ $f_5 = 24.46,$ $f_6 = 29.35$ $f_7 = 34.24$ $f_8 = 39.13,....$
	S3	
Double magnet demagnetization	N1N2	
	S1S2	
Triple magnet demagnetization	N1N2N3	
	S1S2S3	
2 Pair demagnetization	N1N2S1S2	

These frequencies could be used for detection purposes. According to the figures and data from table and considering that the frequency of the stator sinusoidal current is known the frequency spectrum could be determined using the following formula:

$$f_{dem} = \frac{k}{2P} \cdot f_e \qquad k = 1,2,3,..... \tag{4.5}$$

Where, P and f_e are the number of magnetic pole pairs and stator current frequency, respectively. The magnetic flux density components will be calculated using field reconstruction method for 1 electrical cycle. Then these components would be used to determine flux passing each stator tooth which will finally be used to calculate the flux linkages of the stator phases. Next step is to compare the expected flux linkage with the actual quantities. By applying the FFT and low pass filtering the signature frequencies can be extracted.

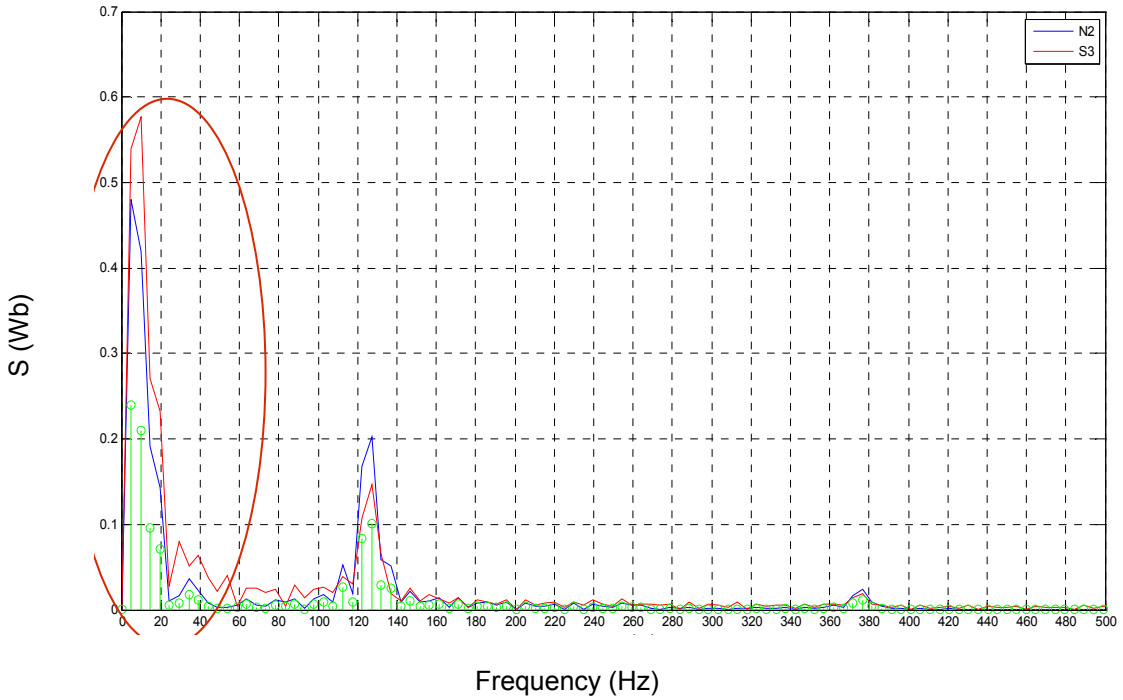

Figure 4.14: Fault signature frequency spectrum. Single magnet demagnetization

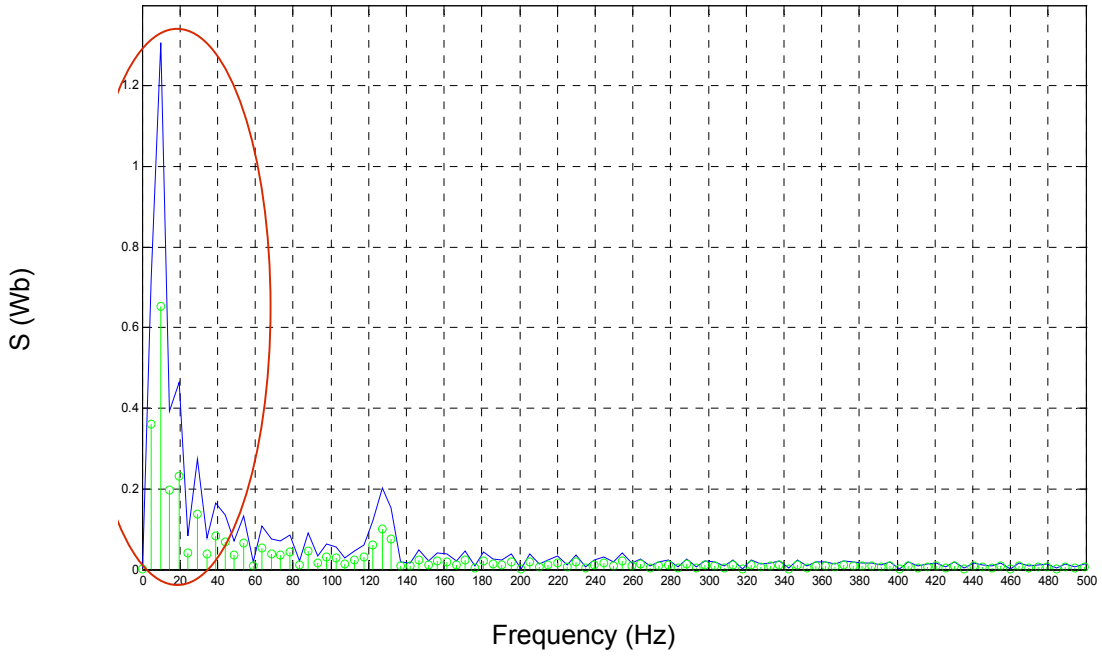

Figure 4.15: Fault signature frequency spectrum. Double magnet pair demagnetization

4.3.3 Rotor Eccentricity detection

In case of eccentricity as the rotor is closer to a set of windings the balance no longer exists in the electrical quantities, so for the same amount of current applied as of the healthy case some of the stator teeth would have higher levels of magnetic flux due to the proxomity to the permanent magnets. Figure 4.16 depicts the comparison of the magnetic flux distribution in the machine in case of a healthy machine and the one with an eccentric rotor. It can be seen that the peak of magnetic flux is higher in case of eccentric rotor. Also, in case of eccentric rotor the distribution of the magnetic flux around the airgap is no longer uniform. This signature can be used to determine the eccentricity of the rotor. Similar to the partial demagnetization case, in case of an eccentric rotor the magnetic flux can be written as:

$$\Phi_j(\theta_e) = \Phi_{PM,j}(\theta_e) + \sum_{j=1}^{5} i_j(\theta_e - j\frac{2\pi}{5}).\Phi_j(\phi_S - j\frac{2\pi}{5}) \Rightarrow \int_0^{2\pi} \Phi_j(\theta_e) d\theta_e \neq 0 \quad (4.6)$$

This unbalance in the magnetic flux linking each stator phase can be used to detect the eccentricity. The flux passing each stator tooth is measured using the FRM module and compared with the flux for the healthy case and the unbalance of the flux shows the eccentricity of the rotor. It should be mentioned that in case of an eccentric rotor there is no deformity in the magnetic flux wavefrom as observed in case of PM demagnetization and the difference is in the magitude of the flux. Figure 4.17 depicts the flux passing stator teeth in case of eccentric rotor compared with the healthy machine. In this case an eccentricity of 30% has been considered for the rotor.

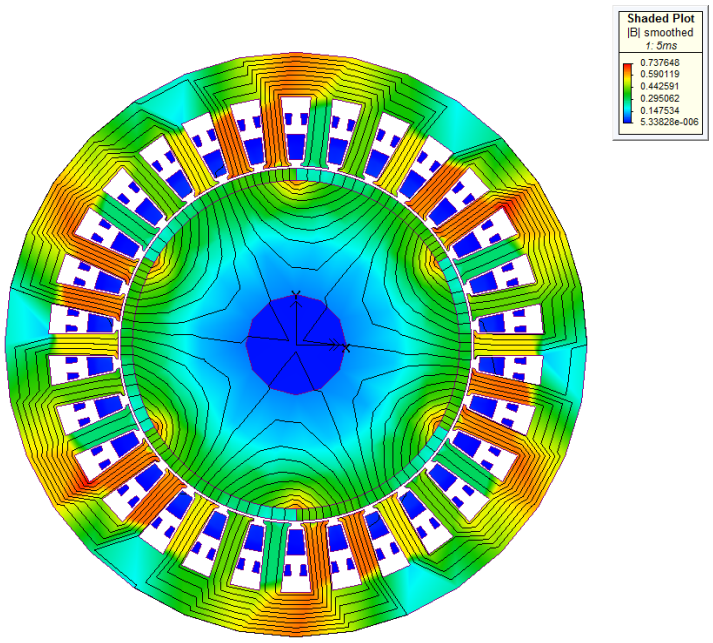

(a)

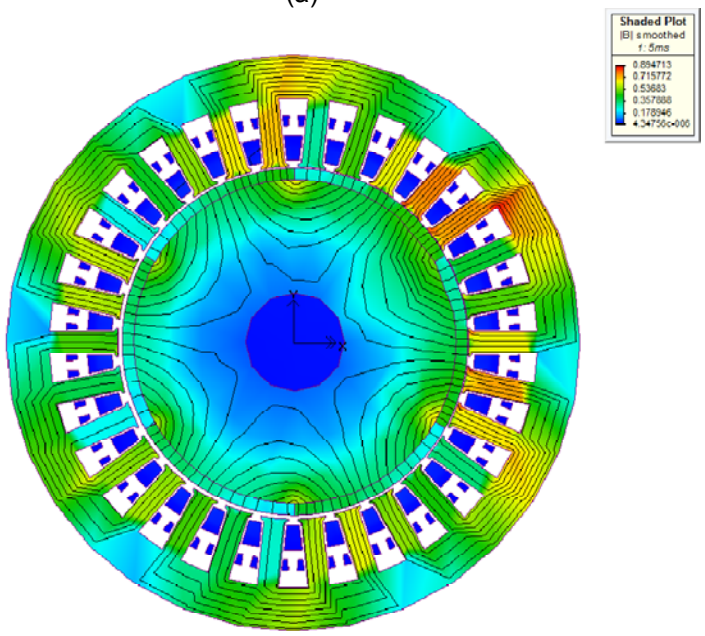

(b)

Figure 4.16: Magnetic flux distribution (a) healthy machine (b) eccentric rotor

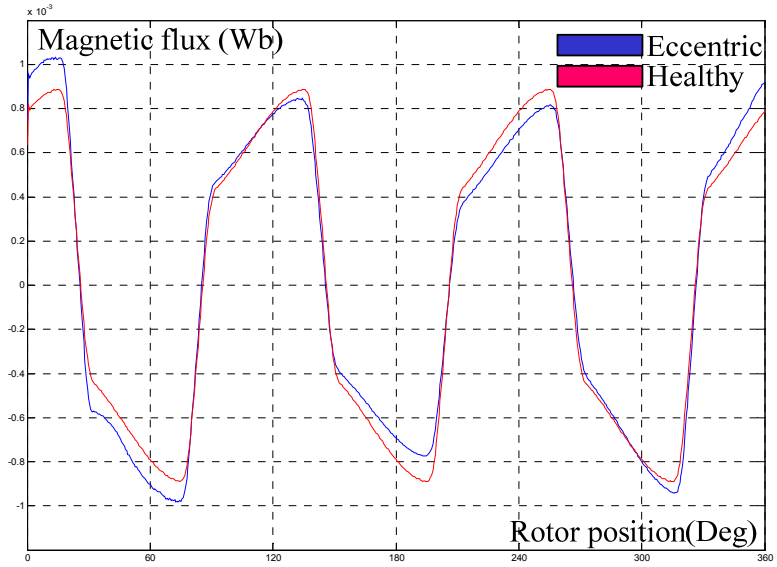

(a)

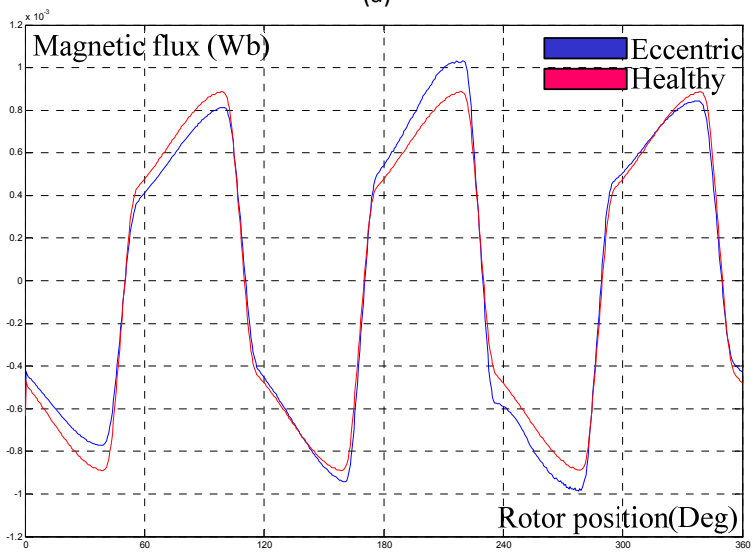

(b)

Figure 4.17: Comparison of magnetic flux distribution (a) tooth#3 (b) tooth#20

4.4 Fault Treatment

Fault teartment is equally important as the fault detection in terms of machine performance. Most of the research conducted on the fault detection is concentrated on the methods of the fault detection. These valuable researches simply ignore what happens to the system operation after the fault. Some of the fault tolerance methods suggest increasing the redundancy of the system to compensate for the component loss in case of the fault. Although

helpful, increasing the redundancy of the system is not always possible because of the limitation in the available space or due to the high price of the equivalent replacement device. On the other hand increasing the redundancy leads in to a more complicated control strategy which includes higher cost of control modules. In this dissertation the optimal excitation of the remaining healthy components of the EMEC is considered as a survival technique to compensate for the missing components.

The optimal currents for all the fault scenarios would be obtained and stored as explaind later. In case the fault happens, based on the type and location of the fault the appropriate set of currents would be applied to the PMSM stator phases to squeeze the maximum torque possible. The optimization criteria can be changed based on the application. Here the maximum average torque is considered while the torque ripple is minimized.

4.4.1 Open-circuit fault treatment

In most applications it is desirable to have the maximum output torque possible while the torque ripple is minimized. This is not necessarily the most efficient way of running the motor drive especially in terms of losses and harmonics. For example, considering the case of the healthy 5 phase PMSM where no faults exist.

Normally, the sinusoidal excitation is used to drive the system because it introduces fewer harmonics into the power electronics hardware hence reducing the losses and eliminating the need to the filters. By the way, in applications where the maximum torque per RMS input current is targeted sinusoidal excitation might not be the best choice. Figures 4.18 and 4.19 represent the sinusoidal and optimal excitation of the 5 phase PMSM machine.

To obtain the optimized waveforms the FRM code has been used in conjunction with the MATLAB optimization toolbox. It can be seen that in case of the optimal excitation the average output torque is higher than the case of the sinusoidal excitation as well as the torque per ampere ratio. Table 4.5 depicts the numerical comparison of these two cases. Based on this

the optimal excitation for the case of a single phase open circuit in the stator winding has been calculated. This data is stored in the memory and in case of a fault the optimal currents would be applied to the remaining healthy phases to get the maximum torque per ampere in the output.

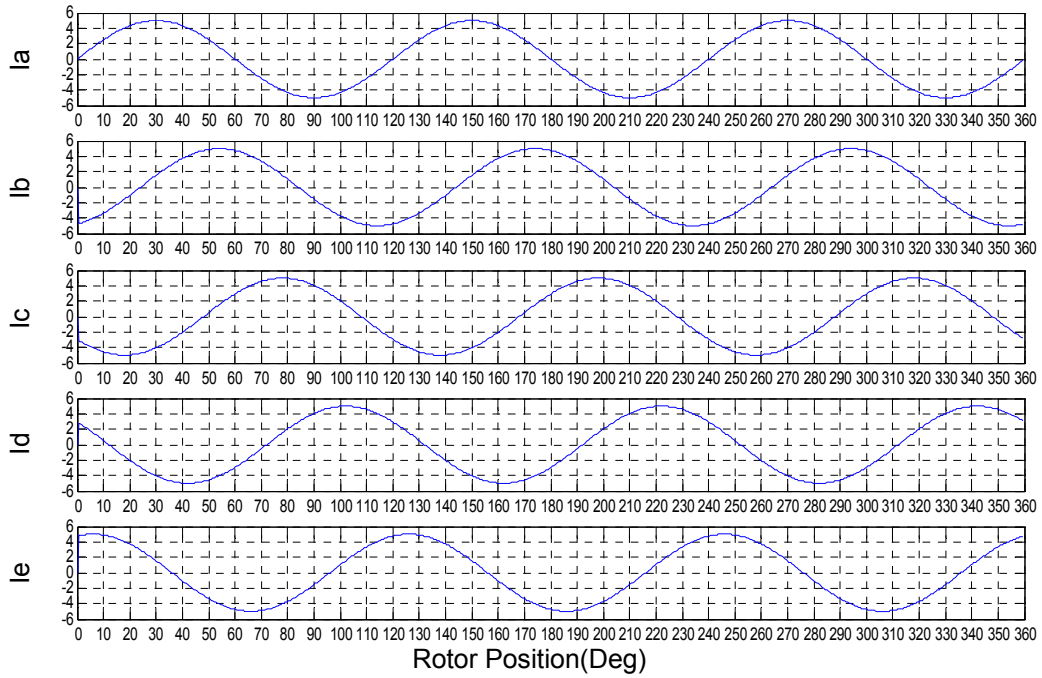

(a)

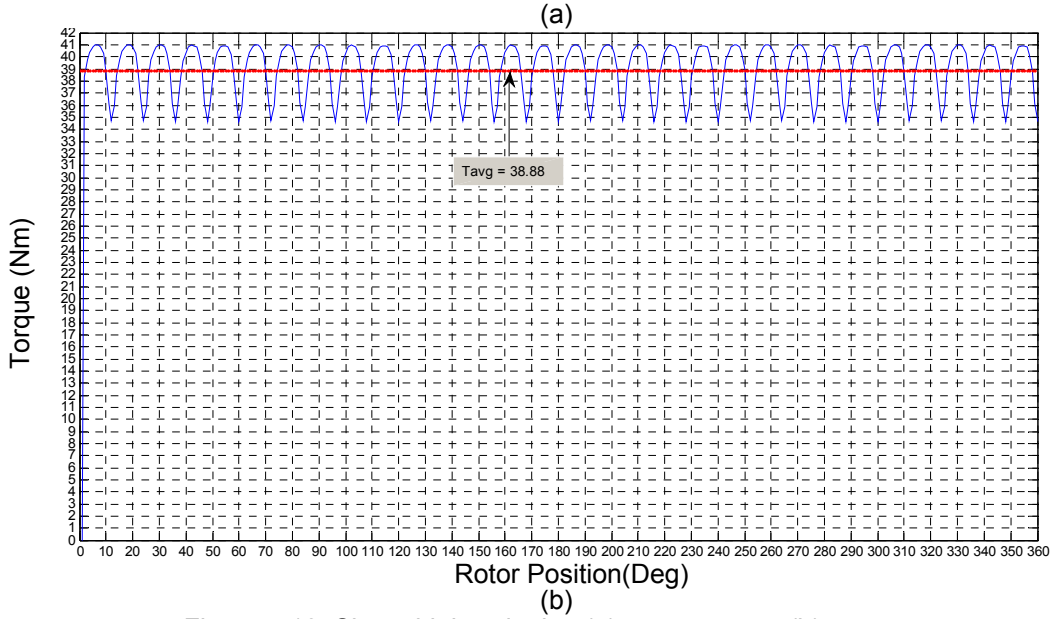

(b)

Figure 4.18: Sinusoidal excitation (a) stator current (b) torque

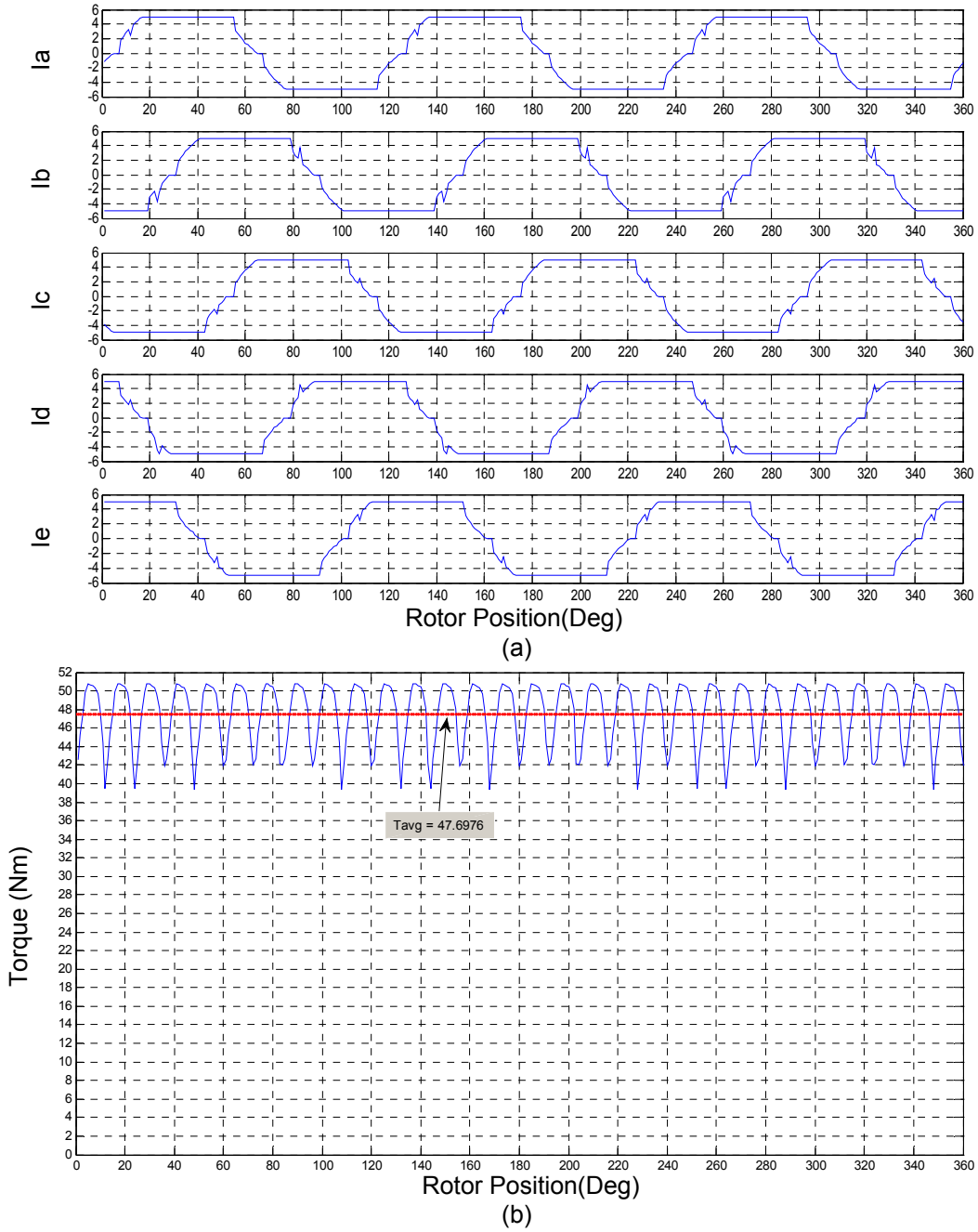

Figure 4.19: Optimal excitation (a) stator current (b) torque

Figure 4.20 depicts the optimal current waveforms in case of an open circuit fault in phase “D”. Figure 4.21 depicts the resulting toque in case the optimized currents have been applied to the remaining healthy phases. It can be seen that the average torque is decreased

comparing to the case of healthy 5 phase but the machine still can continue its operation with the reduced power level. The same analysis can be accomplished for the case that any other phases are out.

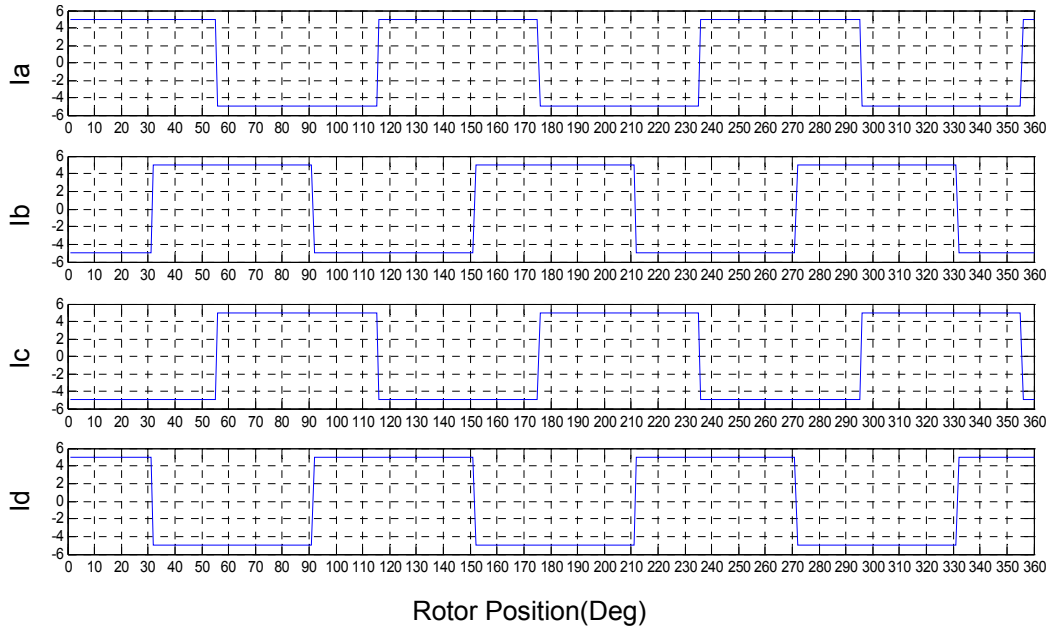

Figure 4.20: Single phase open circuit fault - Optimal current

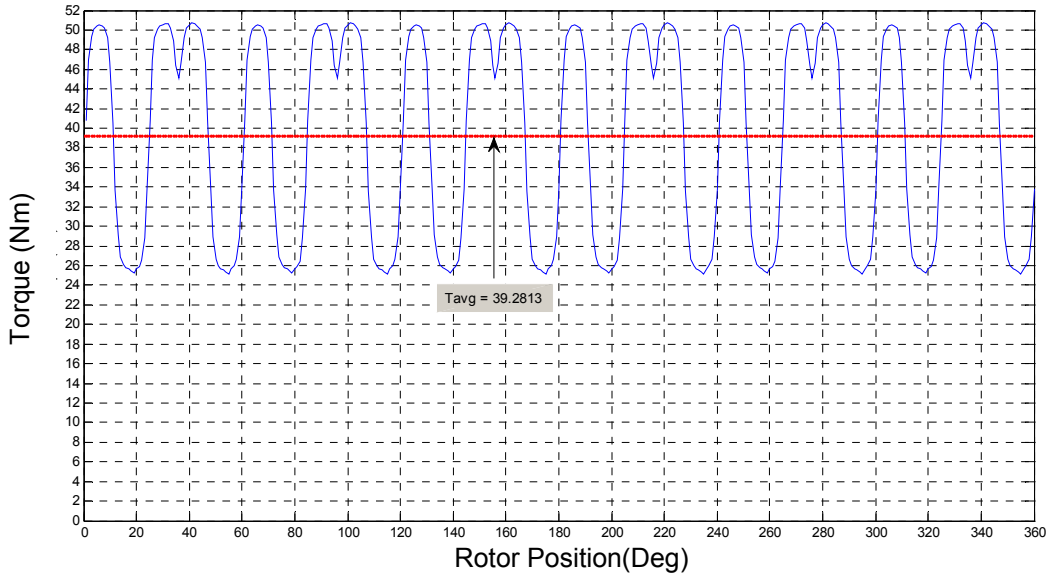

Figure 4.21: Single phase open circuit fault - Output torque

Table 4.5: Torque comparison for sinusoidal and optimal currents

Type of Excitation	T/I_{rms}
Sinusoidal	$T/I_{rms} = 38.88/3.5355 = 10.997$
Optimal	$T/I_{rms} = 47.6976/4.2979 = 11.098$

4.4.2 Partial demagnetization treatment

Depending on the service continuity strategy, various scenarios can be deployed after the demagnetization fault is detected. In case, the service can be provided by another module the machine could be stopped and the magnets being replaced. In case of an emergency application in which service discontinuity is not possible the stator applied currents can be modified in a way the maximum possible average torque could be squeezed out of the machine shaft. Of course the presence of the harmonics in the current would result in extra torque pulsations. For this purpose the field reconstruction method would be used in conjunction with the optimization methods to attain the optimal current waveforms. Figure 4.22 depicts the output mechanical torque of the machine for healthy and demagnetization fault cases in case sinusoidal currents are applied to stator phases. It is shown that the average torque has decreased almost 25% as a result of the magnet demagnetization. Also torque ripple has been increased almost 30%. Using the optimization methods the optimal waveforms are determined in case, demagnetization occurs. The Matlab optimization toolbox is linked to the FRM code.

For each rotor position, the optimization code calculates a set of currents based on the optimization criteria. These currents are used to calculate the magnetic field components in the machine. Then, using the magnetic field components the torque is calculated. In case the calculated torque complies with the target values, the currents would be stored and a new rotor

position would be considered. Figure 4.23 depicts the optimal stator phase currents and the output torque of the machine.

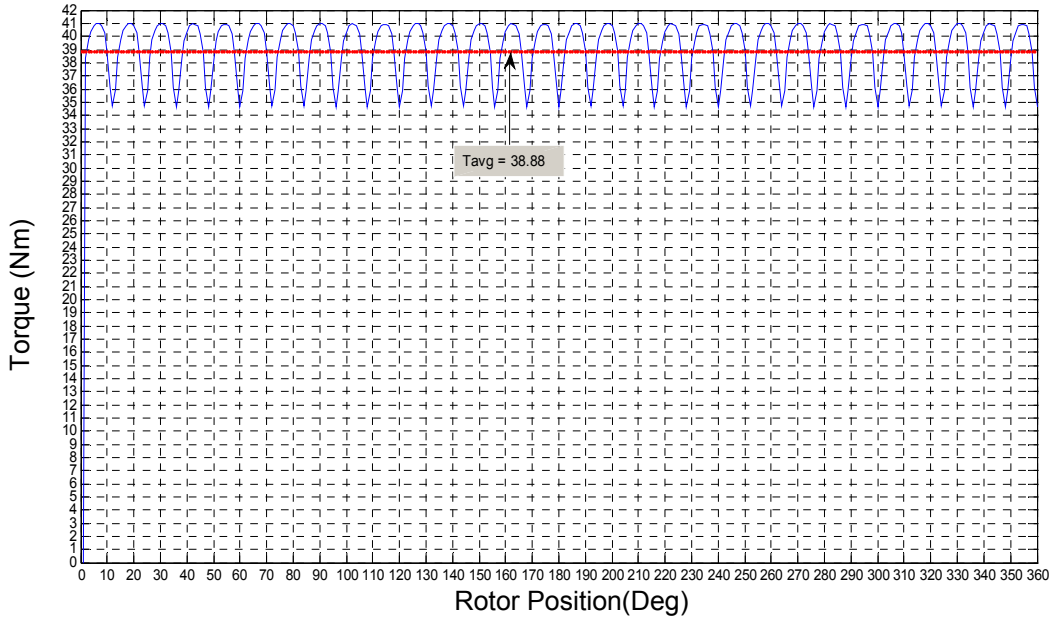

(a)

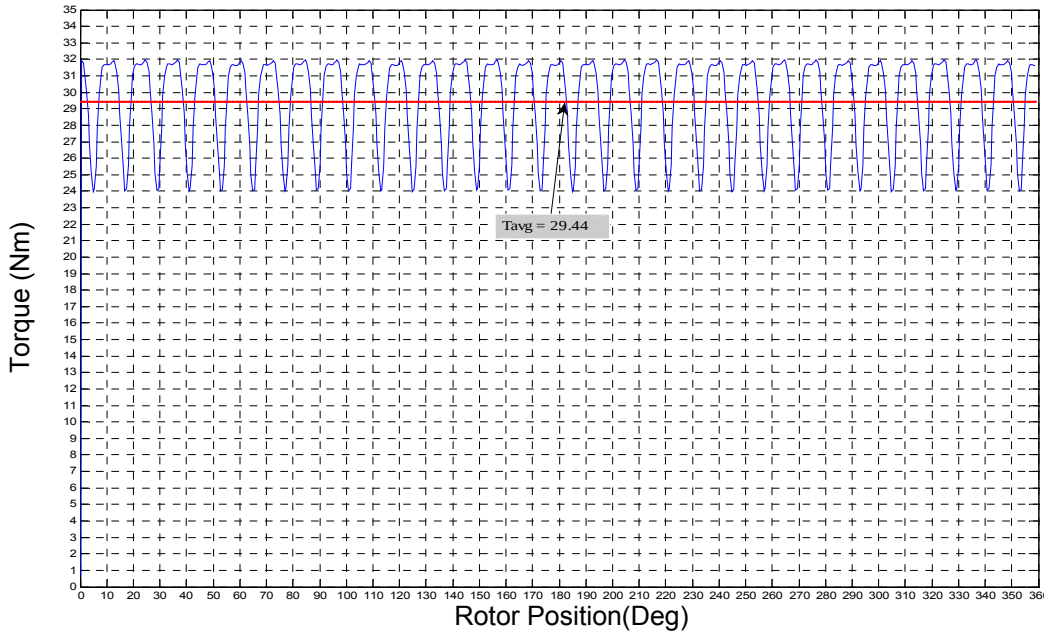

(b)

Figure 4.22: Torque Analysis. (a) Healthy machine, (b) Partially demagnetized magnets

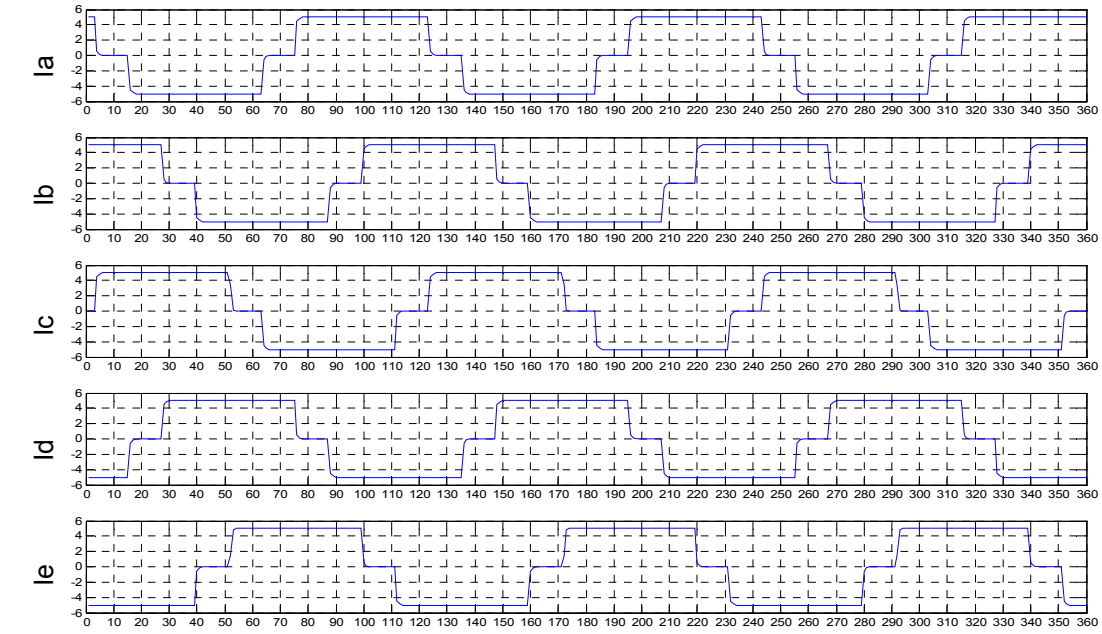

(a)

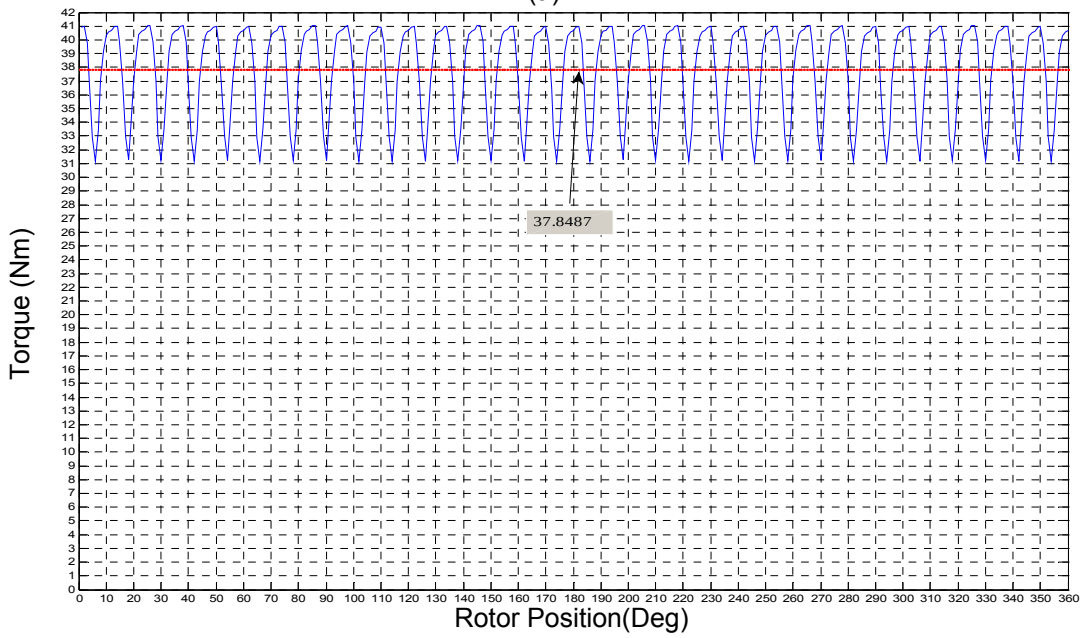

(b)

Figure 4.23: Torque Analysis. (a) Optimal stator currents, (b) Output torque, partially demagnetized magnets

The optimization criteria can be chosen to achieve the following cases regarding the target application:

- Maximum average torque
- Maximum average and Minimum torque ripple
- Minimum torque ripple

Here, the optimization process is targeted towards the maximum average torque. It can be seen that the average torque is about 3% less than that of the healthy machine with sinusoidal stator currents. The torque ripple is increased as expected. Different optimization scenarios can be considered and the optimal currents for each case can be achieved and stored in look up tables in the control unit. Based on the application, the appropriate currents can be applied to stator phases in case the fault is detected.

4.4.3 Rotor eccentricity treatment

As mentioed before, depending on the service continouity strategy, the appropriate control scheme should be deployed. In this dissertation the goal is to squeeze the maximum average power out of the healthy components of the machine. For this purpose the optimal currents for each case of the fault is calculated. In case a fault is detected, the optimal currents would be applied to the stator phases. To obtain the optimized waveforms the FRM code has been used in conjunction with the MATLAB optimization toolbox. The optimization criteria which are determined based on the application are specified in the optimization code. The optimization code is linked to FRM. Based on the initial values of the currents estimated in optimization module, the resulting torque is calculated and compared with the target value. In case the target is reached the optimal currents will be calculated for a new rotor position. This procedure has been implemented for all the faulty cases. The output torque for the eccentric rotor for sinusoidal stator currents has been shown in figure 4.24. It can be seen that the average torque is reduced compared with the healthy machine while the ripple is almost %30 more.

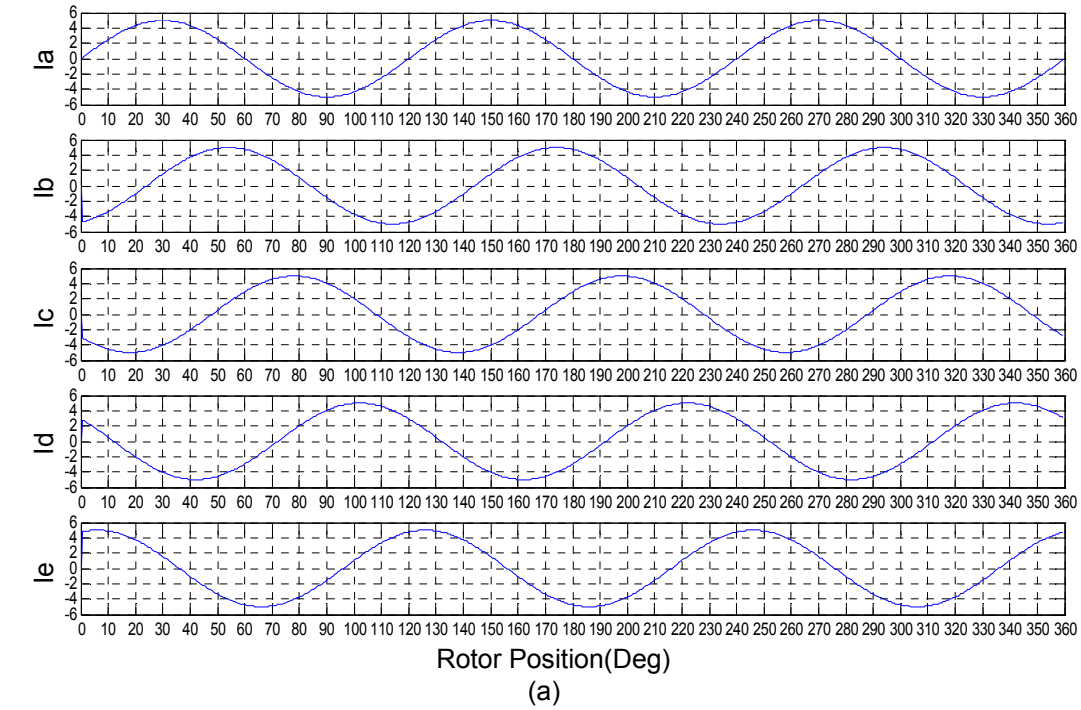

(a)

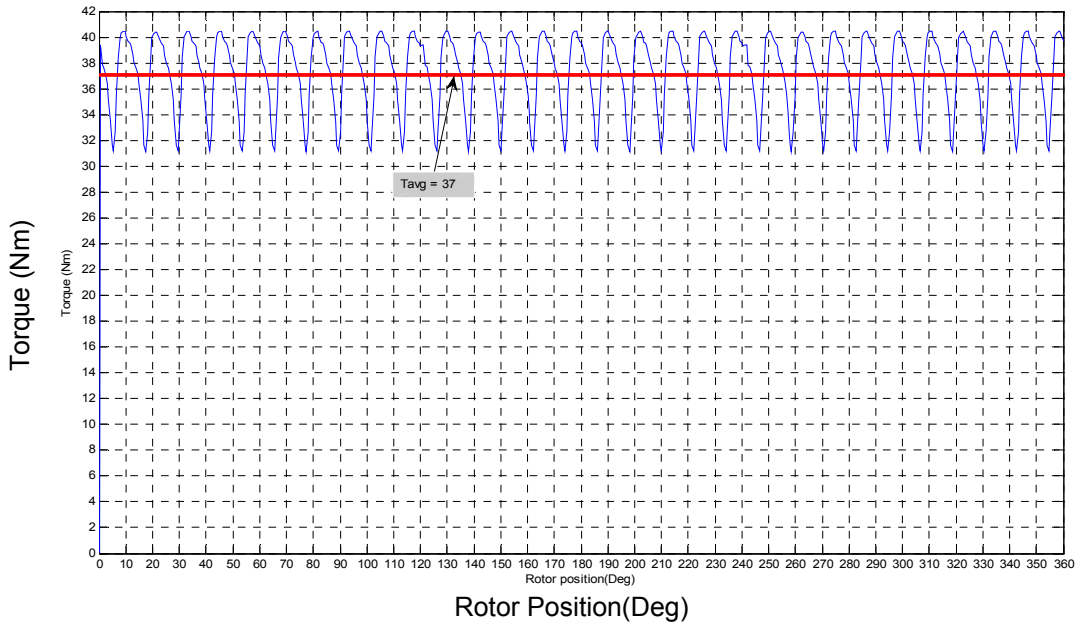

(b)

Figure 4.24: Sinusoidal Excitation. (a) Stator currents, (b) Output torque, Eccentric rotor

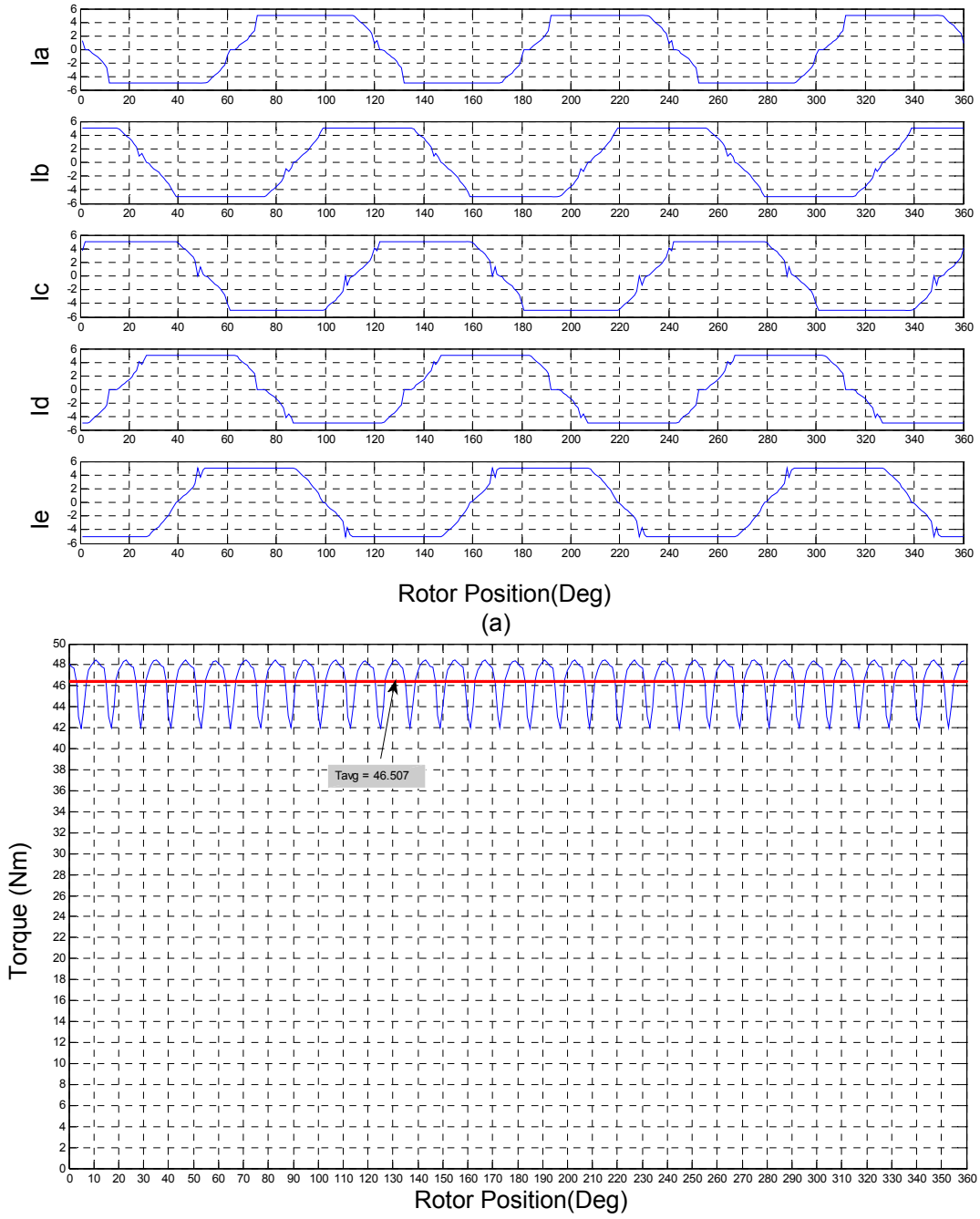

Figure 4.25: Optimization. (a) Optimal stator currents, (b) Output torque, Eccentric rotor

Figure 4.25 depicts the output torque while the optimal currents have been applied to stator phases. The optimization criteria are chosen so that the torque ripple would be minimized and the average torque would be maximized.

4.5 Experimental Results

For independent control of phase currents which is required by fault tolerance, a full bridge inverter has been used, which refers to the use of four switches connected in a bridge arrangement as shown in figure 4.26. Control is performed by regulating the flow of current through the stator windings of the machine. Current controllers are used to generate gate signals for the inverter. Proper selection of the inverter devices and selection of the control technique will guarantee the efficacy of the drive.

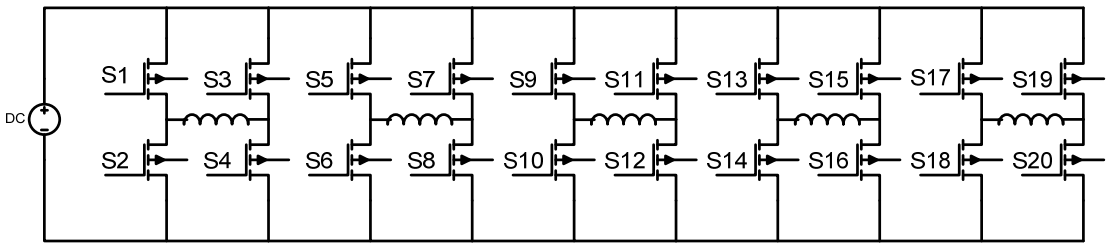

Figure 4.26: Current regulated full-bridge inverter used for the experimental 5-phase motor drive system

An electronically controlled PM motor drive system uses continuous rotor position feedback and hystersis control to supply the motor with the appropriate current. The need of knowing rotor position requires the development of devices for position measurement. In the present drive system, the position sensor is mounted on the shaft of the rotor.

There are four devices that are commonly used for the measurement of position-potentiometers, linear variable differential transformers, optical encoders and resolvers. Of these, resolvers and encoders are most commonly used for motor drive applications.

Depending on the accuracy of performance and sampling frequency available, an appropriate rotor position sensor with the required resolution can be selected.

There are several kinds of encoders. For applications where a device is inactive for long periods of time or is rated relatively low speeds, absolute encoders are used. The machine designed for the present application was rated to a maximum of approximately 1800 rpm. Therefore the position encoder selected for this application was an analog absolute encoder manufactured by AMCI. These encoders are also typically recommended in systems that need to retain position information through a power outage.

The performance of the inverter is shown in figure 4.27. In this figure the sinusoidal currents has been shown versus the rotor position. The absolute position sensor generates an analog voltage according to the relative rotor position. This voltage is then fed into the DSP A/D module. The sinusoidal currents are generated according to the current position of the rotor.

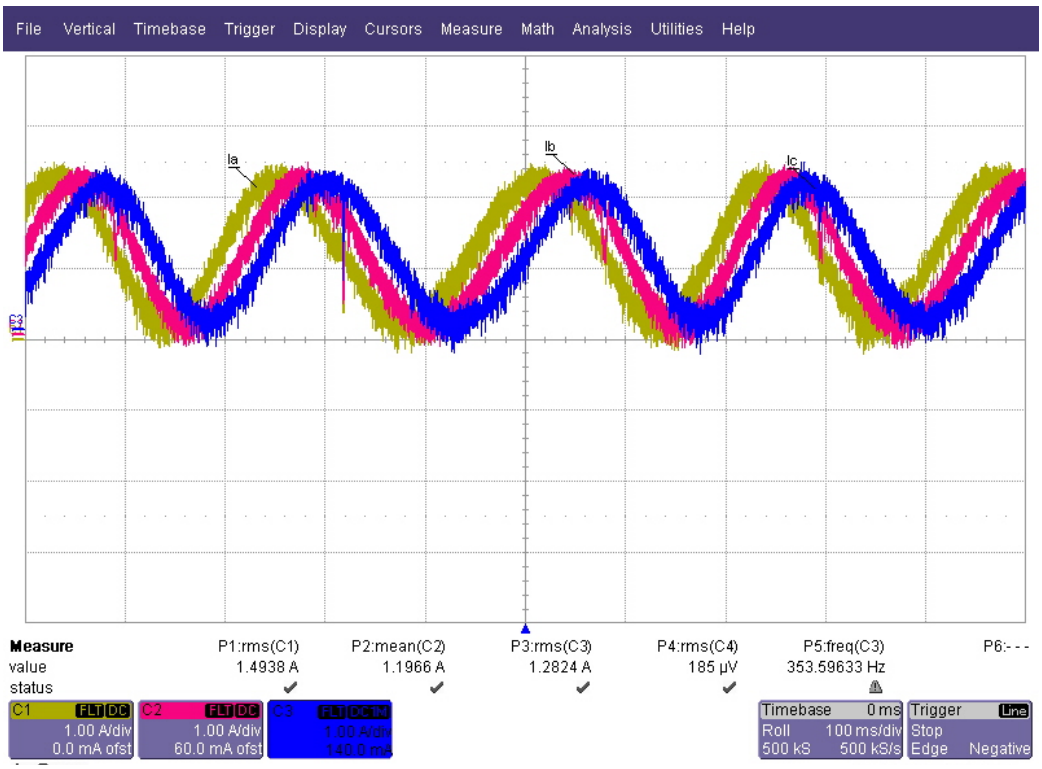

Figure 4.27: Sinusoidal currents regulated by full-bridge inverter using hystersis control

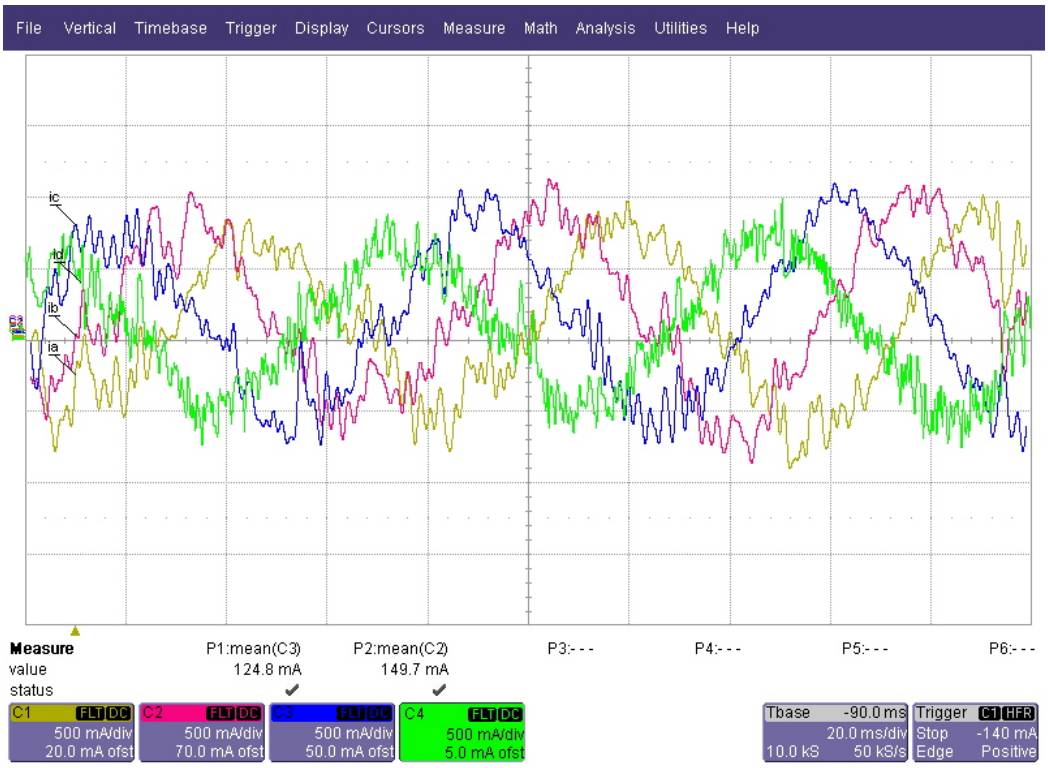

Figure 4.28: Sinusoidal currents Applied to the motor

The sinusoidal excitation of the stator phases has been shown in figure 4.28. This figure indicates the currents applied to phases “A” to “D”. In case one or more of the machine phases undergo the open circuit fault, the DSP should be able to diagnose the fault location and apply the appropriate currents to the remaining healthy phases. Figure 4.29 depicts the case in which phase “B” of the machine is lost. The optimal currents have been calculated and stored using Matlab optimization toolbox. These currents have been shown in figure 4.29(a). Figure 4.29(b) depicts the actual currents obtained from the experimental test bed. The current waveform is alos shown in figure 4.30 for a single phase.

Figure 4.31 depicts the optimal current applied to phase “A” of the motor. Figure 4.32 depicts the optimal currents in case of the double phase open circuit fault on the stator phases “D” and “E”. The calculated optimal currents are shown in figure 4.32(a). The actual currents applied to the stator healthy phases are shown in figure 4.32(b).

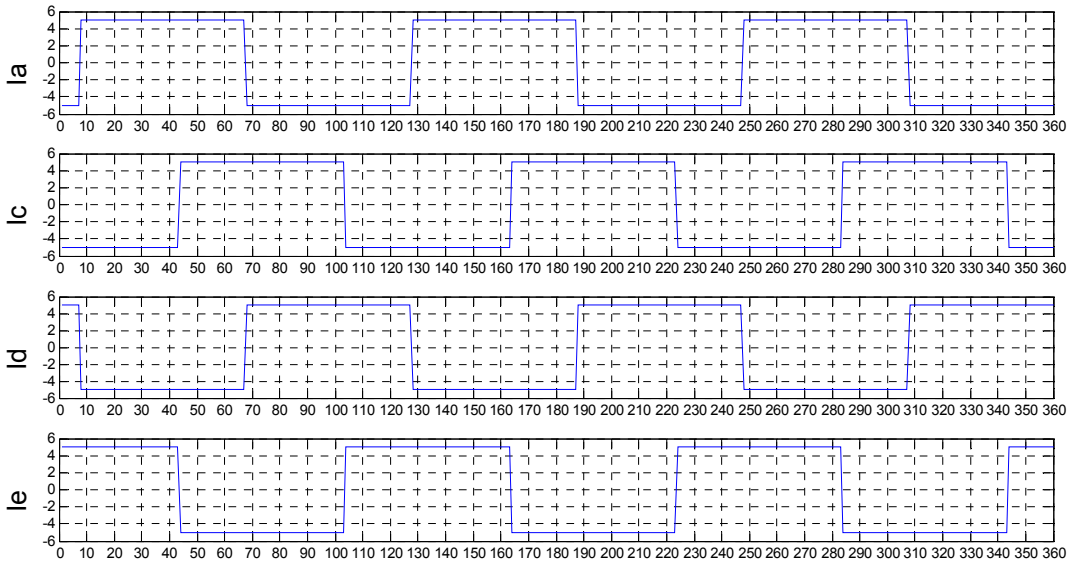

(a)

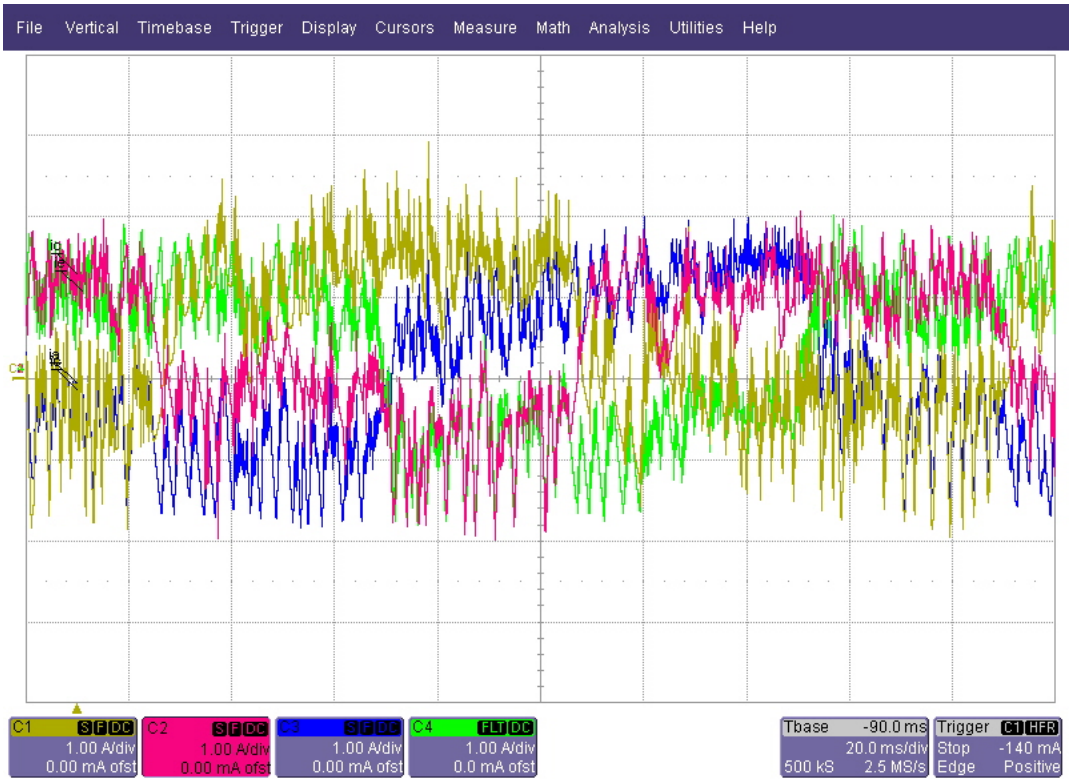

(b)

Figure 4.29: Optimal currents: Single phase open circuit on Phase “B”

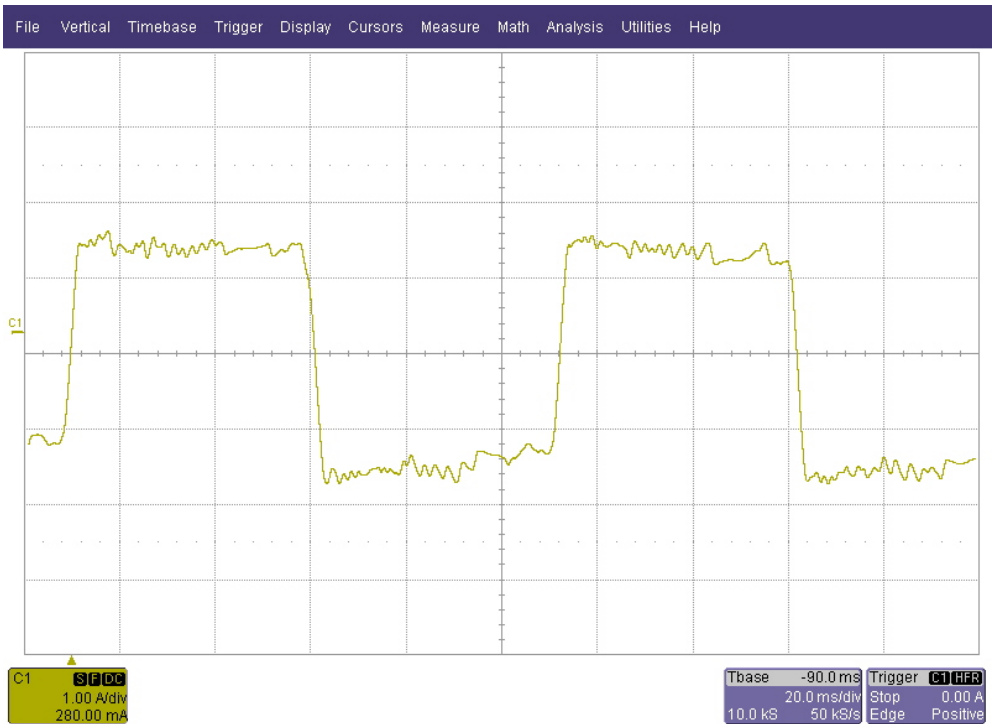

Figure 4.30: Single phase open circuit optimal currents: Phase “C” current.

Figure 4.31: Double phase open circuit optimal currents: Phase “A” current.

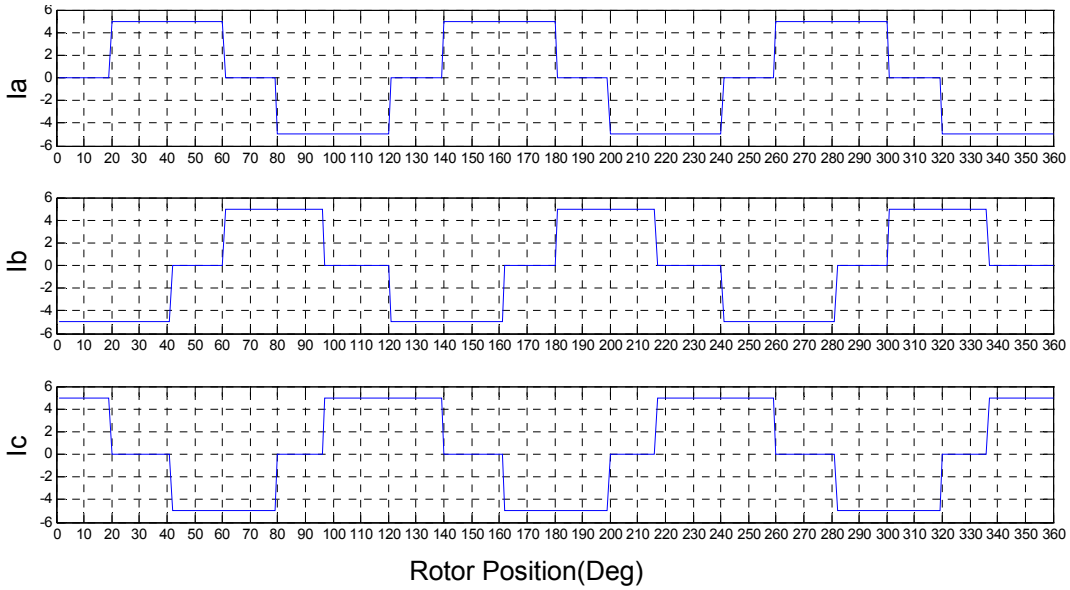

(a)

(b)

Figure 4.32: Optimal currents: Double phase open circuit on Phases “D” and “E”

Figure 4.33 compares the sinusoidal excitation of the stator phases compared with the optimal case. The DC link voltage is 92(V). The rms value of the sinusoidal current is 0.7(A) while the rms value of the optimal current is 0.63(A). The output torque of the machine in each case has been shown in figure 4.34. According to this figure the output optimal torque is almost %10 higher than the sinusoidal case. The significant achievement here is the reduction in the torque ripple for optimal currents compared with sinusoidal excitation.

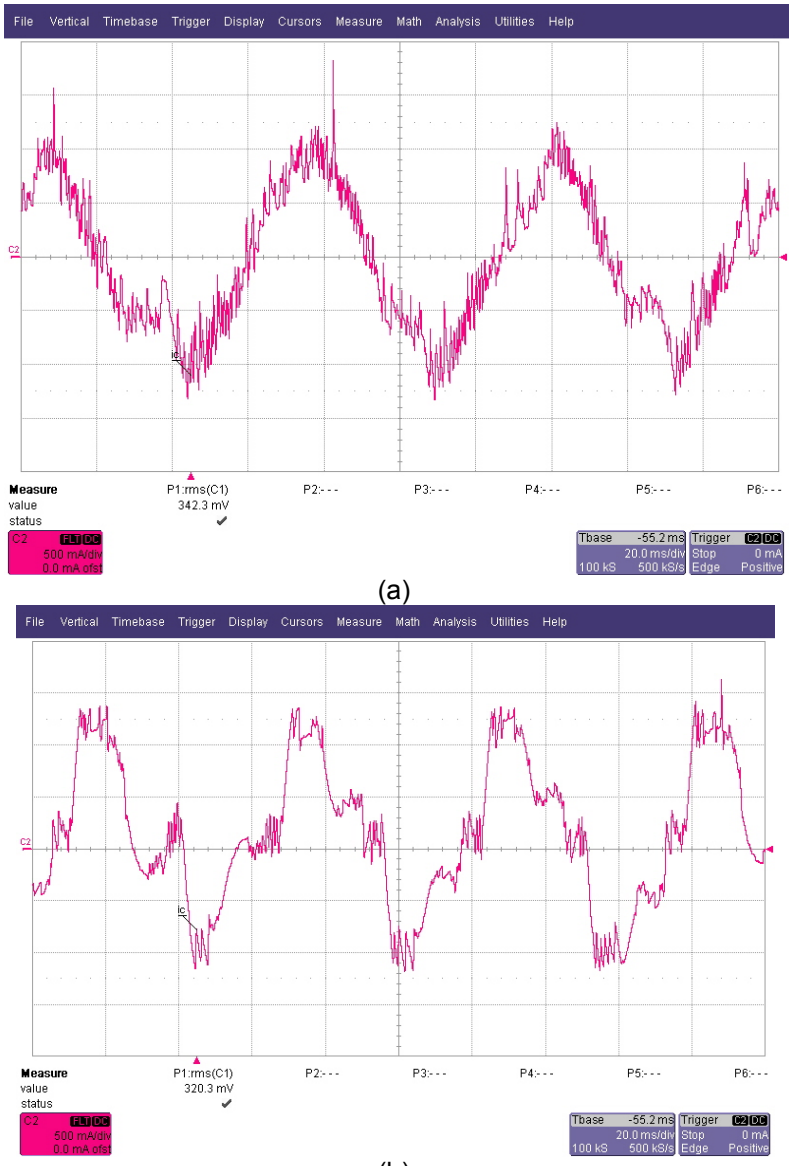

Figure 4.33: Torque Analysis. (a) Sinusoidal current, (b) Optimal current.

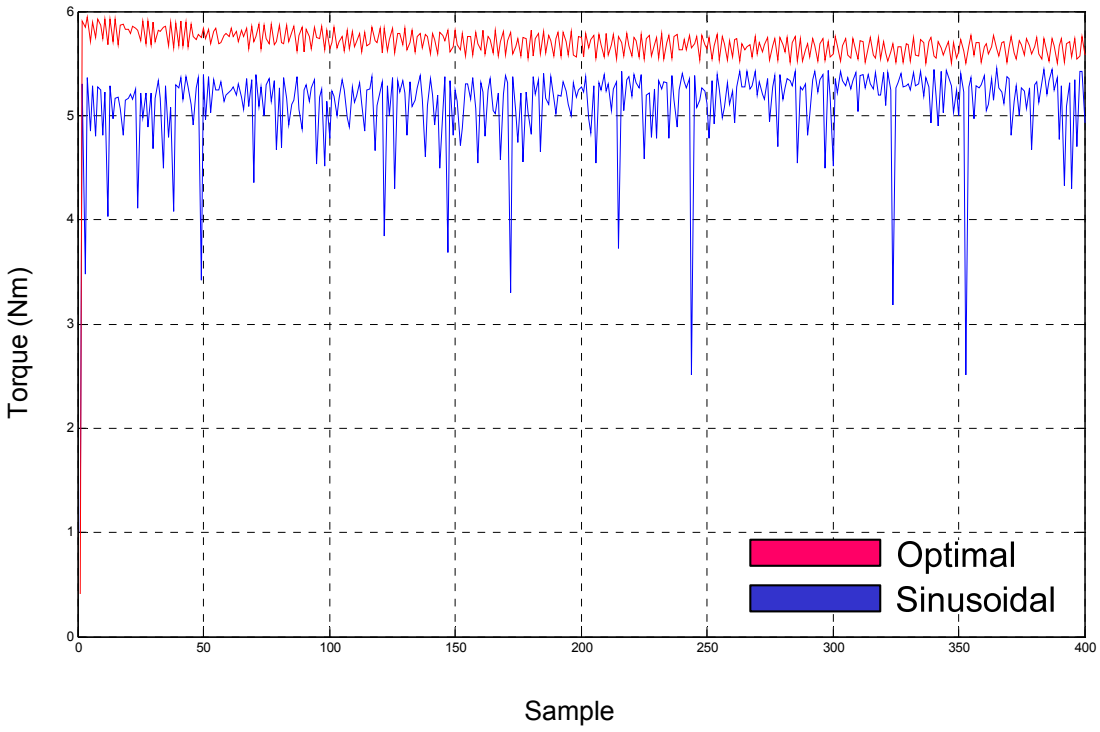

Figure 4.34: Torque comparison for 5-phase PMSM: Optimal versus Sinusoidal

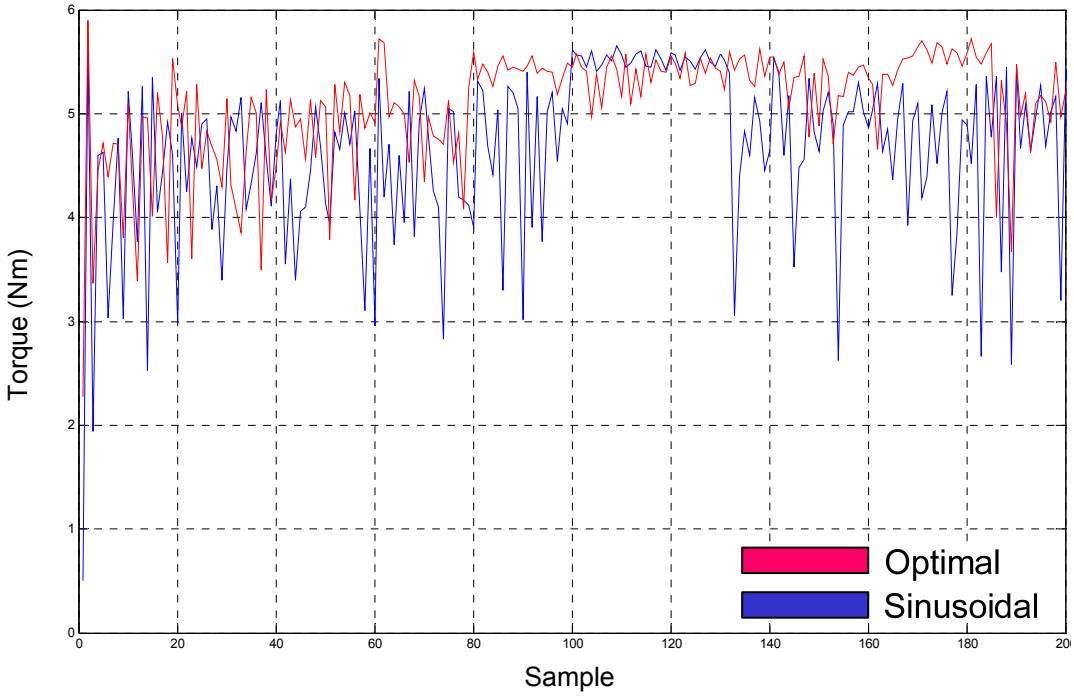

Figure 4.35: Torque comparison for 3-phase PMSM: Optimal versus Sinusoidal

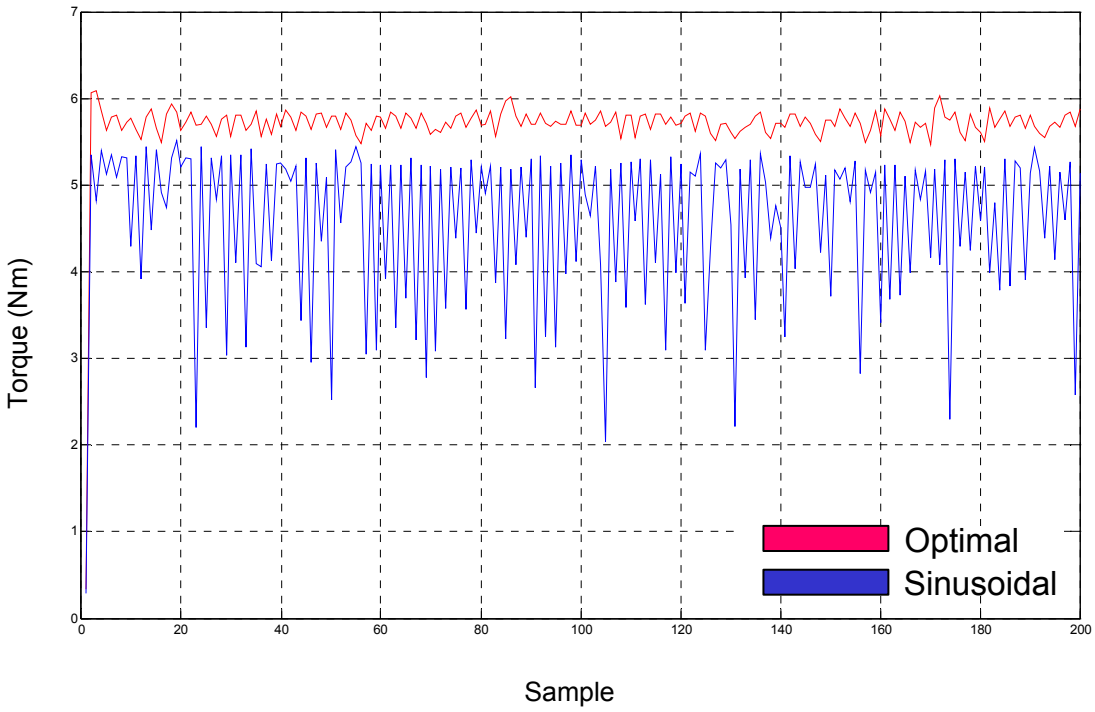

Figure 4.36: Torque comparison for 4-phase PMSM: Optimal versus Sinusoidal

Figures 4.35 and 4.36 depict the torque comparison for the double and single phase open-circuit faults. According to the figures, the average torque is higher in case of optimal excitation compared with the sinusoidal operation of the machine. The torque per ampere is better in case of 5–phase and 3-phase operation while in case of 4-phase operation sinusoidal excitation gets better results. In terms of ripple the optimal excitation is significantly better compared with the sinusoidal case.

CHAPTER 5

CONCLUSIONS

Fault tolerance operation of the adjustable motor drives is crucial in high impact applications. Fault detection and optimal post fault treatment of the fault are the basic requirements for the operation.

In this dissertation, a field reconstruction method based on Finite Element Analysis has been developed. This method involves the reconstruction of the electromagnetic fields due to the phase currents using basis functions obtained using one single solution from FEA. The field reconstruction method presents a new numerical technique for analysis and design of a PMSM. This technique is time- efficient and offers an insightful vision of the magnetic field in the machine. It combines ideas from electromechanical energy conversion, signal reconstruction, pattern recognition, and power electronics to create novel solutions. By manipulating the tangential and normal components of magnetic field in the airgap of the machine, the magnetic flux passing through each stator tooth can be estimated. These fluxes are used to estimate the flux linking each stator phase. The flux estimated is used to detect the signatures related to each of open circuit, partial demagnetization and rotor eccentricity faults. The fault treatment has been investigated by comparing the optimal and sinusoidal excitation of the stator phases. It is shoen that in case of optimal currents the average torque is higher compared with the sinusoidal and the ripple is smaller.

APPENDIX A

EXPERIMENTAL TESTBED SETUP

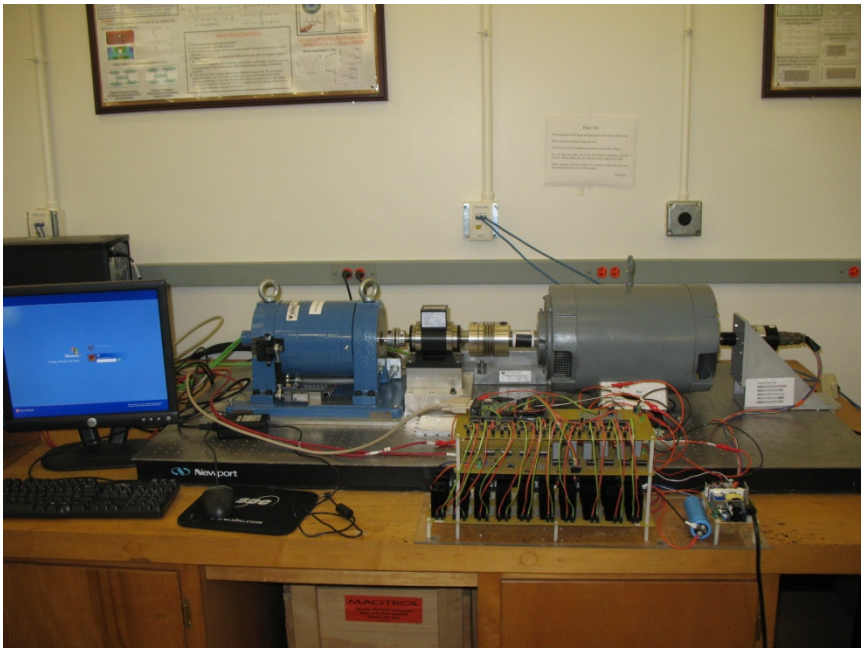

Experimental test bed including the 5-phase PMSM, Torque meter, Dynamometer and Power Electronics boards

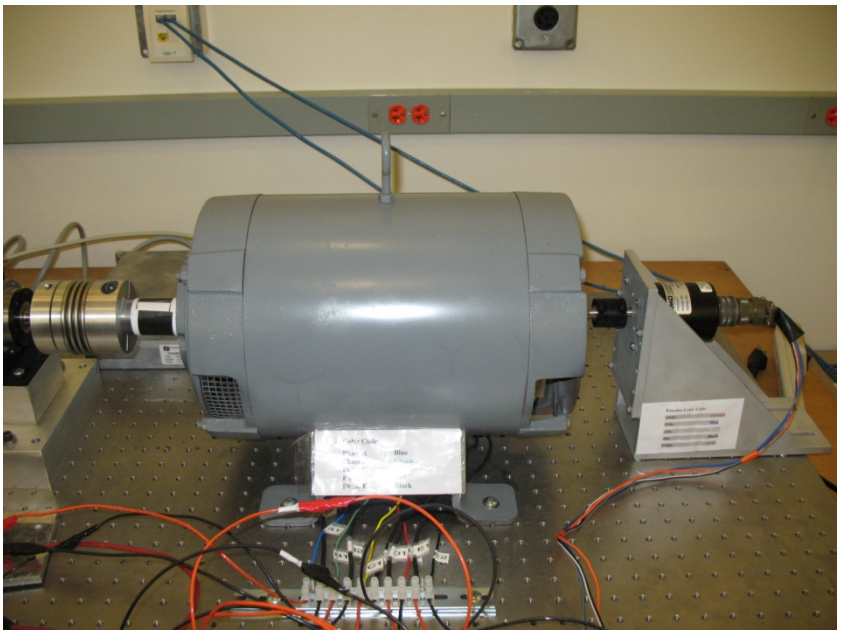

5-phase PMSM coupled to the absolute position encoder

APPENDIX B

ROTOR AND STATOR LAMINATION

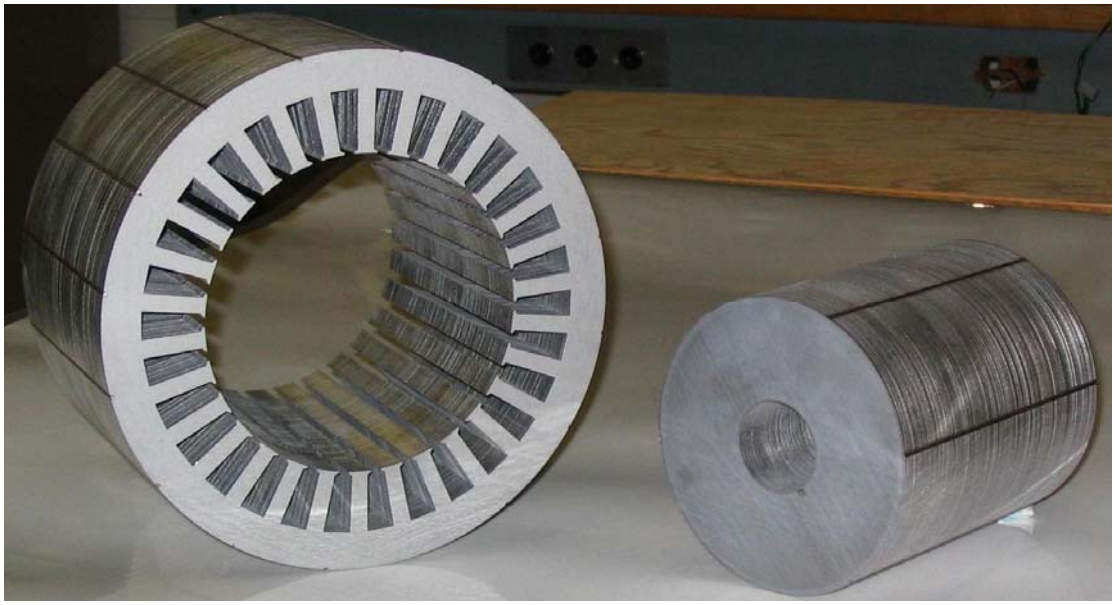

5-phase PMSM stator and rotor laminations

APPENDIX C

COIL WINDINGS ARRANGEMENT

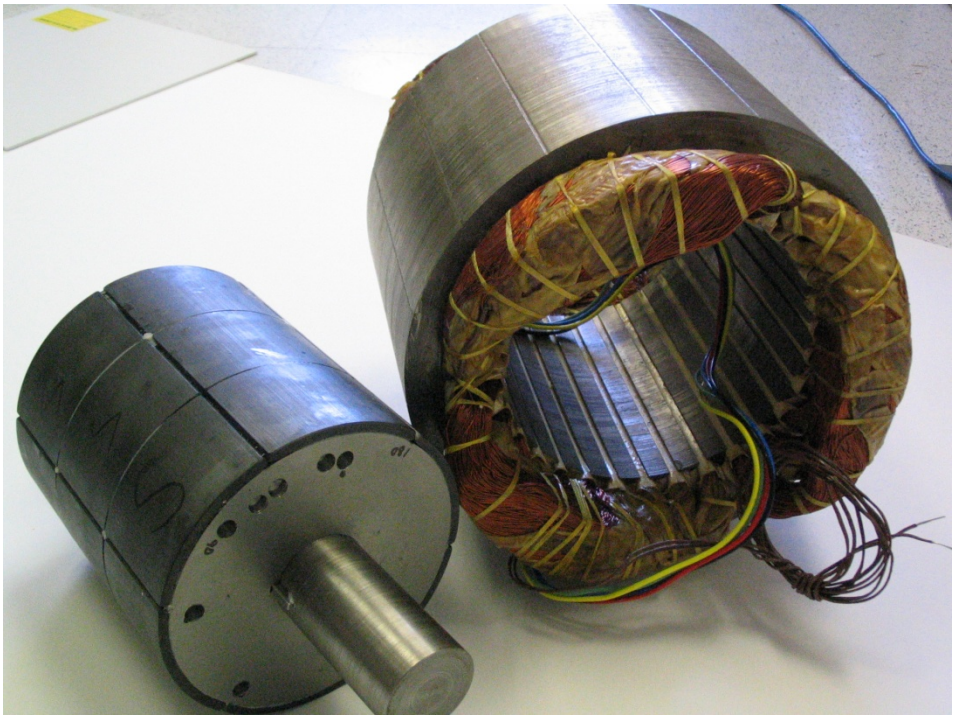

PMSM 6-pole, 5-phase, 30-slot stator and 6-pole rotor

APPENDIX D

POWER ELECTRONICS CONVERTER

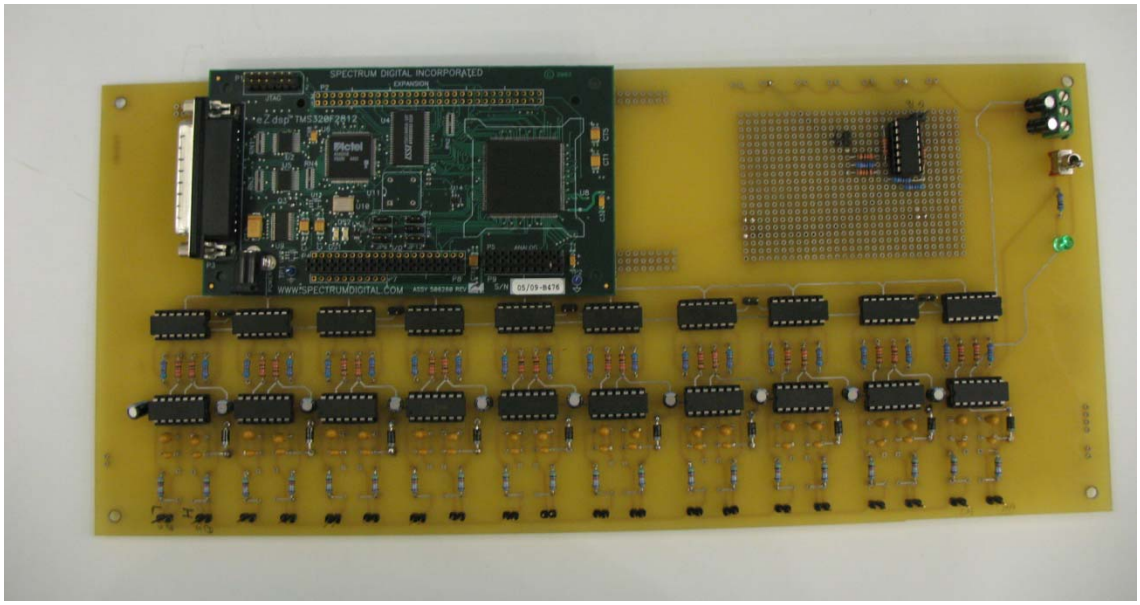

Gate drivers and DSP

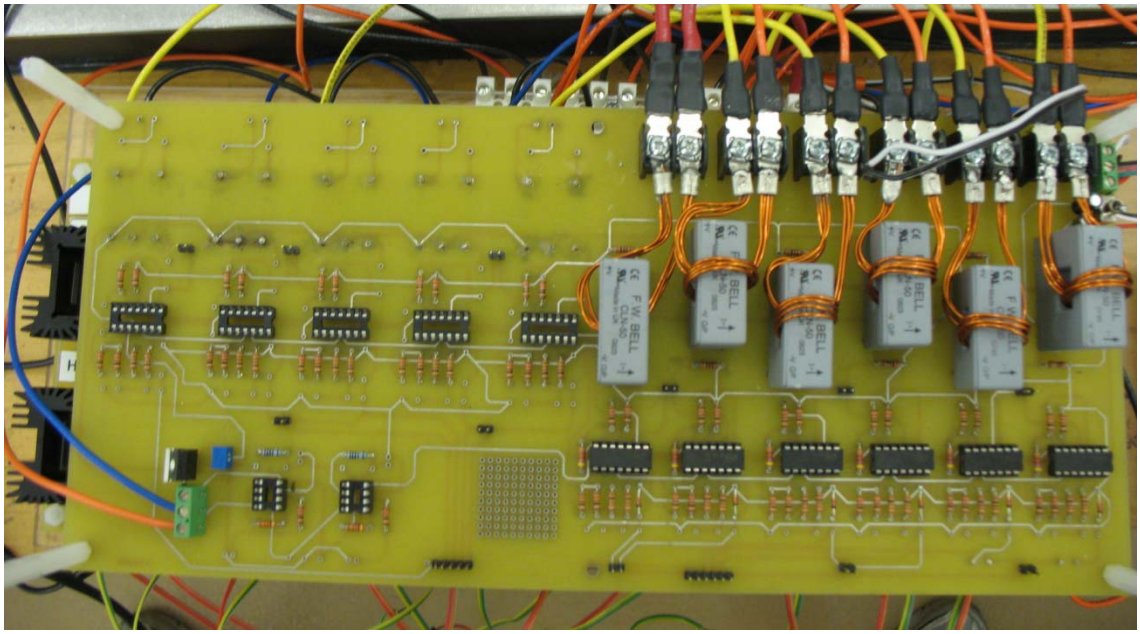

Sensor board: current sensors

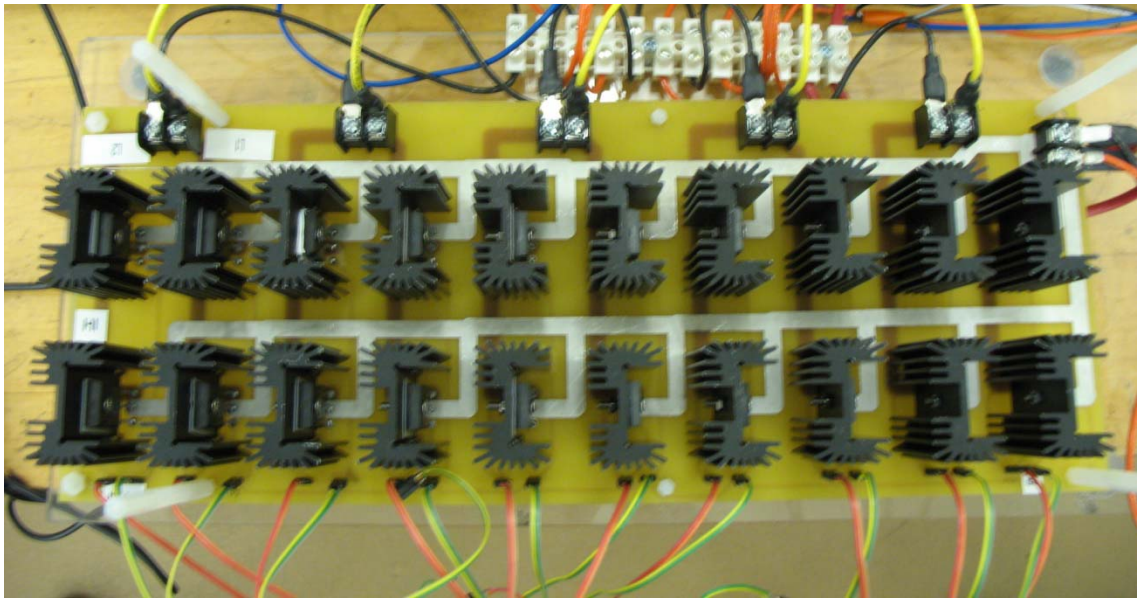

Power MOSFETs

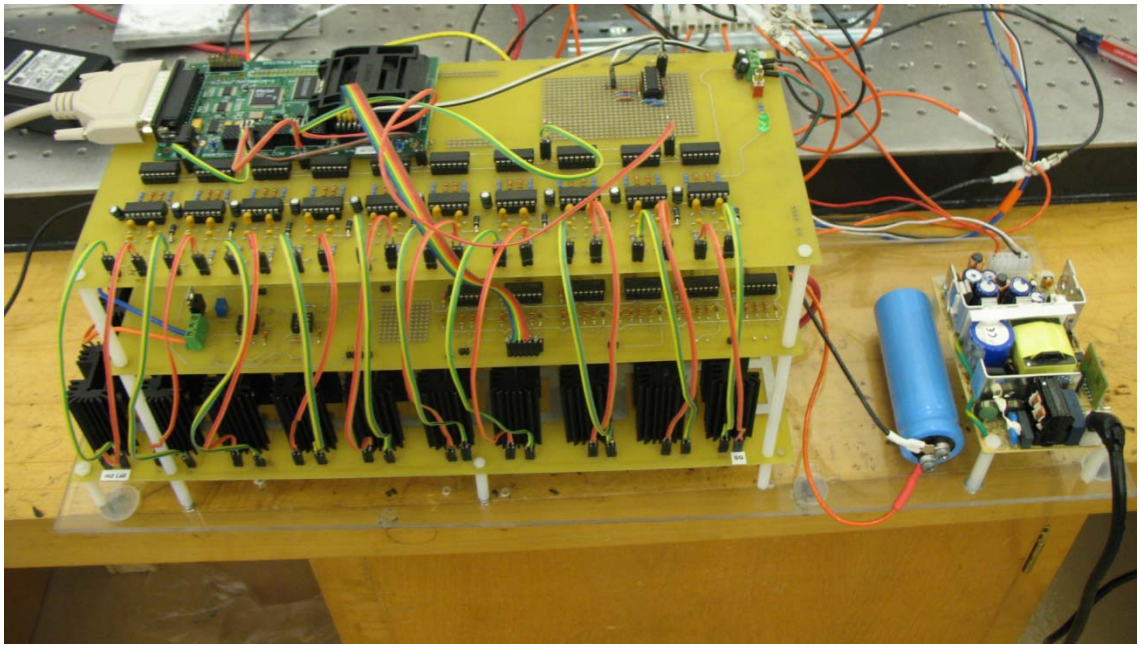

5-Phase H-bridge inverter

REFERENCES

[1] Magnetic Materials Producers Association, “MMPA Standard 0100-Standard Specifications for Permanent Magnet Materials”, originally published 1964.

[2] A. Emadi, *Handbook of automotive electronics and motor drives,* Taylor and Francis group, 2005.

[3] S. Bolognani, M. Zordan, M. Zigliotto, “Experimental fault-tolerant control of a PMSM drive”, *IEEE transactions on Ind. Electron.*, Vol. 47, No. 5, pp: 1134 – 1141, 2000.

[4] C. Jie, W. Jiabin, K. Atallah, D. Howe, “Performance Comparison and Winding Fault Detection of Duplex 2-Phase and 3-Phase Fault-Tolerant Permanent Magnet Brushless Machines”, *IEEE Conf. on Industry Applications*, pp. 566 – 572, 2007.

[5] O. Wallmark, L. Hamefors, O. Carlson, “Control Algorithms for a Fault-Tolerant PMSM Drive”, *IEEE Transactions on Industry Applications*, Vol. 54, No. 4, pp. 1973 – 1980, 2007.

[6] C. Gerada, K. Bradley, M. Summer, “Winding Turn-to-Turn Faults in Permanent Magnet Synchronous Machine Drives”, *IEEE Conf. on Industry Applications*, Vol. 2, pp. 1029 – 1036, 2005.

[7] R. L. de Araujo Ribeiro, C. B. Jacobina, E. R. C. da Silva, A. M. N. Lima, “Fault detection of open-switch damage in voltage-fed PWM motor drive systems”, *IEEE Transactions on Power Electronics*, Vol. 18, No. 2, pp. 587 – 593, 2003.

[8] L. B. Kuk, K. T. Hyung, M. Ehsani, “On the feasibility of four-switch three-phase BLDC motor drives for low cost commercial applications: topology and control”, *IEEE Transactions on Power Electronics*, Vol. 18, No. 1,pp. 164 - 172, 2003.

[9] B. C. Mecrow, A. G. Jack, J. A. Haylock, J. Coles, “Fault tolerant permanent magnet machine drives” *IEEE Int. Conf. on Electrical Machines and Drives*”, pp. 433 – 437, Sep 1995.

[10] A. G. Jack and B. C. Mecrow, J. A. Haylock, “A comparative study of permanent magnet and switched reluctance motors for high-performance fault-tolerant applications”, *IEEE Transactions on Industrial Applications*, Vol. 32, No.4, pp. 889 – 895, 1996.

[11] J. A. Haylock, B. C. Mecrow, A. G. Jack and D. J. Atkinson, “Operation of a fault tolerant PM drive for an aerospace fuel pump application”, *IEE Proceedings on Electric power Applications*, Vol. 145, No.5, pp. 441 – 448, 1998.

[12] J. A. Haylock, B. C. Mecrow, A. G. Jack, D. J. Atkinson, “Operation of fault tolerant machines with winding failures”, *IEEE transactions On Energy conversion*, Vol. 14, No. 4, pp.1490 – 1495, 1999.

[13] J. E. Hill, S. J. Mountain, “Control of a variable speed, fault-tolerant permanent magnet generator” *Int. Conf. on power electronics, Machines and Drives,* pp. 492 – 497, 2002.

[14] B. C. Mecrow, A. G. Jack, D. J. Atkinson, S. Green, G. J. Atkinson, A. King, B. Green, “Design and testing of a 4 phase fault tolerant permanent magnet machine for an engine fuel pump”, *Int. Conf. on Electric Machines and Drives*, Vol. 2, pp. 1301 – 1307, 2003.

[15] S. Green, D. J. Atkinson, A. G. Jack, B. C. Mecrow, A. King, “Sensorless operation of a fault tolerant PM drive”, *IEE Proceedings on Electric power Applications*, Vol. 150, No.2,pp. 117 – 125, 2003.

[16] M. T. Abolhassani, “A novel multiphase fault tolerant high torque density permanent magnet motor drive for traction application”, *IEEE Int. Conf. on Electric Machines and Drives*, pp. 728 – 734, 2005.

[17] Z. Jingwei, N. Ertugrul, W. L. Soong, “Fault Analysis and Remedial Strategies on a Fault-Tolerant Motor Drive with Redundancy”, *IEEE Int. Conf. on Electric Machines and Drives*, Vol. 2, pp. 1119 – 1124, 2007.

[18] T. M. Jahns, “Improved Reliability in Solid State AC Drives by means of Multiple Independent Phase-Drive Units”, *IEEE Transactions on Industrial Applications*, Vol. 16, No. 3, pp. 321 - 331, 1980.

[19] A. G. Jack and B. C. Mecrow, “Safety Critical Drives for Aerospace Applications”, *Proceedings of ICEM 94*, Vol. 1, pp.91-96, 1994.

[20] R. V. White, “Fault tolerance in distributed power systems”, *Proceedings of EPE’95*, pp. 2 851-2 857, 1995.

[21] J. Zhu, N. Ertugrul, W. L. Soong, “Performance Investigation of a Fault-Tolerant Brushless Permanent Magnet AC Motor Drive” *IEEE Int. Conf. on Power Electronics and Motion Control*, Vol. 2, pp. 1 – 5, 2006.

[22] Z. Jingwei, N. Ertugrul, W. L. Soong, “Detection and Remediation of Switch Faults on a Fault Tolerant Permanent Magnet Motor Drive with Redundancy”, *IEEE Conf. on Industrial Electronics and Applications*, pp. 96 – 101, 2007.

[23] J. Penman, H. G. Sedding, B. A. Lloyd, W.T. Fink, “Detection and Location of Inter turn Short Circuits in the Stator Windings of Operating Motors”, *IEEE Transactions on Energy Conversion*, Vol. 9, No. 4, pp. 652-658, Dec. 1994.

[24] E. Wosdmagg “Turbo generator Field Winding Shorted Turn Detection by AC Flux Measurement”, *IEEE Transactions on Energy Conversion*, Vol. 9, No. *2*, pp. 427.431, June 1994.

[25] K. Weinreh, P. Drozdavski, “Detection of Winding Faults of a Salient Pole Synchronous Modeling by a Spectral Analysis of Currents”, *ICEM 94*, Vol. 2, pp. 56-61, 1994.

[26] W. Jiabin, K. Atallah, D. Howe, “Optimal torque control of fault-tolerant permanent magnet brushless machines”, *IEEE transactions on Magnetics*, Vol. 39, No. 5, pp. 2962 – 2964, 2003.

[27] W. Zhu, B. Fahimi, S. Pekarek, **“**A field reconstruction method for optimal excitation of permanent magnet synchronous machines”**,** *IEEE Trans. on Energy Conversion,* vol. 21, no.2, pp. 305 – 313, June 2006.

[28] B. Fahimi, “Qualitative approach to electromechanical energy conversion: Reinventing the art of design in adjustable speed drives”, *ICEMS Int. Conf. on Electrical machines and Systems*, pp. 432 – 439, Oct 2007.

[29] W. Jiang, M. Moallem, B. Fahimi, S. Pekarek, **“**Qualitative Investigation of Force Density Components in Electromechanical Energy Conversion Process”, *IEEE Conf. on Ind. Electron.,* pp.1113-1118, Nov. 2006.

[30] W. Zhu, B. Fahimi, S. Pekarek, **“**Optimal excitation of permanent magnet synchronous machines via direct computation of electromagnetic force components”, *IEEE Int. Conf. on Electrical machines and Drives*, pp. 918 - 925 , May 2005.

[31] P. *C.* Krause, *Analysis of Electric Machinery,* McGraw- Hill, 1986, New York.

[32] J. Holtz, “Methods for speed sensorless control of AC drives,” in *Sensorless Control of AC Motor Drives,* K. Rajashekara, A. Kawamura, and K. Matsuse, Eds. Piscataway, NJ: IEEE Press, 1996.

[33] J. Jinsheng, J. Holtz, “High dynamic speed sensorless AC drive with on-line model parameter tuning for steady state accuracy”, *IEEE Trans. on Ind. Electron.,* vol. 44, no.2, pp. 240 – 246, Apr 1997.

[34] J. Holtz, Q. Juntao, “Sensorless vector control of induction motors at very low speed using a nonlinear inverter model and parameter identification”, *IEEE Trans. on Ind. Appicatl.,* vol. 38, no.4, pp. 1087 – 1095, July 2002.

[35] J. Holtz, “Acquisition of position error and magnet polarity for sensorless control of PM synchronous machines”, *IEEE Trans. on Ind. Appicatl.,* vol. 44, no.4, pp. 1172 – 1180, July 2008.

[36] J. Holtz, “Sensorless position control of induction motors - an emerging technology”, *IEEE Trans. on Ind. Electron.,* vol. 45, no.6, pp. 840 – 851, Dec 1998.

[37] P. L. Jansen and R. D. Lorenz, “Transducerless position and velocity estimation in induction and salient AC machines,” *IEEE Trans. Ind. Applicat.,* vol. 31, pp. 240–247, Mar./Apr 1995.

[38] Y. A. Chapuis. D. Roye, J. Davoine, “Principles and implementation of direct torque control by stator flux orientation of an induction motor”, *IEEE IAS annual meeting,* vol. 1, pp. 185 – 191, 1995.

[39] B. K. B. And, N. R. Patel, “A programmable cascaded low-pass filter based flux synthesis for a stator flux-oriented vector-controlled induction motor drive”, *IEEE Trans. on Ind. Electron.,* vol. 44, no.1, pp. 140 – 143, Feb 1997.

[40] M. F. Rahman, M. E. Haque, L. Tang, L. Zhong, “Problems associated with the direct torque control of an interior permanent magnet synchronous motor drive and their remedies ”, *IEEE Trans. on Ind. Electron.*, vol. 51, no. 4, pp. 799 - 809, Aug 2004.

[41] K. K. Shyu, L. J. Shang, H. Z. Chen, K. W. Jwo, “Flux compensated direct torque control of induction motor drives for low speed operation”, *IEEE Trans. on Power Electron.*, vol. 19, no. 6, pp. 1608 - 1613, Nov. 2004.

[42] S. Mir, M. E. Elbuluk, D. S. Zinger, “PI and fuzzy estimators for tuning the stator resistance in direct torque control of induction machines”, *IEEE Trans. on Power Electron.* vol. 13, no. 2, pp. 279 – 287, Mar 1998.

[43] L. Zhong, M. F. Rahman, K. W. Lim, Y. Hu, Y. Xu, “A fuzzy observer for induction motor stator resistance for applications in direct torque control”, *IEEE Int. Conf. on Power Electronics and drive systems* , pp. 91 - 96, 1997.

[44] F. Zidani, D, Diallo, M. E. H. Benbouzid, R. Nait-Said, “Direct torque control of induction motor with fuzzy stator resistance adaption”, *IEEE Trans on Energy Conversion*, Vol. 21, no. 2, pp. 619 - 621, June 2006.

[45] E. Wosdmagg, “Turbo generator Field Winding Shorted Turn Detection by AC Flux Measurement”, *IEEE Trans on Energy Conversion*, Vol. 9, no. 2, pp. 427 - 431, June 1994.

[46] C. C. Wang, C. H. Fang, “Sensorless scalar controlled induction motor drives with modified flux observer”, *IEEE Trans. on Energy Conversion,* vol. 18, no.2, pp. 181 – 186, June 2003.

[47] V. Vasic, S. N. Vukosavic, E. Levi, “A stator resistance estimation scheme for speed sensorless rotor flux oriented induction motor drives”, *IEEE Trans. on Energy Conversion,* vol. 18, no.4, pp. 476 – 483, Dec 2003.

[48] S. B. Lee, T. G. Habetler, R. G. Harley, D. J. Gritter, “An evaluation of model-based stator resistance estimation for induction motor stator winding temperature monitoring”, *IEEE Trans. on Energy Conversion,* vol. 17, no.1, pp. 7 – 15, Mar 2002.

[49] H. D. Glass, B. C. Brown, G. W. Foster, W. B. Fowler, R. Gustafson, G. P. Jackson, J. F. Ostiguy, J. T. Volk, “Stability tests of permanent magnets built with strontium ferrite”, *Particle Accelerator Conference*, Vol. 3, pp. 3260 – 3262, May 1997.

[50] S. Ruoho, A. Arkkio, “Partial Demagnetization of Permanent Magnets in Electrical Machines Caused by an Inclined Field”, *IEEE Trans. on Magnetics*, Vol. 44, pp. 1773 – 1778, July 2008.

[51] J. R. Riba Ruiz, J. A. Rosero, A. Garcia Espinosa, L. Romeral, “Detection of Demagnetization Faults in Permanent-Magnet Synchronous Motors Under Nonstationary Conditions”, *IEEE Trans. on Magnetics*, vol. 45, No. 7, pp. 2961 – 2969, 2009

[52] J. Rosero, L. Romeral, J. A. Ortega, J.C. Urresty, “Demagnetization fault detection by means of Hilbert Huang transform of the stator current decomposition in PMSM”, *Int. Sym. on Industrial Electronics (ISIE)*, pp. 172 – 177, 2008

[53] J. A. Rosero, J. Cusido, A. Garcia, J. A. Ortega, L. Romeral, “Study on the Permanent Magnet Demagnetization Fault in Permanent Magnet Synchronous Machines”, *IEEE conf. on Industrial Electronics*, pp. 879 – 884, 2006.

[54] B. M. Ebrahimi, J. Faiz, M.J. Roshtkhari, “ Static-, Dynamic-, and Mixed-Eccentricity fault diagnoses in permanent-magnet synchronous motors”, *IEEE Trans. on Ind. Electron.*, Vol. 56, No. 11, pp. 4727– 4739, 2009.

BIOGRAPHICAL INFORMATION

Amir Khoobroo was born on November 19, 1979 in Tehran, Iran. He received his Bachelor of Science from Sharif University of technology, Tehran, Iran, in 2003 and Master of Science in Electrical Machines and Drives from the Isfahan University of techology, Isfahan, Iran, in 2006. He started his PhD in Spring 2007 at the University of Texas at Arlington.During his PhD, he was employed at Renewable Energy and Vehicular technology Laboratory as a Research Associate where he was involved in the design and implementation of Electrical machines and Power Electronics modules. At the University of Texas at Arlington, he was also involved in various projects including the design of linear Switched Reluctance machines and development of the power electronics drilling applications. His research interests include power electronics, motor drives, renewable energy and vehicular systems.